STUDY ON CONCRETE INFILLED TUBES AS COMPRESSION MEMBERS IN TRUSS TYPE LIGHT VEHICULAR BRIDGES

P. B. M. R. Bogahawaththa

198023U

Degree of Master of Science

Department of Civil Engineering

University of Moratuwa

Sri Lanka

April 2021

STUDY ON CONCRETE INFILLED TUBES AS COMPRESSION MEMBERS IN TRUSS TYPE LIGHT VEHICULAR BRIDGES

P. B. M. R. Bogahawaththa

198023U

Thesis submitted in partial fulfilment of the requirements for the degree Master of Science in Civil Engineering

Department of Civil Engineering

University of Moratuwa

Sri Lanka

April 2021

DECLARATION

I declare that this is my own work and this thesis does not incorporate without acknowledgement any material previously submitted for a Degree or Diploma in any other University or institute of higher learning and to the best of my knowledge and belief it does not contain any material previously published or written by another person except where the acknowledgement is made in the text.

Also, I hereby grant to University of Moratuwa the non-exclusive right to reproduce and distribute my thesis, in whole or in part in print, electronic or other medium. I retain the right to use this content in whole or part in future works (such as articles or books)

…… Date:

P. B. M. R. Bogahawaththa

The above candidate has carried out research for the Masters under my supervision.

…… Date:

Dr. H. D. Hidallana-Gamage

…… Date:

Dr. K. Baskaran

ABSTRACT

Applicability of concrete filled steel tubes (CFST) for compression members in truss type steel light vehicular bridges is studied in this research as an economical solution for the lack of light vehicular bridges in Sri Lanka. There are many places in Sri Lanka where people have to travel long distance to cross rivers or access the nearby city for their day to day needs. CFST is a composite material which is getting more popular in the civil engineering industry. So, it is important to examine the properties of CFST as a composite material. The use of CFST in truss bridges has several advantages such as deflection reduction of the bridge, improved seismic performance, improved load carrying capacity, dynamic performance, and cost reduction. To achieve an economical structural performance, CFST section has to be designed properly. Optimum positions to use CFST have to be identified depending on the truss type. Replacing larger steel I sections with CFST will reduce the cost since the same amount of force can be carried out with less steel amount in CFST. Also, the tendency to local buckling is reduced when thinner sections are filled with concrete. Therefore, to achieve a higher span with a lesser cost (steel tonnage), usage of CFST sections for compression members have been accessed in this study. Also, the tendency to local buckling was examined with experimental and numerical simulations. Hence first, a desk study was carried out focusing Gin Ganga area to identify the problems in the area due to lack of bridges. Two experimental model bridges were tested in this study as one with only hollow aluminium tubes and other with cement grout filled in selected top chord members. Using a real scale numerical simulation of a CFST bridge model, practical applicability and cost figures were compared with a conventional steel truss bridge.

Keywords: truss type steel light vehicular bridges, concrete filled steel tubes, composite material, axial compression, finite element modelling

DEDICATION

To my loving parents, brothers and sisters for encouraging me throughout the milestones of my life and my supervisor, Dr. Hidallana-Gamage H. D. and co-supervisor Dr. Baskaran K. for the unwavering motivation and mentorship they provided.

ACKNOWLEDGEMENT

First and foremost, I would like to express my sincere gratitude towards my supervisor, Dr. Hidallana-Gamage H. D. for motivating me to explore the bridge engineering arena and supporting me to build up my research. His invaluable guidance to help me keep up with the timeline and produce results, while overcoming the hurdles is greatly acknowledged. I would also like to express my thanks to my co-supervisor, Dr. Baskaran K., for the enthusiasm and motivation he planted in me to pursue my research.

Next, I extend my sincere gratitude to Prof. M. T. R. Jayasinghe and Dr. (Mrs.) J. C. P. H. Gamage for their valuable comments, recommendations and suggestions given during the progress reviews which helped me to further improve my work. Then I would like to thank Dr. (Mrs.) M. T. P. Hettiarachchi and Dr. G. Tharmarajah for their valuable comments and recommendations given as members of the examination panel. I would also like to take this opportunity to express my sincere gratitude to all the academic staff of the Department of Civil Engineering, University of Moratuwa, for laying a strong technical foundation in my undergraduate studies.

I thank my fellow research assistants for the constructive discussions we had that supported me in using numerous approaches to overcome research questions, and I appreciate the support they have given for conducting the laboratory experiments. I would also like to thank the technical staff members in the Department of Civil Engineering, who supported me in building the experimental models. I am also grateful to all other academic and non-academic staff of the Department of Civil Engineering and my colleagues for their support during the research.

Finally, I would like to thank the Senate Research Grants Committee (SRC) for the financial assistance provided throughout this project.

CONTENTS

LIST OF FIGURES

LIST OF TABLES

LIST OF ABBREVIATIONS

Abbreviation	Description
CFST	Concrete Filled Steel Tubes
GI	Galvanised Iron
LB	Local Buckling
GB	Global Buckling
CF	Compression Failure
FEM	Finite Element Model
K_t	Tensile strength factor
N_{tu}	Tensile strength of tested CFST specimens
f_y	Yield strength of steel
A_s	Cross-sectional area of the steel tube
E_s	Elastic modulus of steel
E_c	Elastic modulus of concrete
A_s	Cross-sectional area of concrete
N_1	Applied axial force during corrosion stage
ρ_s	Ratio of reinforcement area to concrete area
δ	Steel contribution ratio
$N_{pl,Rd}$	Design plastic resistance
f'_{cc}	Maximum concrete stress
J	Second stress invariant of the stress deviator tensor
GFAT	Grout filled Aluminium Tubes

CHAPTER I

1. BACKGROUND

1.1. Introduction

Sri Lanka is a country which is rich with a lot of natural resources. One of the most valuable things in the country is having its natural beauty which has been comprised of beautiful forests, mountains, waterfalls and rivers etc. So, the people who reside closer to river valleys and catchment areas have to move across rivers. But the problem existing in developing countries such as Sri Lanka for decades is non availability of proper connectivity across the rivers. Perhaps, when considered the rural areas which are far away from the congested cities, the development of the infrastructure is rare. In Sri Lanka, there are many villages without proper connectivity beside a river such as Lankagama close to Neluwa which came to discussion in the country due to a bridge and a road project recently. The attention given by the local government to such areas is very less. Only a smaller number of foreign-funded projects was also directed in those areas to build bridges over the rivers.

Construction of a bridge at wherever required is a vital task. A bridge is an expensive engineering creature, engaging precise design considerations that try to optimise the resources, while minimising the cost, but ensuring the structural adequacy. Perhaps bridges have become one of the most vital necessity for travel as well as in logistics dating back to the ancient era. With time, the need for bridges to cross rivers and also valleys have been increased. The roman citizens who lived in roman era greatly mastered theory behind this, with architectural essences, which can be witnessed even today. Throughout the Europe, above fact can be well supported with the ruins of ancient as well as functioning bridges. Present, normally one person has to cross at least one bridge in daily basis just to reach their work place. When a discontinuity presents in a terrain, bridges come to the scenery as an important element of the transportation infrastructure, while costing extremely. Almost in every engineering venture, bridges need to be designed, constructed and also functioned as the safest they can be, while being economical. Hence, bridge design is of the utmost importance due its functionality. Compared to other creatures, truss bridges are largely

cost effective, since they yield a high strength to weight ratio. Furthermore, compression members can be more strengthened by infilling concrete into them and improve load bearing capacity as well as improve the resistance to different buckling effects. Concrete filled steel tubes (CFST) can be formed as a composite material to fulfil above criteria.

CFST is formulated with two major building materials: concrete and steel. CFST has become a popular composite construction material used in many countries for a wide variety of construction purposes. Compared to those of individual materials, the properties of CFST are far better and have greater advantages over individual materials. The likelihood of steel tubes to deform locally is greater in compression. Also, concrete alone does not perform in high ductile manner when considered separately and steel has a major drawback for fire resistance. Therefore, by combining both materials together, the weaknesses of both can be controlled. CFST has greater resistance to compression due to the confinement provided by steel core. CFST has greater resistance to local instability due to its greater rigidity. Fire resistance is also greater due to the increased fire performance inhabited with the concrete core. The steel tube behaves like a mould during the construction, which leads to a fast construction while reducing the cost. Henceforth, CFST can be developed and further investigated to achieve greater performance as a good quality construction material for the industry. Different types of research were carried out to determine the effects of various parameters on the compression behaviour and failure criteria of CFSTs in experimental programs.

The first CFST arch bridge was constructed in Soviet Union in 1930s. However, it has been later abandoned with the construction of two such bridge structures, due to an unforeseen failure to take advantage of its structure and construction. The CFST arch bridge is an excellent type of steel-reinforced concrete composite bridge, in which the local stability of a steel tube is improved by concrete infilling, while the toughness and confinement is improved by the external confinement of the steel tube. The mechanism, technology and construction methodology of CFST arch bridges have deeply examined by Chinese engineers and have conducted an extensive research in this area. Also, they have been promoting the

CFST bridges by building a huge number of CFST arch bridges in China since 20th century. This study is directed towards the applicability of CFST in the local context, and examining the potential of using the CFST in truss type light vehicular bridges to solve the existing scarcity of bridges in Sri Lanka.

1.2. Importance and Identification of Knowledge Gap

Even though CFST related structural techniques have been established a popularity globally, it is not much popular due to the novelty in the local context. It should be noted that only the Classes 1, 2 & 3 sections as specified in the Euro code 3 have been assessed in a comprehensive manner and no attention has been given to Class 4 sections which are prone to buckle locally. Moreover, in local context, no study has been carried out to assess the load carrying capacity of commercially available Galvanized Iron (GI) sections and also for slender (Class 4) GI sections.

Variable height truss type light vehicular bridges have been constructed in Sri Lanka in recent past. Lateral buckling of the unbraced top chord members close to the supports is a critical issue in those bridges, where bigger GI sections are required for those unbraced members. This will considerably increase their cost, and hence a more practical and feasible method is required to enhance the lateral stability of variable height bridges. This research will investigate the applicability of CFST in that context which has not been studied in detail to date. Due to the practical constrains in terms of construction, the use of CFST should be experimentally verified where as a comprehensive numerical model are required to predict their behaviour.

Truss members which are prone to fail due to lateral buckling resulting a lower overall capacity for the bridge, have never been experimentally tested in terms of an experimental truss bridge model. A comprehensive experimental program has to be carried out to investigate the strength enhancement with CFST as individual members and also as a complete truss. Finally, steel truss type light vehicular bridges should be designed by incorporating CFST for selected compression members, and their structural performance and the economic feasibility have to be determined before introducing the proposed technique to the construction industry.

1.3. Aim and Objectives of the Research

The aim of this research is to investigate the applicability of CFST for compression members in truss type steel light vehicular bridges. This research utilized an experimental testing and numerical simulations of steel hollow sections, CFST and application of those in truss bridge models. The aim of this research was achieved by undertaking following objectives.

1. Investigate the effects of different geometrical parameters such as width and height of a truss for the performance and economy of different truss type light vehicular bridges.
2. Investigate the behaviour of the hollow and concrete infilled GI sections under uniaxial compression, compare the failure modes and loads with those obtained from the theoretical calculations and numerical simulations.
3. Conduct a scaled down testing of bridge models to investigate the strength enhancement of bridges when infilled sections are used for the unbraced members in variable height bridges
4. Design steel truss type light vehicular bridges in cooperating CFST for selected compression members, and investigate their performance and economic feasibility

1.4. Methodology

This research has investigated the applicability of CFST as compression members in steel truss type light vehicular bridges. First a thorough literature survey was done to examine economical truss types for various spans. Henceforth, the selected truss types were used for further studies, where a preliminary numerical analysis was carried out using the SAP2000 finite element (FE) software to investigate the effects of geometrical parameters such as width and height of a truss for the structural performance and economy of a truss bridge. At the same time, a desk study comprising with field survey was done to identify the needs of bridges in rural areas and to assess the condition of the existing bridges.

The experimental program was conducted in two phases. In Phase 1, the effects concrete infilling into steel sections were examined by conducting uni-axial

compression tests for commercially available GI hollow and CFST sections with different lengths and thicknesses. Experimental results for failure loads and modes were compared with those obtained from the theoretical calculations and also numerical analysis using the ABAQUS FE software. In Phase 2, Uni-axial compression tests were conducted for Aluminium hollow and grout filled Aluminium tubes (GFAT) having different lengths. Then these GFAT were used for the unbraced top chord members (subjecting to compression) in scaled down model bridges with variable height to investigate their strength enhancement. The failure modes and the failure loads of the model bridges were compared with those obtained from the numerical analysis.

Finally, the applicability CFST in steel truss type light vehicular bridges was examined by considering a 50 m span bridge. Modified Warren, Pratt and Parker (variable height truss) truss type light vehicular bridges were analysed incorporating CFST members into appropriate positions. MIDAS CIVIL FE software was used in this exercise as it facilitates the analysis and design of bridges as per the relevant design codes incorporating composite sections. Structural performance and economic feasibility of these truss types with proposed modifications were compared to see the advancements which can be gained by introducing CFST for the selected compression members.

1.5. Significance of the research

This research has investigated the applicability of CFST as compression members in steel truss type light vehicular bridges. The extensive testing program conducted in this research, and detailed information presented by comparing the experimental results with those predicted from theoretical calculations and numerical analysis, will give a better idea about the behaviour of CFST under uni-axial compression loading depending on their strength class. The testing of scaled down model bridges illustrates the failure loads, failure modes and the critical members in a variable height truss such as Parker which will be useful to design engineers. This research has shown that the structural performance of a Parker truss can be improved, while minimising the cost when CFST sections are incorporated into the top chord members. The outcomes of this research will therefore enable design engineers to

come up with an economical truss type having optimum sections for a given span. This will considerably reduce the total project cost of a light vehicular bridge by encouraging government authorities such as RDA and PRDA to propose light vehicular bridges in many locations in Sri Lanka.

1.6. Outline of the Thesis

Chapter 1: Background of the study, an introduction to the CFST construction techniques, discussion on the knowledge gap, aim and objectives of the study, research methodology, significance of the research

Chapter 2: Review of previous work found in literature by giving an introduction to trusses bridges, CFST techniques and finite element (FE) modelling of CFST.

Chapter 3: Desk study about the existing problems around the country due to lack of bridges and practical applicability of CFSTs in Sri Lanka

Chapter 4: Experimental Program Phase 1 – Uni-axial compression testing of GI hollow and CFST.

Chapter 5: Experimental Program Phase 2 – Uni-axial compression testing of Aluminium hollow and Grout Filled Aluminium Tubes (GFAT), Testing of model bridges

Chapter 6: Numerical modelling of the behaviour of GI hollow and CFST using the ABAQUS CAE finite element software

Chapter 7: Application of CFST in truss type light vehicular bridges, Analysis of bridges using MIDAS software, Feasibility study

Chapter 8: Conclusions, Recommendation for future research

CHAPTER II

2. REVIEW OF PREVIOUS LITERATURE

2.1. Background

Concrete filled steel tubes (CFST) are being used in various applications of civil engineering for a long time all over the world. Advantages which it possesses as a composite material, compared to two individual materials is the main reason to use CFST in constructions.

First technical paper about the CFST was written in 1961 in Japan. Since it is a composite material it has more advantages than the individual material. Specially CFST is more effective when it is subjected to compression. CFST has higher compressive strength due to the confinement effect. CFST has a higher stiffness. Therefore, it is more resistible to local buckling. Concrete core inside the steel tube, provides a proper fire resistance to the material. CFST has high strength-to-weight ratio which makes it a more suitable construction material for bridges. Han, Wei and Reidar (2014) mentioned that ductility of the CFST is highly enhanced, compared with steel and concrete as discrete materials.

Concrete filled steel tubes are made up with various shapes characterising based on the confining steel tube's shape, such as square, rectangular, circular, elliptical, as shown in Figure 2.1. Square and circular CFST sections are the mostly used sections in construction of bridge structures. The shape and size of CFST tube cross section, diameter to thickness and width-to-thickness ratios of the steel tube determines the load carrying capacity of a CFST column. Circular and square CFST have more compression capacity than other shapes.

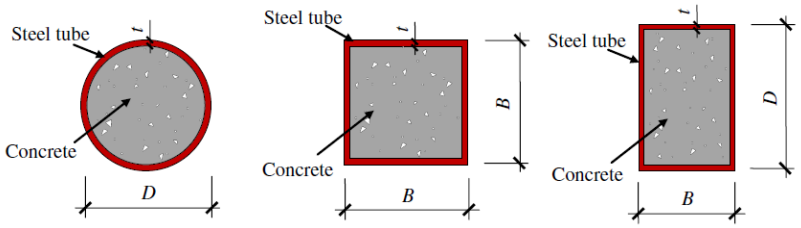

Figure 2.1: CFSTs with different shapes (Han et al., 2014)

Han et. al (2014) compared the compression capacity of several materials as shown in Figure 2-2. According to those details, compression capacity of the CFST is almost twice as a normal reinforced concrete column.

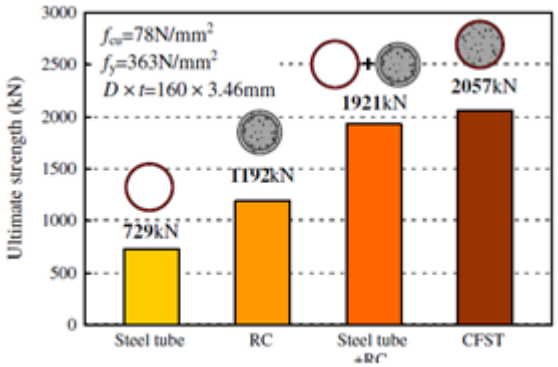

Figure 2.2: Comparison of compression capacity among materials (Han et al., 2014)

When CFST is being used, there is no need of formwork. Steel tube itself behaves as the formwork. It helps to carryout rapid construction and reduce the cost.

2.2. Concrete filled steel tubes

Performance of the CFST depends on many parameters. Geometry of the section, Properties of concrete and steel are some parameters which affect the behaviour of CFST.

There are a few types of sections in CFST; square, circular, rectangular and hexagonal. Circular section provides the most effective confinement effect. Therefore, it has higher compressive strength. Also, circular section is less likely to buckle when compared to other sections. But mostly square and rectangular sections are used for the construction, because it is easy to connect those sections by using bolts.

Since CFST is a composite material, it has characteristics of both concrete and steel, and also a unique behaviour when compared to concrete or steel. Many researches have been carried out to identify the behaviour of the CFST under different stress conditions and other parameters which affect the performance of CFST. Information which are relevant to this research, were gathered from previous researches and books and those are presented in this chapter.

2.2.1. Behaviour of CFST under different stress conditions

Mainly a few types of stress conditions were considered in this research. Generally, truss bridges are subjected to axial forces. Therefore, axial tension and axial compression are mainly considered. Chloride corrosion of CFST directly affects the behaviour and durability of the material. Therefore, chloride corrosion is also considered in the literature review.

[1] Behaviour of CFST subjected to axial compression

CFSTs are especially effective as compression members. Since there is steel tube outside of the concrete core it creates a good confinement effect. This confinement effect helps to increase the compressive strength of the CFST.

Hu et al. (2003) investigated the confined effect of CFST using 24 circular, square shaped specimens, while varying the D/t (diameter/ steel tube thickness) ratio in the range of 17 to 150. Maximum confined effect was observed in circular shape CFSTs with D/t less than 40. Results showed that circular steel tubes create three-dimensional confinement in a concrete core.

O'Shea & Bridge (2000) studied the effect of loading condition on the strength of the CFST. Three types of loading conditions; axial loading of concrete, axial loading of steel & simultaneous loading of both concrete and steel were tested. Considering the results, it was found that the strength of the CFST depends on the loading condition. Highest confinement effect occurred when only concrete was loaded.

Gupta et al. (2007) investigated the effect of the D/t ratio (diameter/ steel tube thickness ratio), concrete grade and volume of the fly ash in concrete on the load carrying capacity of circular CFST. From the result observed by testing 81 specimens including 9 hollow steel tubes, they came up with three main conclusions.

1. CFST essentially fails by local buckling when subjected to axial loading

2. Confinement effect decreases with the increase of the concrete strength

3. When the D/t ratio is smaller, the confinement effect is better

Burak, Kivanc and Tuncan (2014) investigated the behaviour of CFST under axial compression. The effect of width/thickness ratio, compressive strength of the concrete and geometrical shape of the cross section on the ultimate load, axial stress, ductility and the buckling behaviour were investigated in their study. Burak et al (2014) calculated ductility values as the ratio between maximum deformation at the ultimate load point and also the deformation values at elastic limit. All the CFST specimens had higher ductility values than steel hollow tubes and circular type CFST had maximum ductility behaviour. Result proved that rounded specimens have higher ductility than the angular shaped specimens.

Also, from their study Burak et al (2014) concluded, that concrete core inward buckling of the steel tube and steel tube provides a confinement effect for CFST which were axially loaded at the same time. Axial compressive strength values of CFST were compared with the unconfined compressive strength values of the core concrete. Maximum increment ratio of 167.8% was observed in circular CFST. Increasing the steel tube thickness and reducing compressive strength of the concrete were identified as the reasons for above increment.

[2] Behaviour of CFST subjected to axial tension

Relatively limited research has been carried out to identify the behaviour of CFST under axial tension. According to existing design codes; AISC 2005, CEN 2004 tension capacity of the composite section is taken as the yield strength of its steel section. However, Han et al. (2011) showed that tensile strength of a circular shaped CFST is 9-13.5% higher than the hollow circular tube, depending on different steel ratios. Experimental results collected by Pan and Zhong (1990) showed that concrete fill increase the tensile strength of the CFST approximately by 10%. In 2016, using test results of Pan and Zhong (1990) and Han et al. (2011), Meng et al. (2016) conducted a research and concluded that the tensile strength of a circular type CFST is approximately 10.2% higher than that of a circular hollow tube and the effective

stiffness of circular type CFST is approximately 28.7% higher than a steel circular hollow tube.

Han et al. (2011) studied the performance of CFST under axial tension by varying many parameters. He carried out a FEM analysis and an experimental model analysis. In their research, there were three testing parameters.

1.Steel ratio. α (α = Cross sectional area of steel/ Cross sectional area of concrete)

2.Type of concrete fill (self-consolidating concrete or fibre reinforced concrete)

3.Bonded/ unbonded between steel and concrete

Final result obtained from the tests are shown in figure 2.3. For the convenience of the analysis K_t is defined as below.

$$K_t = \frac{Ntu}{fyAs} \quad (1)$$

Where;

K_t − Tensile strength factor

N_{tu} − Tensile force of tested CFST specimens

f_y − Yield strength of steel

A_s − Cross-sectional area of the steel tube.

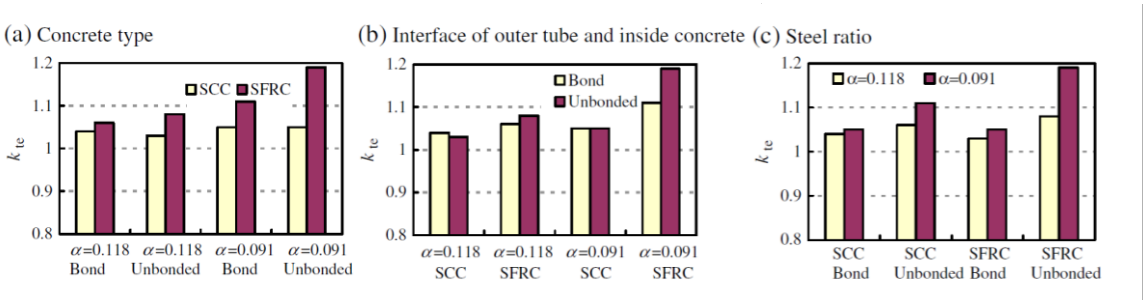

Figure 2.3: Comparison of results (Han et al.,2011)

Using above result Han et al. (2011) concluded that,

 Tensile strength of the CFST with SCC concrete fill has higher values than CFST with normal concrete. He mentioned the reason for this behaviour is SFRC concrete has higher post-cracking strength compared to normal concrete.

 When considering the bond between concrete and steel, Han et al (2011) mentioned that in practical engineering it is not an important factor that affects the tensile capacity.

 As seen in the graph, K_t decreases when α is increases. It means tensile strength increases with the increase of the cross-sectional area of steel.

Some simple equations were derived in this research.

$$(EA)_t = E_s A_s + 0.1 E_c A_c \tag{2}$$

$(EA)_t$ = Elastic tensile stiffness of CFST member, as shown in Figure 2.4(a);

Es = Elastic modulus of steel

E_c = Elastic modulus of concrete

A_s = Cross-sectional area of steel tube

A_c = Cross-sectional area of concrete

The elastic tensile stiffness $(EA)_t$ determined is somewhat higher than that of the corresponding hollow steel tube.

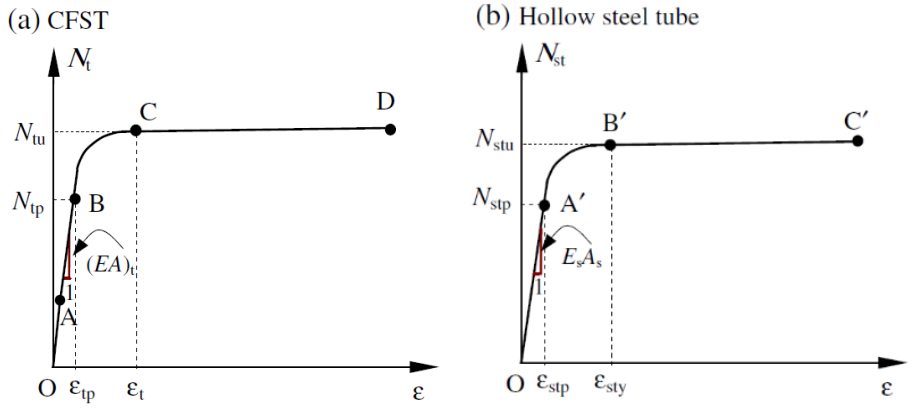

Figure 2.4: (a) & (b) - Typical $N_{t-\varepsilon}$ curves (stress strain curve)

$$N_{tu}=(1.1-0.4\alpha)f_y A_s \quad (3)$$

Where;

N_{tu} – Tensile strength

f_y − Yield strength of steel

The validity limits of the equation are α = 0.04–0.2, f_y = 235–420 MPa, and f_{cu} = 30–80 MPa.

2.2.2. Effect of corrosion on CFST

Corrosion is an important factor which affects the durability of CFST. Since the outer steel is subjected to different exposure conditions, there is a risk of corrosion. Specially in offshore areas, chloride corrosion effect can be crucial. Therefore, it is important to identify the effect of corrosion and the possible measures to reduce it for sustainable design.

Corrosion of the CFST is different from the normal steel tube since the presence of composite effect of two materials. Han et al. (2011) studied the square type CFST stub column behaviour under corrosion environment, which was simulated with electrolytic solution. Test results showed that corrosion has noticeably reduced the strength of the CFST. Loading ratio under different corrosion conditions were investigated during the experiment. Loading ratio, n was defined as below.

$$\mathrm{n} = \frac{N_1}{N_u} \quad (4)$$

Where;

N_u – Ultimate strength of the specimen under short-term loading without corrosion

N_1− Applied axial force during corrosion stage

Three types of corrosion conditions were selected.

1. Fully-immersed
2. Half-immersed
3. No-corrosion

By analysing the test results, following findings were concluded.

1. Increase of the corrosion extent reduction the ultimate strength and ductility of CFST. With higher corrosion extent, higher strength decrease will be yielded.

2. Inward and outward buckling was observed in steel tube while CFST showed outward buckling. Support effect of the core concrete resist the local buckling of CFST under long-term loading and also corrosion environment.

When the degree of corrosion is larger, local buckling of the CFST is also larger.

When compared to square CFST columns, circular CFST provides more effective support to outer steel tube. Therefore, local buckling of circular CFST column is less than square shaped CFST column under corrosion.

3. The graph below shows the relative strength of corroded specimen to short-term loading specimen.

N_{ue} is the ultimate strength of the specimen under long-term corrosion

N_{ue0} is the ultimate strength of the column under no corrosion

According to Figure 2.5, effect of the corrosion on steel hollow tubes is much higher than on CFST stub columns. In steel tubes, ultimate strength solely depends on the steel thickness. Loss of the steel thickness due to corrosion creates a major impact on its ultimate strength due to the lack of inner concrete support in steel tubes.

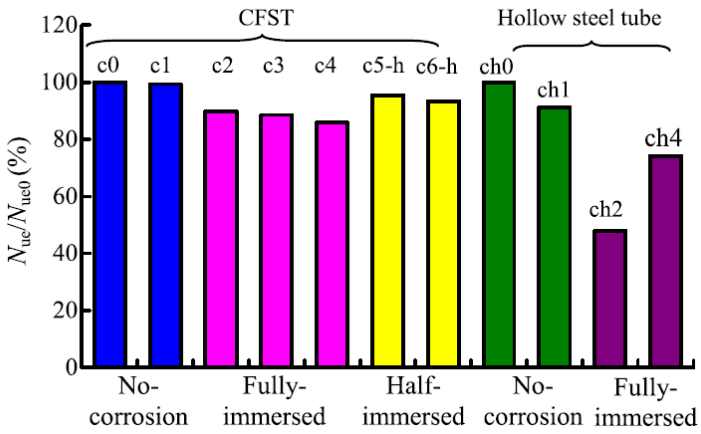

Figure 2.5: Relative strength of corroded specimen Han et al. (2011)

Kayser and Nowak (1989) described 5 types of corrosion in steel tubes; general, pitting, crevice, galvanic and stress corrosion. Most common one is the general corrosion which is defined as the section loss of steel tubing.

2.2.3. Constructability

Han et al (2011) investigated the composite action between concrete and steel. Since most of the research have been carried out on reduced scale, practicing engineers are concern about the composite behaviour of concrete and steel. Field experiment was carried out and two circular type CFST columns were casted using self-consolidating concrete as shown in Figure 2.6. Columns were cut after test. It showed that concrete is well compacted. Maximum gap between concrete and steel was 0.1mm. Test results showed that the longitudinal shrinkage is larger than the shrinkage in transverse direction.

(a) (b)

Figure 2.6: Casting of a column on site and a cross-section of CFST

2.3. Truss Bridges

2.3.1. Introduction

Truss is a special type of structure where individual straight members are connected at joints. It is assumed that members are allowed to rotate at joints. Therefore, members are subjected to axial force only. Often in construction, joints do not allow free rotation, which makes the assumption of the truss structure is an approximate.

For truss bridges main mechanism for load distribution is the truss. Top chord is under compression and the bottom chord is under tension. Depending on the type of the truss, axial force can be different in other members.

Truss bridges are very versatile, due to the large number of possibilities in shape. There are many types of truss bridges as shown in Figure 2.7. Depending on the application, a suitable truss type can be selected. Truss bridges have the ability to withstand very high concentrated loads. Therefore, truss bridges are often used for heavy railway traffic.

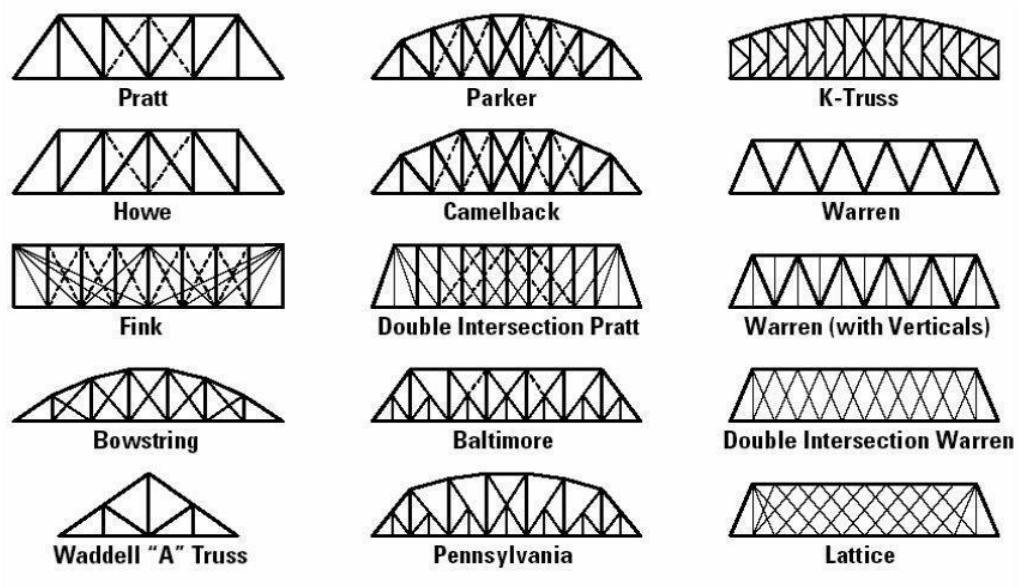

Figure 2.7: Different truss types used for the bridges (Miss, n.d.)

Pratt, Howe, Warren, Camelback are the most common types used in the bridges. Truss bridges can be categorized depending on the position of the deck as shown in Figure 2.8. In a through truss bridge, deck is positioned at the bottom chord and the trusses on the either side are connected by cross-bracings. This is the most common truss type in Sri Lanka. In semi through type trusses deck is located at the intermediate level and in deck type trusses it is positioned below the deck.

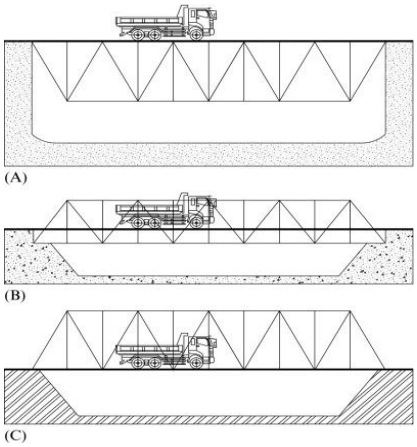

Figure 2.8: Truss types according to deck location. (A) Deck truss. (B) Half-through truss. (C) Through truss (Weiwei L., 2017)

2.3.2. Truss bridges in Sri Lanka

In Sri Lanka, there are many truss type steel bridges. Most of the railway bridges are truss bridges. Steel is used as the construction material for most truss bridges. In terms of the classification, several types of truss bridges can be seen in Sri Lanka. Pratt and Warren are the most common types which can be seen in Sri Lanka. There are very few bridges with spans over 100m in Sri Lanka. Most of the bridges have spans less than 100 m. This is one major difference between other countries and Sri Lanka. Some truss bridges which can be seen in Sri Lanka are shown in Figure 2.9.

Figure 2.9: Different truss bridges in Sri Lanka

2.3.3. Force distribution in truss bridges

Usually, truss is designed to maximize the loading per unit weight of material. Truss bridge can be considered as an optimized beam. As seen in the Figure 2.10, beam mass is removed in a way that it will not reduce the mechanical properties. In this way efficient trusses can be fabricated. Top flange is under compression and bottom flange is under tension. Usually in truss bridges, members in mid span are subjected to high tensile and compressive forces.

Tension members are lighter and efficient than compression members in the trusses. It is because most materials have higher tensile strength capacity than compressive capacity. But depending on the situation tension trusses might not be the best solution.

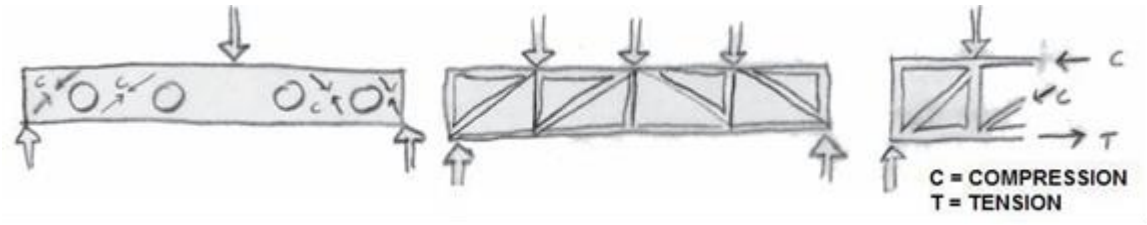

Figure 2.10: Force distribution of a truss bridge

2.4. CFST in truss bridges

Karunarathna et. al, (2015) mentioned that, since CFST has higher compressive capacity and ductility, CFST are mostly suitable for the applications in bridges where members are subjected to compressive forces and bending. The aim of the study was to investigate the benefits of square type CFST members in railway steel truss bridges susceptible to earthquake loads. In this study CFST only used in the end-rakers of the bridge. End raker is the diagonal member of main truss which creates the end frame of the bridge.

Karunarathna et al. (2015) found that vertical displacement under static loads were significantly reduced when CFST is used in end-rakers. Therefore, they suggested that CFST would be a solution for controlling the displacements in railway truss bridges. Also, when CFST was used, maximum steel stress occurred in the end-

raker was decreased. Therefore, it is clear that CFST can be used to improve the seismic performance of truss bridges.

Although steel stress is reduced, when higher grade concrete is used, concrete stresses were high. Karunarathna et al. (2015) mentioned that further studies are required to identify the maximum and minimum concrete grades to be used in CFST economically.

Fong et. al, (2011) compared the behaviour of bare steel and the CFST as an individual column and as a member of a truss. Figure 2.11 shows the specimens which were tested underpinned and fixed end conditions.

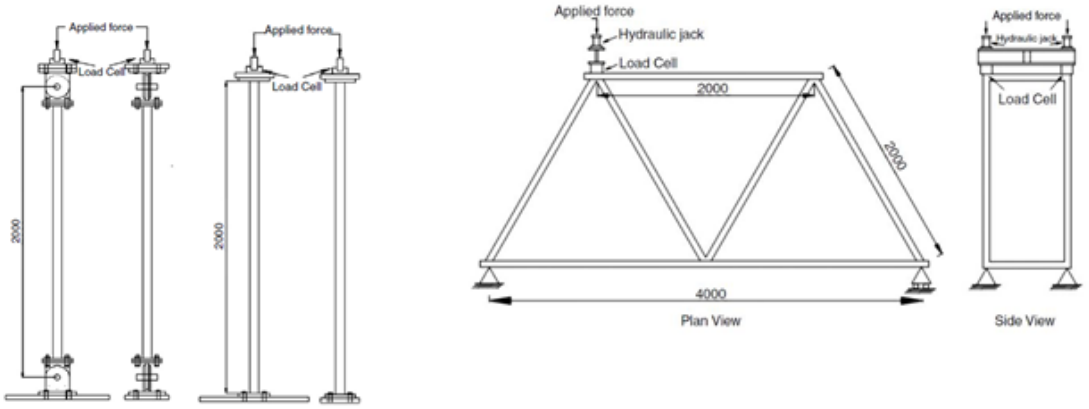

Figure 2.11: Side view and end condition details of the truss (Fong et. al, 2011)

In the truss, members were allowed to rotate at ends, but it was partly restrained by other members. Therefore, the end conditions of the members in the truss was assumed to be in between pinned and fixed. Result obtained from the test is shown below.

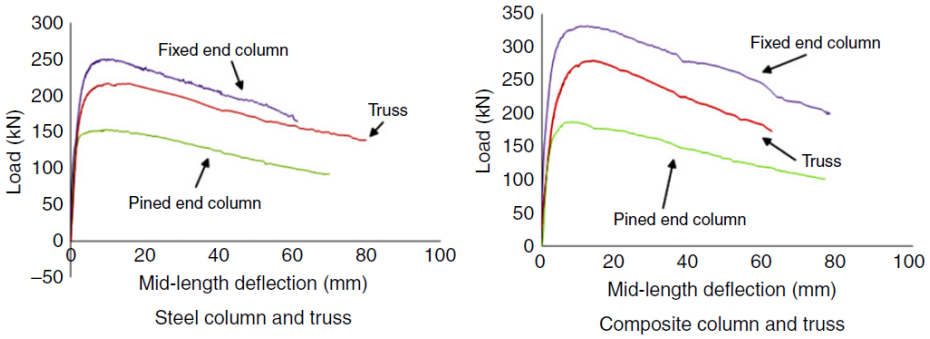

Figure 2.12: Load vs. deflection curve (Fong et. al, 2011)

Column with fixed end conditions had a higher load capacity than the column with the pinned end conditions. Observing Figure 2.12, it is clear that truss bridge with CSFT can withstand higher load without failure than a steel truss.

For the analysis of this test two methods were used.

1. Using design codes (EC3, EC4, CoPHK, AISC LRFD, AS5100)
2. Second order method – nonlinear analysis

According to design codes, there are correction factors for length depending on end conditions. When compared with test results, pinned end calculations according to the design codes are under-estimated which led to expensive design while fixed end calculations according to the design codes are over-estimated. This study showed that main disadvantage of using the method of effective length is that the idealized end conditions do not exist in practice and results are inaccurate.

2.4.1. World practice

Many countries in the world currently use this technology for different types of bridges. Figure 2.13 shows CFST bridges in China. CFST can be used as piers, bridge towers, arches and also in bridge decks. Specially in china, many research have been carried out relevant to CFST. In China many bridges were constructed using CFST. There are special characteristics of CFST which makes it a better construction material for bridges.

1. Higher compression capacity and ductility
2. Excellent seismic resistance
3. Higher strength-to-weight ratio
4. Easy to perform the erection of the truss

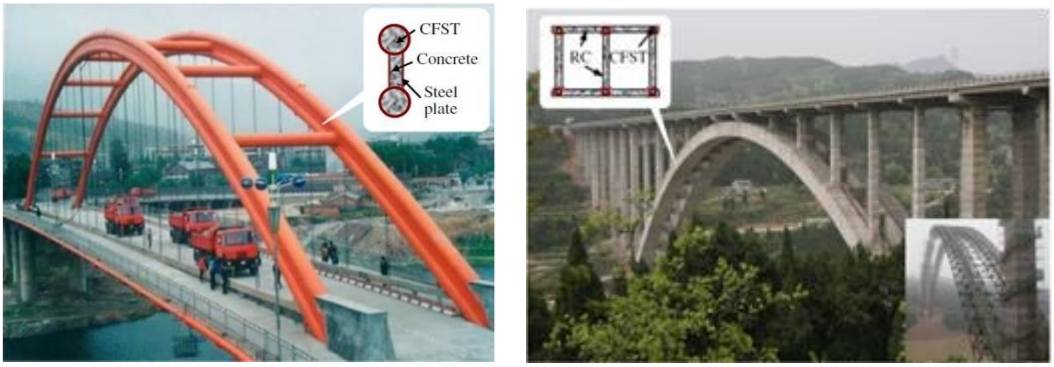

Figure 2.13: Arch bridges constructed in China

But currently CFST in truss bridges is not much common due to lack of research carried out on topic in local context.

2.4.2. Sri Lankan practice

A few research has been carried out relevant to CFST in Sri Lanka. Due to the lack of experiments and exposure to this technique, currently CFST is not used in Sri Lanka for bridge construction.

2.5. Theoretical analysis of steel tubes for compression

2.5.1. Hollow steel tubes

Hollow steel tube failure in compression can be categorised into 3 main criteria.

Local failure: Thin-walled hollow steel tubes can fail in local buckling prior to achieve the full strength of the whole section. For an example, an individual element in the section (one of the walls) can fail before achieving the capacity of the whole section. EC 3 checks for local buckling as described in section 4.4.2, as if $c/t > 42\sqrt{\frac{235}{f_y}}$ (c = square section size, t = thickness of the section, f_y = yield strength of steel) sections are classified as class4 and hence prone to buckle locally.

Compressive failure: When whole section is compressed under axial load without showing major deformations, it is classified as compressive failure of steel section. Sections having non slender dimensions are failed in this mode. When L/r ration (L= length of the member, r= radius of gyration) of the section is lesser compared to the

critical L/r value, sections are prone to fail in compression. Compression capacity of the section is given by the following equation.

$$Nc = A_s f_y \tag{5}$$

Where, N_c = compression capacity, A_s = area of steel, f_y = yield strength of steel

Euler Buckling*:* Sections categorised in to slender sections are failed demonstrating global buckling mode. When L/r is exceeded the critical L/r value sections are prone to fail in global buckling failure mode. The global buckling failure load of structural members can be calculated using the Euler's formulae.

$$N_b = \frac{n\prod^2 EI}{L^2} \tag{6}$$

Where, N_b = Euler buckling load, n = factor accounting for the end conditions (n=1 for both ends pin condition), E = modulus of elasticity, L = length of column, I = Second moment of area

2.5.2. CFST sections

Similarly, there are three types of failure modes that can be identified for CFST sections.

Local failure: According to EC4 all CFST sections have to check for the condition for local buckling. Condition of the local buckling is used to determine minimum wall thickness. Local buckling effect has been omitted in EN 1994-1-1 by limiting the section slenderness ratio D/t to 90(235/f_y) for circular sections and B/t to $52\sqrt{235/f_y}$ for rectangular sections with B, D and t being the diameter, depth and thickness of hollow steel sections, respectively, and f_y being the yield strength of steel.

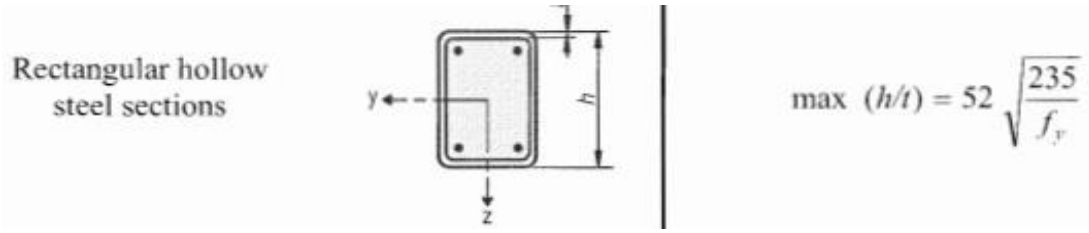

Figure 2.14: Rectangular and square sections design details (EN 1994-1-1)

Compressive failure: For non-slender CFST sections, compression capacity can be determined using the sectional capacity of the whole section. Capacity of the section is given by the following equation as stated in the Section 6.7.3.2 of EC4.

$$N = A_s f_y + A_c f_c \quad (7)$$

Where, A_s = area of steel, f_y = yield strength of steel, A_c = area of concrete, f_c = compressive strength of concrete.

Buckling failure: Slender CFST sections fail in global buckling, which can be determined using the Euler formulae as given in Equation 6. However, flexural effective stiffness of the composite section $(EI)_{eff}$ should be used in the Euler's formula, which should be calculated using the following equation, which has been used in previous research (Kuranovas et. al., 2009)

$$(EI)_{eff} = E_a I_a + 0.8 E_{cd} I_c \quad (8)$$

Where, E_a = Modulus of Elasticity of steel, I_a = Second moment of area of structural steel section, I_c = second moment of area of un-cracked concrete section.

Here, $E_{cd} = E_{cm}/\gamma_c$

Where, E_{cm} = Secant modulus of the concrete, $\gamma_c = 1.35$ (which is used to determine the effective stiffness of concrete according to EC2)

A similar procedure has been given in the Section 6.7.3.3 of the EC4 to calculate the effective flexural stiffness of CFST.

2.6. Finite element modelling

2.6.1. Introduction

Finite element modelling has been used in many of the previous researches to analyse the behaviour of CFST. When experimental modelling is costly or not possible, especially when there are large structures to analyse, Finite Element Analysis (FEA) is the easiest method to analyse.

In most of the studies FEA results were compared and verified with the experimental result and extended to check various parameters which are not possible to evaluate experimentally. To perform FEA mainly ANSYS and ABAQUS software

have been used in previous research to perform extensive analysis such as nonlinear buckling analysis etc.

Accuracy of the FEA results is directly depending on the input parameters. Especially material properties and the interface between steel and concrete have to be correctly defined. Therefore, it is important to identify parameters which have been used for previous research and its variation with experimental result to identify most suitable method for FEM.

There are 4 main considerations of analysis.

1. Material properties
    a. Concrete
    b. Steel
2. Element mesh
3. Boundary conditions
4. Steel-concrete interface

Several research which include details about FEM of CFST, were studied during the literature review.

2.6.2. Mander, Priesley and Park (1988)

A stress-strain model for concrete subjected to uniaxial compressive loading and confined by any kind of general type of confining steel (either spiral or circular hoops) was developed by Mander et al (1988).

As stated in this research, previous researchers found that the strength and the corresponding longitudinal strain of the strength of concrete confined through an active hydrostatic fluid pressure can be determined using below equations:

$$f^{l}{}_{cc} = f^{l}{}_{c} + k_1 f^{l} \quad (9)$$

$$\varepsilon^{l}cc = \varepsilon^{l}c(1 + k_2 f^{l}\, f^{l}{}_{c}) \quad (10)$$

Where;

$f'cc$ − Maximum concrete stress

(uniaxial compressive strength when concrete subjected to confining pressure)

$\varepsilon'cc$ − Corresponding strain when concrete is subjected to confining pressure

f^l − Lateral confining pressure from the steel tube

$$f_l = \frac{2\sigma\theta\ t}{D} \tag{11}$$

$$\sigma_\theta = 0.1 f_y \tag{12}$$

Based on studies of Richart et al. (1928), $k1$ = 4.1 & $k2$ = 20.5. Also, Balmer (1949) found from his experiments that $k1$varies between 4.5 and 7, where higher value occurs at lower lateral pressures.

2.6.3. Hu at el. (2007).

Hu et al. (2007) studied the nonlinear behaviour of axially loaded CFST having the confinement effect.

Material properties- concrete

For FEM of the study Poisson's ratio was taken as 0.2 under uniaxial compression. Stress-strain model shown in Figure 2.15 was used for the analysis.

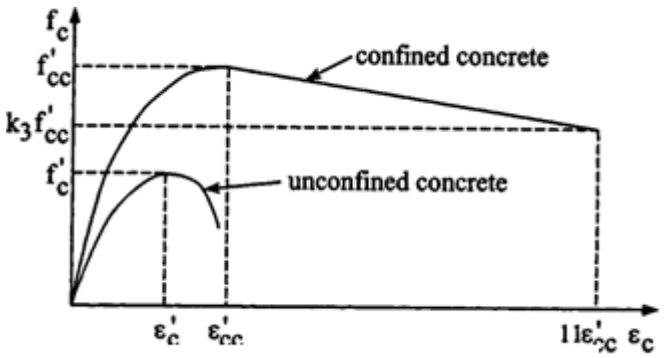

Figure 2.15 Stress-strain curve

$f'c$ =Axial compressive strength

ε'_c = Corresponding strain at $f'c$

$f'c$c = Unconfined concrete strength

ε'_{cc} = Corresponding strain at $f'c$

Compressive strength, $f'c$= unconfined concrete strength which was suggested by ACI committee 318 (1999)

$$\varepsilon'_{cc}=0.003 \tag{13}$$

ε'_c is taken as 0.003 which was suggested by ACI committee 318 (1999).

For confined concrete Hu et al. (2007) used following equations, derived by Mander, Priesley and Park (1988).

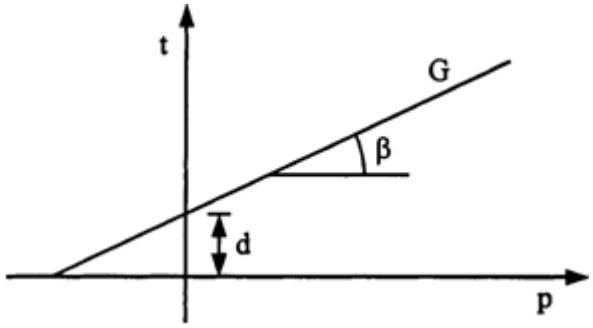

Figure 2.16 Drucker-Prager yield criterion

Because concrete is subjected to tri-axial compressive stresses, Hu et al (2011) mentioned, the failure of the concrete is determined by the compressive failure surface expanding in line with incremental hydrostatic pressure. Therefore, linear Drucker-Prager yield criterion (Figure 2.16) is followed to determine the yield surface of the concrete.

$$G = t - p\tan\beta - d \tag{14}$$

Where,

$$p = \frac{-(\sigma_1+\sigma_2+\sigma_3)}{3} \tag{15}$$

$$d = (1-\frac{\tan\beta}{3})\, f'cc \tag{16}$$

$$t= \frac{\sqrt{3}J2}{2}[1+\frac{1}{K}-(1-\frac{1}{K})(\frac{r}{\sqrt{3}J2})^3] \tag{17}$$

$$r=[\frac{9}{2}(S_1{}^3+S_2{}^3+S_3{}^3)]^{1/3} \tag{18}$$

σ_1, σ_2, σ_3– Principal stresses

S_1, S_2, S_3− Principal stress deviators

K = 0.8 & β=20° (Wu, 2000)

Initial modulus of elasticity is thoroughly correlated to its compressive strength. It was calculated by following empirical equation. (ACI, 1999)

Ec=4700$\sqrt{f/cc}$ MPa

When $\varepsilon c \leq \varepsilon cc$ uni axial stress-strain curve can be presented as below.

$$f_c = (E_c\, \varepsilon_{cc})/(1+(R+R_E-2)(\frac{\varepsilon c}{\varepsilon/cc})-(2R-1)(\frac{\varepsilon c}{\varepsilon/cc})^2+ R(\frac{\varepsilon c}{\varepsilon/cc})^3) \quad (19)$$

Where, $R = \frac{RE(R\sigma-1)}{(R\varepsilon-1)2}-\frac{1}{R\varepsilon}$ and $R_E = \frac{Ec\varepsilon/cc}{f/cc}$

R_σ=4, R_ε=4 values were used by Hu and Schnobrich (1989).

When $\varepsilon c > \varepsilon/cc$ linear descending line was used to analyse the behaviour of concrete. $K3$ was defined as the material degrading parameter. Descending line was assumed to be terminated at the point where $fc=k_3 f/cc$ and $\varepsilon c=11\varepsilon/cc$.

f_c, k_3 values are needed to complete the uniaxial stress-strain relationship. Generally, f_c, k_3 values depend on (D/t) ratio, cross section shape and the stiffening mean. Appropriate values are determined by the numerical result with experimental result by a trial and error method.

From the result of the numerical simulation Hu et al (2011) suggested following equations.

k_3=1 ; ($21.7 \leq D/t \leq 40$)

k_3=0.0000339$(D/t)2$−0.010085(D/t)+1.3491 ; ($40 \leq D/t \leq 150$)

Material properties-Steel

For the steel tube Poisson's ratio and modulus of elasticity were assumed as υ_s=0.3 and E_s=200 GPa respectively. Von Mises yield criterion F was used to define the elastic limit.

$$F=\sqrt{3}J_2=\frac{1}{\sqrt{2}}\sqrt{(\sigma_1-\sigma_2)^2+(\sigma_2-\sigma_3)^2+(\sigma_3-\sigma_1)^2}=\sigma_y \quad (20)$$

Where,

J = second stress invariant of the stress deviator tensor

σ_1, σ_2, σ_3 = principal stresses

Response of the steel tube was modelled by elastic-perfectly plastic theory with the associate of flow rule. Behaviour of the steel was considered as linear, when stress points come inside the yield surface. When the stresses reach the yield surface, the behaviour of the steel tube considered as perfectly plastic.

Element mesh

Hu et al. (2011) only analysed one eighth part of CFST, due to the symmetry (Figure 2.17).

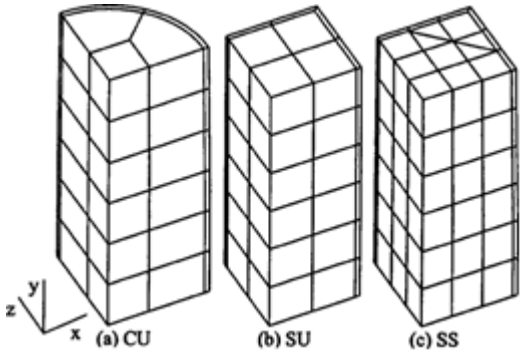

Figure 2.17 Finite element model and mesh details (Hu et al., 2011)

In the finite element mesh, both the concrete core and the steel tube were modelled by 27-node solid elements as demonstrated in Figure 2.17 (a), (b) and (c) (3 degree of freedom per each node).

A study was carried out to identify the convergence of the mesh, using various element sizes for both circular and square CFST (Wu, 2000). It showed that results of the circular columns with 30 (5x6) elements (Figure 2 – 17(a)) are almost similar to those 192 elements. Since Hu et al. (2011) concluded the mesh refinement has less impact on the numerical result, coarse mesh shown in Figure 2 – 17 (b) was used for the analysis.

Boundary conditions

Symmetric boundary conditions were adopted for the symmetric planes. Top surface of the column is allowed to displace only in y direction.

Concrete-steel interface

Special nine-node interface element was used to model the interaction between the concrete and steel. The interface conditions that require matching meshes on the two body's surfaces were used to combine the nodes of concrete and steel tube. The elements can model infinitesimal sliding and friction (Hibbitt et. al., 2000) between the concrete surface and the steel tube. Friction coefficient was taken as 0.25. Separation between the contact surface of steel and concrete was allowed through interface elements, but penetration of each other was not allowed.

Results obtained from the FEM were compared with the experimental results. Figure 2.18 shows that FEM results have good agreement with the experimental results.

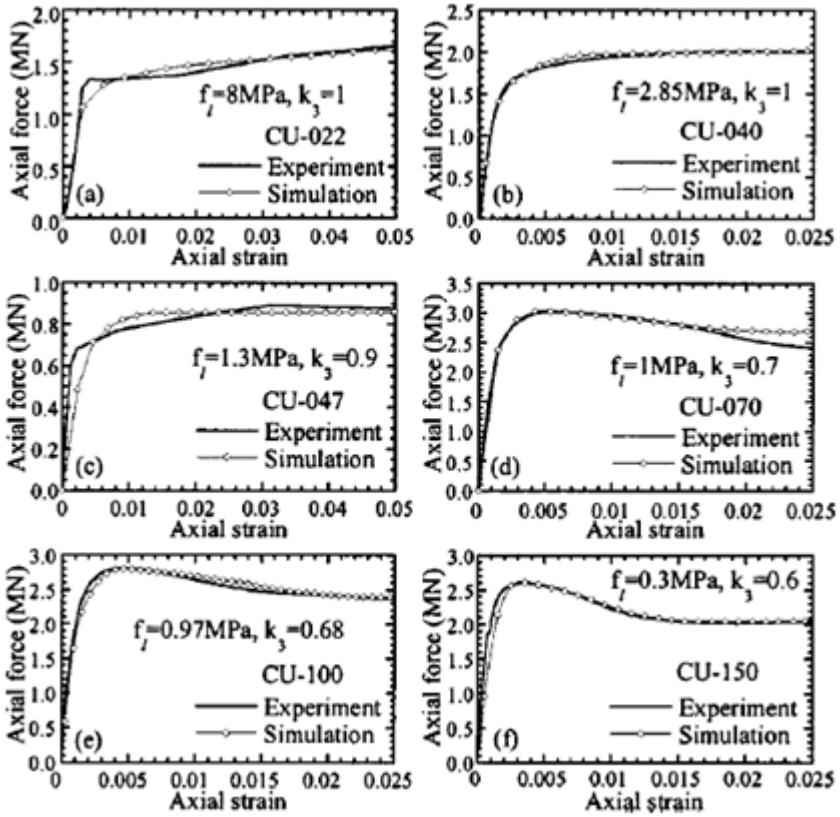

Figure 2.18: Axial strain vs.axial force (Hibbitt et. al., 2000)

2.6.4. Moon et al. (2012)

Moon et al. (2012) conducted a series of parametric studies to identify the effects of D/t ratio and the impact of the material using a FEM. The model was developed to identify the confining stresses, local buckling of the CSFT.

FE Model

ABAQUS was used for the FE modelling. Steel tube was modelled using deformable 4-node shell element (S4R). Concrete was modelled using 8-node solid elements (C3D8R) (refer Figure 2.19). Gap elements were used to model the behaviour of the interface. Friction coefficient between surfaces was taken as 0.47 based on the previous research and the results obtained from the experiments.

Concrete damaged plasticity model based on the studies of Lubliner and Fenves (1989) and Lee and Fenves (1998) was used in this study. Dilation angle, ψ affects the compressive hardening of the concrete. Therefore, it is important to use

proper value for ψ for accurate results. Lee and Fenves proposed ψ=31° for uniaxial stresses and ψ=20° for biaxial stresses. As shown in Figure 2.19, $P_{u,\,FEM}/P_{u.test}$ was plotted as a function of D/t for different ψ values. FEM results and the experimental results are compared well when ψ=20°. Therefore, dilation angle was taken as ψ=20° for the model.

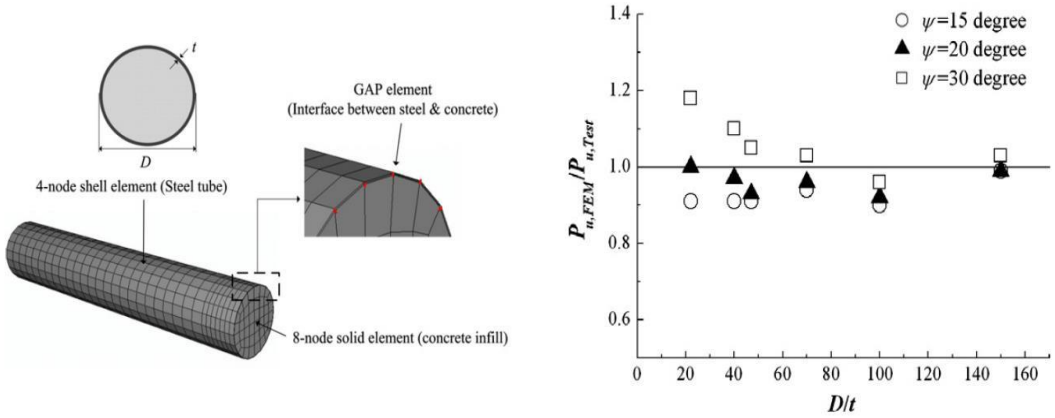

Figure 2.19: Finite element details and P (FEM)/ P(test) vs D/t graph

Concrete steel surface

Concrete core and steel tube were modelled separately and connected using interface elements. Relative movement between two materials, composite action and confinement effects can be modelled directly using this design approach.

Material properties- Concrete

The stress-strain relationship of the concrete was taken according to Figure 2.20(a). Value of the proportional limit stress was taken as $0.5f'c$/ ($f'c$/= compressive strength of the concrete). Initial modulus of elasticity was taken as,

$$Ec = 4700\sqrt{f'c}\ \text{MPa} \tag{21}$$

Stress-strain relationship of the concrete was defined by the same equation used by Hu et al. (2011).

$$f_c = \frac{E_c\varepsilon_c}{1+(R+R_E-2)(\varepsilon_c/\varepsilon'_{cc})-(2R-1)(\varepsilon_c/\varepsilon'_{cc})^2+R(\varepsilon_c/\varepsilon'_{cc})3} \tag{22}$$

Tensile strength of the concrete was assumed as 9% of the compressive strength of the concrete.

Material properties-steel

Linear stress–strain relationship used for steel is illustrated in Figure 2.20(b). Young's modulus Es was approximated as 200,000 MPa and the Poisson's ratio was taken as 0.3. Plastic behaviour of the steel initiates at f_y.

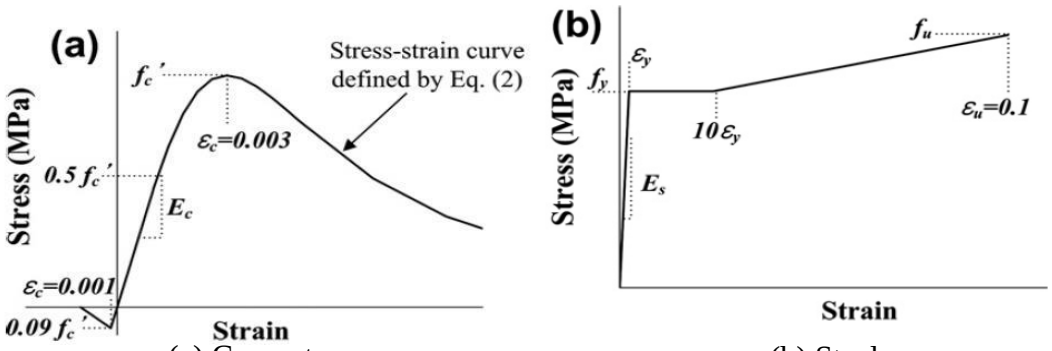

(a) Concrete (b) Steel

Figure 2.20: Stress-strain curves of concrete and steel (Hu et al., 2011)

2.7. Cost benefit analysis

Taylor et al. (2016) investigated the feasibility of the CFS columns in terms of both performance and cost. Actual 20 storey building was selected for the study frame which was designed for steel as per IS800:2007. All the columns in the building were replaced with equivalent circular and square CFST. Standard for the structural calculation of steel reinforced concrete structures, 5th edition Architecture Institute of Japan (AIJ) (2001) was used for the design of CFST. Beam sections of the original design were not changed. Therefore, the cost difference was due to CFS columns only. Cost for both original structure and CFST structure were calculated using same rates for materials. Results showed that;

 Circular CFST frame will cost approximately 38.6% lesser than steel frame.

 Square CFST frame will cost approximately 23.6% lesser than steel frame.

Cost of the CFST directly depends on the material which is used. Geetha and Swedha (2015) investigated the effect of the steel material on compressive strength of CFST. Stainless steel, mild steel, cold form steel were used for the experiment. Effect of

different D/t for different steel types was studied during the research. Tube thicknesses 2mm and 3mm were used in the experiment.

Dimensions of the specimens used for the experiment are mentioned in Table 2.1.

Table 2.1: Dimensions of the specimens

S.N	Type of steel	No of specimen	Length (L) (mm)	Diameter (D) (mm)	Thick ness (t) (mm)
1.	Stainless steel	2	600	150	2
2.	Stainless steel	2	600	150	3
3.	Mild steel	2	600	150	2
4.	Mild steel	2	600	150	3
5.	Cold formed steel	2	600	150	2
6.	Cold formed steel	2	600	150	3

Results showed that increasing thickness of cold form steel is not much effective than other materials (Table 2.2). Geetha and Swedha (2015) have mentioned that even though cost of the stainless steel is higher than two other materials, it is preferable to use stainless steel for CFST in cases where high performance is required.

Table 2.2 Capacity of specimens for different steel types and thicknesses

Specimen type	Average value, P_u (kN)		Increasing % of loadCarrying capacity for 2mm & 3mm
	2mm thick	3mm thick	
Stainless steel	989	1393	40%
Mild steel	721	1064	48%
Cold formed steel	869	907	4%

According to previous research cost of the CFST is usually lesser than ordinary steel columns. But most of the feasibility studies and cost benefit analysis were carried

out for structures where CFST are mainly used as compression members. Cost benefit analysis for other structural behaviour is yet to be investigated. Proper cost benefit analysis study relevant to CFST in truss bridges has to be carried out to identify the effectiveness relevant to Sri Lankan context.

2.8. Chapter Summary

This research was carried out to find the feasibility of using square CFST in truss bridges. Currently a lesser number of research has been carried out relevant to this topic in Sri Lanka. Square CFST has a higher compressive strength when compared to steel hollow tube. Also, Square CFST has higher confinement effect rather than CFST with other geometric section. Therefore, it has a higher compressive strength, ductility and buckling resistance.

Performance of Square CFST is affected by the following parameters according to the literature.

1. Concrete grade

2. Diameter/ thickness (D/t) ratio

3. Loading condition

When CFST axially loaded, if concrete grade increases the confinement effect will be reduced. Also, ductility of CFST is reduced when high strength concrete is used. Decrease of D/t ratio will increase the confinement effect. Therefore, compressive strength and the stiffness of CFST will be increased. When different loading conditions are considered, maximum confinement effect can be observed, when only concrete is axially loaded.

Chloride corrosion reduces the compressive strength and the ductility of CFST. Effect of the corrosion on steel hollow tubes are much higher than on CFST stub columns. Compressive strength will reduce up to higher extent when steel tube is corroded.

Using CFST in truss bridges will provide better seismic performance for truss bridges. And it will reduce the vertical deformation of the truss bridge. Especially usage of steel tonnage will be utilized properly to yield a higher load carrying capacity

when concrete infilling is done for compression members and members prone to buckle locally in truss bridges.

Previous studies show that cost of the CFST is 25% lesser than ordinary steel material when they are used as compression members.

CHAPTER III

3. DESK STUDY

3.1. Existing Pedestrian bridge types and condition in Sri Lanka

Sri Lanka has a wide highway road network connecting cities as well as rural villages. There are about 103 major rivers in Sri Lanka, where this road network has to be crossed in many situations. At most, bridges have been constructed for highways and major roads to cross over the rivers or to connect major roads. There are a lot of villages in Sri Lanka, where the people have to travel a long distance to cross the river through the highway bridges, while on the other hand, if there are at least pedestrian bridges, people could have used those to cross the river and get into the other village or a major road.

People have to cross over the rivers to do their day-to-day work, and for this purpose, they use several tricks as shown in Figure 3.1. It shows how school children cross the river with a temporally constructed bridge with stones, which cannot be used when the water level is high in the river. In extreme instances such as funerals, people have to cross the rivers with a lot of difficulties as seen in Figure 3.2. Figure 3.3 shows how a person crosses a river through a boat, with a supporting structure connected at the ends. This is also popular in some of the rural areas, where the safety condition is very poor for the people. All these are very sensitive incidents, where people have to put their lives in danger to cross over the river.

Figure 3.1: School children crossing over a river

Figure 3.2: Carrying a dead body across a river

Figure 3.3: Crossing the river using a boat

Figure 3.4 shows an older pedestrian bridge located in Kothmale Sri Lanka, which is still used to cross the Kothmale River, though it is in very poor condition for pedestrian usage. Based on the field survey it was identified that most of the pedestrian bridges constructed during the colonial period or even slightly later are not in good condition for use. On the other hand, people in rural areas need pedestrian bridges in many locations than what is available at the moment to do their routine activities smoothly. Therefore, an investigation is vital to determine whether an economical steel truss type bridge can be proposed for pedestrian usage by considering the guidelines given in the local and international standards.

Figure 3.2: Old pedestrian bridge in poor condition in Kothmale

Beginning with the colonial period of the country, several bridges were established for pedestrian use as well as highways. Most of those bridges served for a long time until they have been closed for existing traffic very recently. When looking at the nature of them, most of them can be categorized as steel truss type bridges. That is because of the benefits such as faster construction compared to concrete deck bridges and the aesthetical appearance. Therefore, a variety of steel truss type bridges can be seen all over the country.

The number of pedestrian bridges can be identified as increasing with the population increase across many major rivers in the country. Along with the pedestrian usage light vehicular traffic is also a present trend in these areas. Since most of these rivers are situated in the upcountry region, the pedestrian bridges constructed above rivers have to accommodate lightweight lorries, which are used for tea leaves transportation. For the pedestrian and light vehicle usage, Modified Warren and Pratt trusses are being used very frequently. Also, variable height truss type bridges are very popular among designers. Figure 3.5 shows the variable height pedestrian and light vehicular traffic bridge located in the Thawalama area over the Gin Ganga.

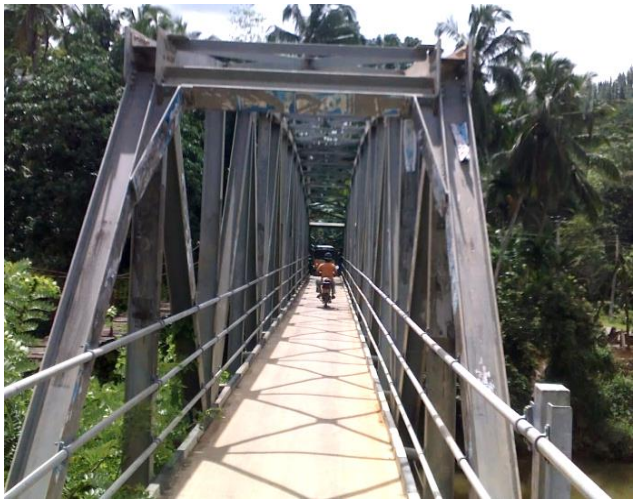

Figure 3.3: Variable height Gangasiriya Bridge

3.2. Reasons for the scarcity of pedestrian bridges in necessary areas

Along the Gin Ganga the main road lies next to the river valley. Therefore, one side is separated by the river, and hence people live in those areas are unable to come to the road side to fulfil their day today necessities. At least one bridge per village is needed to reduce the travel time and cost of villagers to cross the river.

Special point observed in the field visits is that, most of the existing bridges are located in places where there are narrow sections of the river to minimise the span of the bridges. That also have been led people to travel more distance. Figure 3.6 shows

Figure 3.4: Broken old bridge parts used by villagers to cross the river in Lankagama

a part of a broken bridge which is used by people to cross over the river in Lankagama. This place can be identified as a wide section along the river compared to most of the other locations. Therefore, relevant authorities such as PRDA needs to design a bridge according to the situation rather than trying to implement design of an existing bridge.

This is just an example for a such place, where immediate solution must be given by the relevant authorities. As villagers witnessed, sad truth about these problems in Sri Lanka is that many politicians come and visit these places, but no actions are taken to build a bridge.

3.3. Preliminary truss analysis using numerical software

Bridges can be classified based on their functional usage, the position of the deck etc. Highway, railway and pedestrian (most of the times pedestrian plus light vehicular) bridges are the main three types of bridges based on functional usage. In another way, bridges can be classified as deck type, through type and semi through type. When the deck is at the bottom level of the truss it is known as through type and is the most common type in Sri Lanka. In semi through type bridges, the deck is located at the middle level of the truss, while the deck is completely above the truss in the deck type bridges. Furthermore, bridges can be classified according to form or type of superstructures, the material of construction of superstructure, inter-span relationship, etc.

An innovative solution for the steel pedestrian bridges has been introduced as a new structural system of pedestrian stress-ribbon bridges. It includes suspension members with bending stiffness and a pre-stressed tie (Sandoviča et.al 2012).

The applicability of hollow structural section members for heavily loaded bridges and large span bridges were assessed in China and also the problems associated with joints and interfacial debonding was sorted out (Zhijuan et.al 2019).

A new concept in the field of bridge engineering was introduced as a tubular truss bridge for pedestrian use. The innovativeness, slenderness as well as the aesthetical appearance added to the truss bridge construction. This innovative collaboration took bridge construction to a new level and increased the closeness between the architect and the structural engineer (Backer et.al 2007).

Studies for evaluating the existing condition after passing ages have been assessed by university students to obtain natural frequency, material condition review and also to verify whether the structure is able to withstand the loads applied in the current conditions by structural modelling (Jorge et.al 2010).

Excessive lateral sway motion generated by the crowd caused the excessive vibrations in London Millennium Bridge. It is one of the famous examples of the vibration serviceability problem of steel footbridges. Addressing the lack of research in that area, first steps have been done identifying the vibration path as mass, damping and stiffness of the footbridge. Also, the modelling of the crowd-induced dynamic force has not been clearly defined (Dushyant et.al 2015).

Full arch and Vierendeel truss type steel pedestrian bridge models were tested with time history analysis by changing the span by Monika et.al (2017). Obtained results were compared between Full Arch and Vierendeel trusses for time period and frequency.

Modified Warren, Pratt, Tied Arch, Inverted Tied Arch, Parker, Strengthened Tied Arch and Pratt Type Arch truss types were modelled varying the span for 8 m, 16 m, 24 m, 32 m, 40 m, 48 m and 56 m by Baskaran et.al (2011). Figure 3.7 shows the above-mentioned different truss types and Figure 3.8 shows the span Vs. tonnage graph yielded.

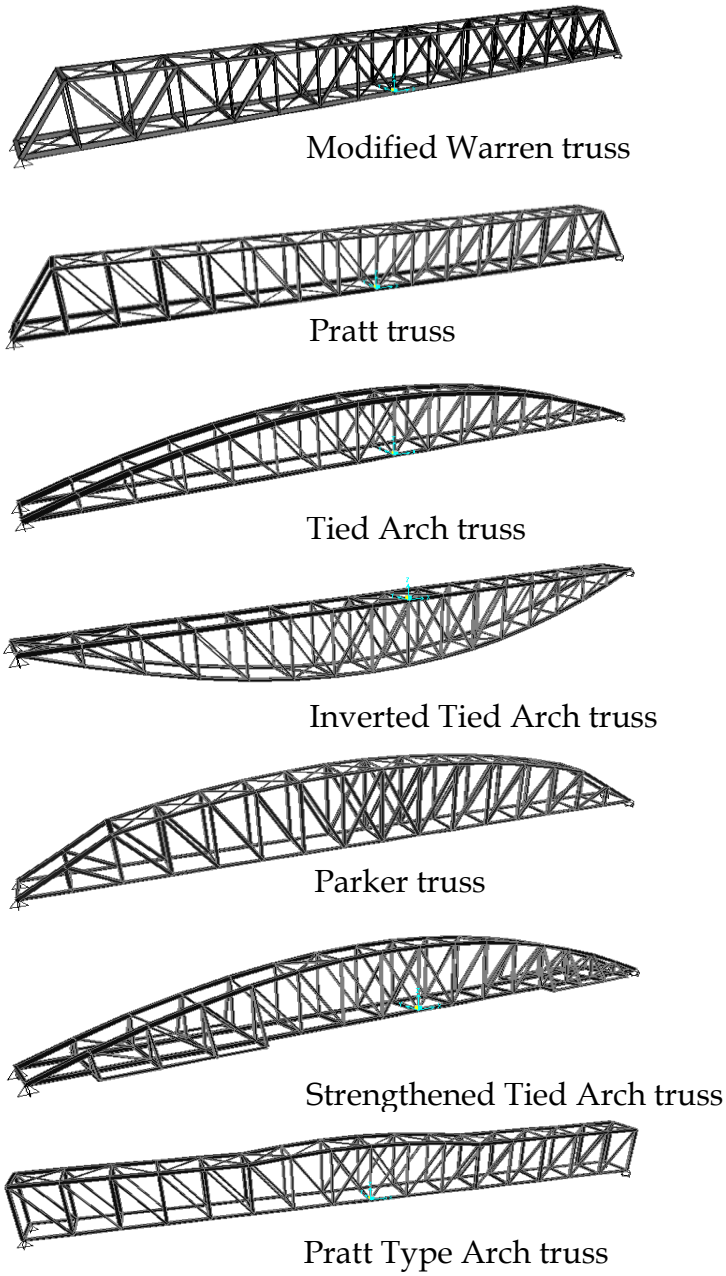

Figure 3.5 Different truss types (Baskaran *et.al.*, 2011)

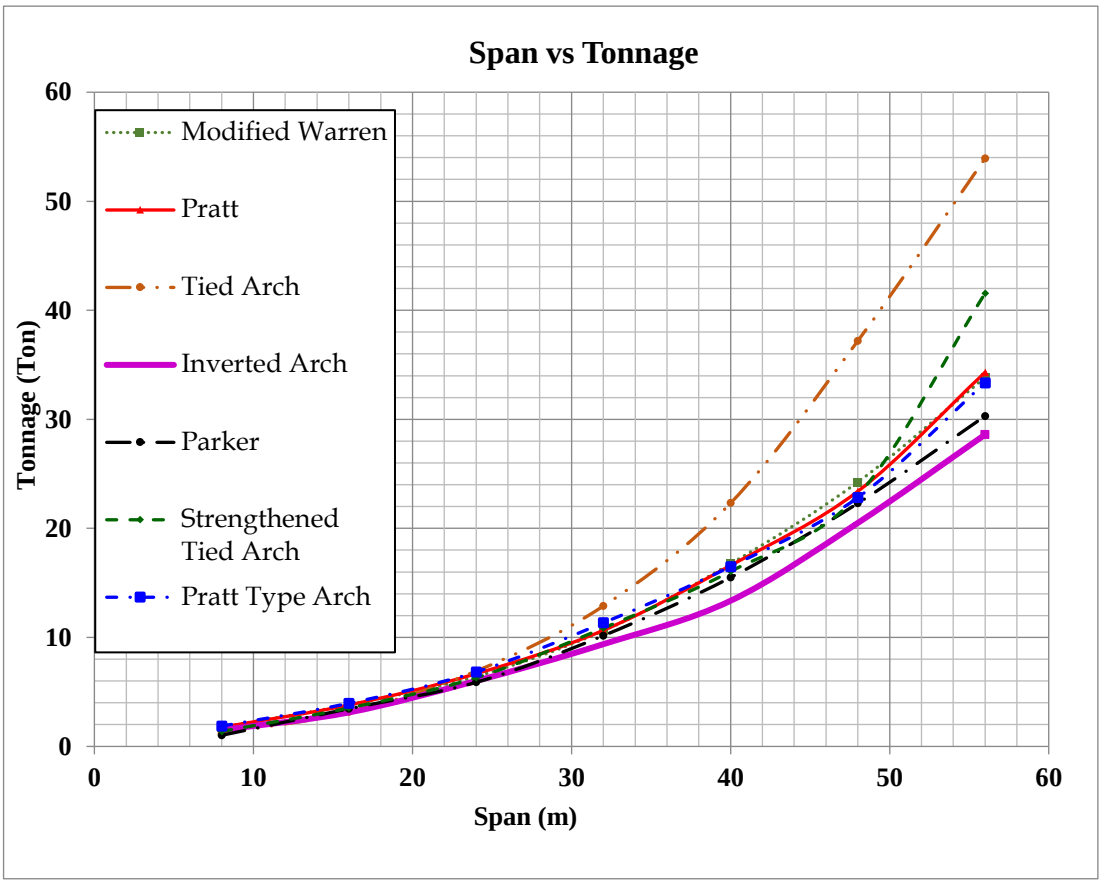

Figure 3.6: Span vs. tonnage graphs for different truss types (Baskaran *et.al*,2011)

Above results showed that almost all the truss types consume similar tonnage up to 25 m span. Inverted Arch truss consumes the least tonnage while the Tied Arch truss consumes the highest tonnage for the selected span range. Parker truss consumes the least tonnage out of the selected through type (carriage way rests on the top of the bottom chord) truss bridges. Both Strengthened Tied Arch and the Pratt Type Arch truss types show a similar variation as Modified Warren and Pratt truss types within the span range of 25-50 m. But Strengthened Tied Arch truss consumes less tonnage compared to the Modified Warren and Pratt truss types and is almost coinciding with the tonnage curve of the Parker truss type within the above span range.

Steel bridges on highways in Sri Lanka were assessed to be upgraded by Chandrasiri et.al., (2001). Most of the highway bridges were identified as narrow bridges and highlighted the need for replacement or rehabilitation. Locally suitable options for rehabilitation of steel bridges were discussed and cost-effectiveness of such options was highlighted in previous research.

Suspension bridges were assessed to carry light vehicular traffic rather than the pedestrian traffic to gain a much more economical solution. In Sri Lankan context there is a greater demand for light vehicular traffic. Since light vehicular traffic can allow transportation of goods, it is much more beneficial to have a suspension bridge with light vehicular traffic is also allowed. Practically Sri Lanka has a smaller number of such bridges. The loading conditions and techniques for accurate modelling of such bridges were obtained and case studies were carried out for 42 m and 60 m span bridges (Rohitha et al., 2001).

For pedestrian bridges as well as ramps, walkways and structures functional requirements, statics and dynamics, materials, design and construction, finishing and economical aspects were discussed in “Detail practice. Pedestrian Bridges” (Keil, 2013). Pedestrian bridge design requirements based on different standards are shown in Table 3.1, and the minimum headroom requirement for pedestrian bridges is shown in Figure 3.9 (Keil, 2013).

Table 3.1: Pedestrian bridge design details according to different standards (Keil, 2013)

Standard	**Country**	**Min. path width [m]**	**Clearance**	**Max. gradient [%]**
Austroads 13, 14, 92	Australia	1.5-1.8 (pedestrians) 1.5-3.0 (Cyclists) 2.5-3.0 (Mixed)	2.1-2.4 (Pedestrians) 2.5-3.0 (Cyclists)	12.5 (pedestrians) 5.0 (Cyclists) 3.0 (Mixed)
Structures Design Manual	Hong Kong	2.0 (pedestrians) 3.0 (In metro stations)	-	5.0-8.3 (Pedestrians) 4.0-8.0 (Cyclists)
Japanese foot bridge Design Code (1979)	Japan	3.0 (pedestrians)	-	5.0
Design Specifications of Road Structures	South Korea	1.5-3.0 (pedestrians) 3.0 (Cyclists)	2.5	-
British Standard 5400	Great Britain	1.8 (Pedestrians) 2.0 (Mixed) 2.7 (Pedestrians and cyclists with separate path)	-	5.0-8.3 (Pedestrians)
DIN 18024-1	Germany	2.0 (Pedestrians) 30.(Mixed)	2.5	6.0

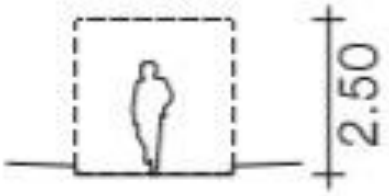

Figure 3.7: Minimum headroom requirement (Keil, 2013)

3.3.1. Finite element (FE) modelling

Baskaran et al. (2011) tested physical models of Pratt truss bridges made out of aluminum sections and loaded until the failure. 3D FE analysis was carried out using SAP2000 software. They confirmed that both failure load and failure mode obtained from FE analysis were agreed well with those obtained from the experiments. 3D FE model of a Pratt truss (16 m span) bridge is shown in Figure 3.10.

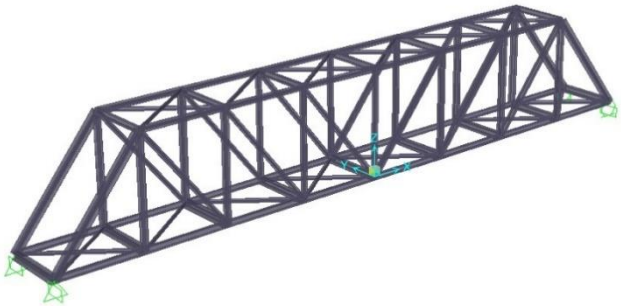

Figure 3.8: FE model of a Pratt truss (Baskaran et al., 2011)

3.3.2. Span Vs. Tonnage graphs

Span vs. tonnage graphs were developed to give an approximate number for the steel tonnage required for a particular span of a particular truss type bridge according to specific design consideration. So, span vs. tonnage graphs were developed for the pedestrian bridges with specified dimensions. Span vs. Tonnage graphs represent the variation of optimum steel weight (in tons) with respect to the span of the bridge. Hence, it can be used to check the design of a particular bridge with a given length and width to do initial cost estimation of a bridge, as the steel weight can be directly obtained from the graph for a given span.

Span vs. tonnage graphs were obtained for three different truss types, which are: Modified Warren, Pratt and Parker truss. For all the bridges, the width was maintained as 1.5 m and the maximum height was kept at 2.5 m. For the variable height truss bridges, the minimum headroom was maintained at 2.5 m (Keil, 2013). Steel was used as the material for all member sections, which is having a modulus of elasticity of 205 kN/mm^2 and minimum yield strength of 275 N/mm^2. Steel member sections were imported from a standard section table available in the SAP2000 software, which is specified according to the requirement of the British Code.

Span vs. tonnage graphs were developed changing the height and the width compared with the above-specified dimensions for width and height. For the Modified Warren and Pratt type,

-• 2 m width and 3.7 m height

• 2 m width and 2.5 m height

• 1.5 m width and 3.7 m height trusses were modelled for the analysis.

For the Parker truss,

• 2 m width, 5 m maximum height and 3m headroom

• 2 m width, 4.5 m maximum height and 2.5 m headroom

• 1.5 m width, 4.5 m maximum height and 2.5 m headroom

3.3.3. Loads on bridges

The loads acting on the pedestrian bridges were calculated based on BS 5400: Part 2: 1978. In the analysis, dead load, superimposed dead load, live load and the wind load were considered. The dead load which is the self-weight of the truss was automatically obtained from the software. The bridge deck was assumed to consist with a 100 mm thick reinforced concrete slab and a 50 mm thick wearing surface, and they were considered as superimposed dead load. The standard; BS 5400: Part 2: (1978) recommends 5 kN/m^2 of live load for pedestrian bridges, as they have access to light vehicles such as three-wheelers. Modification factor was applied for the nominal live load to the bridges spanning more than 30 m. When the pedestrians are standing on the bridge, wind acting on the pedestrians can be transferred to the deck and it was also considered in the design. Four different patterns of live loading were considered for pattern loading since they can be critical for certain members.

FE analysis was carried out using the SAP2000 software. The orientation of the top chord, vertical members and diagonal members were used effectively to provide higher stiffness in the lateral direction and less stiffness in the plane of the truss.

In Parker trusses, first two top chord members close to the support do not have any restraint in the lateral direction. So, in order to calculate the effective length in the lateral direction, the total length of the un-braced members has to be considered.

Giving more considerations to the prevailing construction practices, the same member sections were used within the groups such as top chords, bottom chord, diagonal, vertical, cross beams, bracings, etc. Suited member for a given group was decided based on the critical member in that group. Steel I sections having overall height and width of 100 mm were used to top and bottom chords. 90 mm L angle sections were used for vertical and triangulating members throughout the analysis.

Structural design was also carried out by using the “design check” option in the SAP2000. Demand/capacity ratio was considered as 0.87 in the design and the members were assigned based on the British Standard sections (British Standards for structural steel sections, 1993).

Span Vs. Tonnage graph for Modified Warren truss type is given in Figure 3.11. It can be seen that when the width and height are decreased the tonnage is also reduced, but the variation of tonnage is not much significant up to 24 m spans. Most significantly, when the height is reduced the tonnage difference is larger compared to the width reduction. Pratt type truss also shows the same behaviour as the Modified Warren truss type as shown in Figure 3.12.

In Parker truss type, when the width is reduced the tonnage difference is greater compared to the height reduction as seen in Figure 3.13.

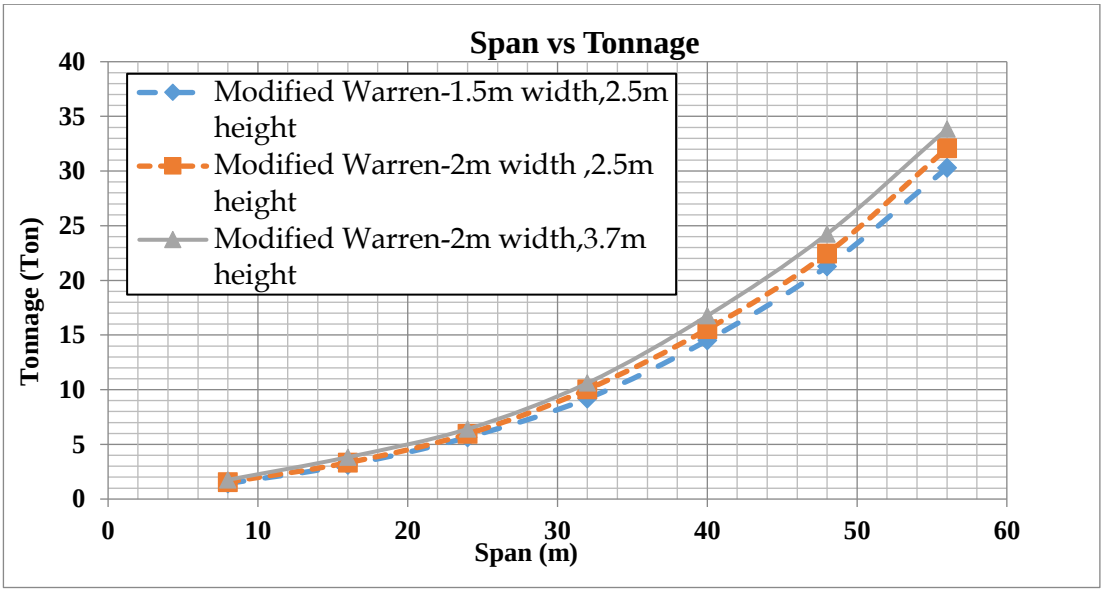

Figure 3.9: Span vs.tonnage graphs for Modified Warren truss type

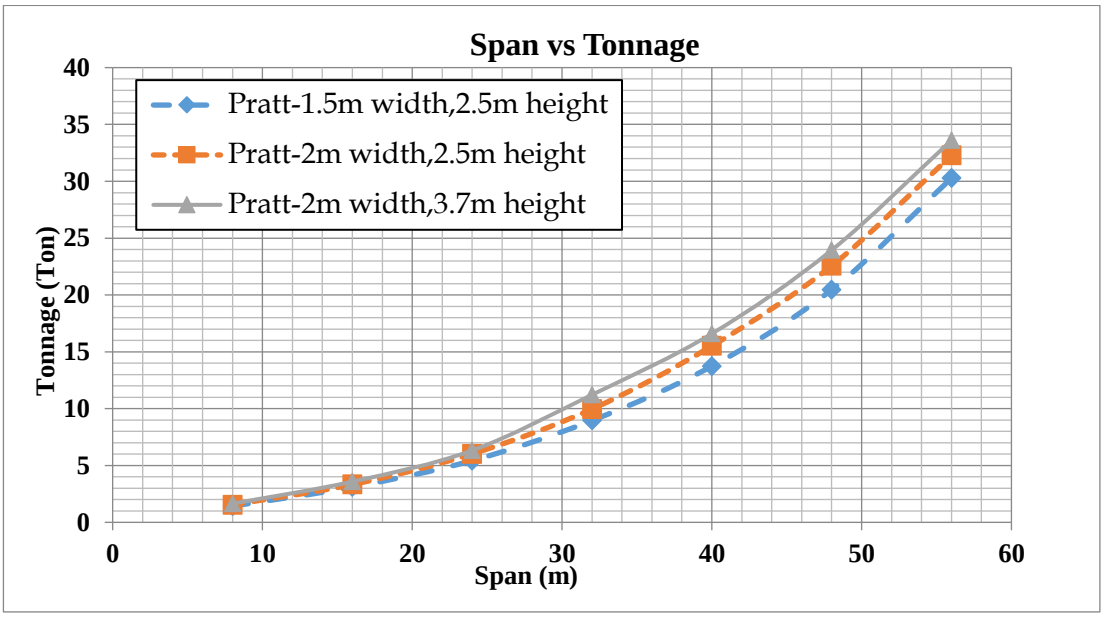

Figure 3.10: Span vs.tonnage graphs for Pratt truss type

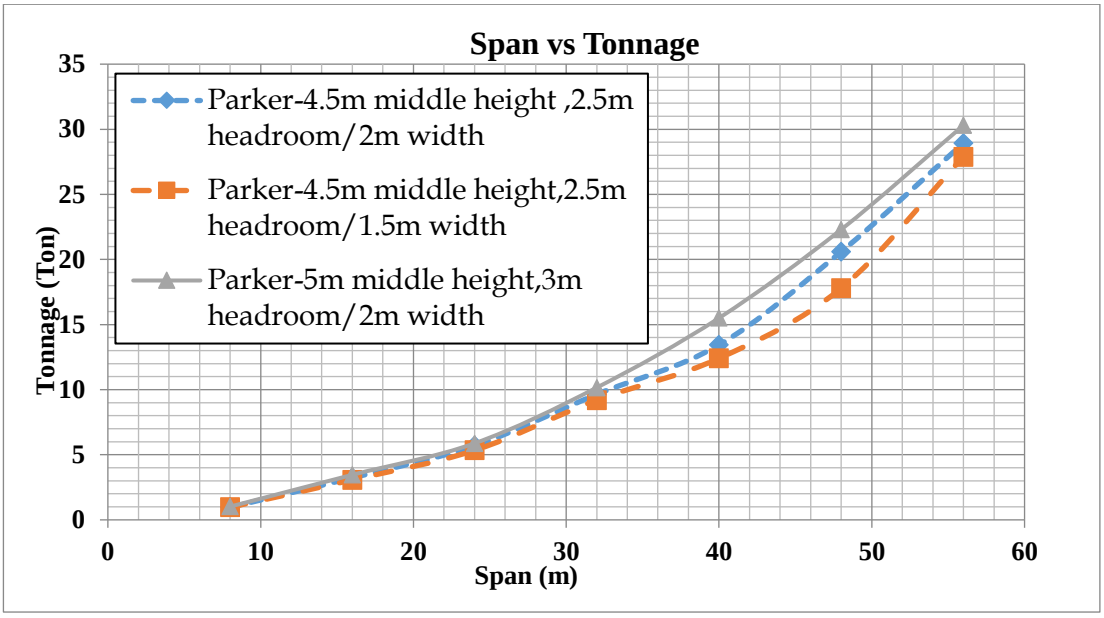

Figure 3.11: Span vs.tonnage graphs for Parker truss type

Figure 3.14 shows the final tonnages for the proposed road width of 1.5 m and a height of 2.5 m. Modified Warren and Pratt trusses consume almost the same tonnages for the higher spans, while Parker truss consumes a lesser tonnage compared to above two truss types.

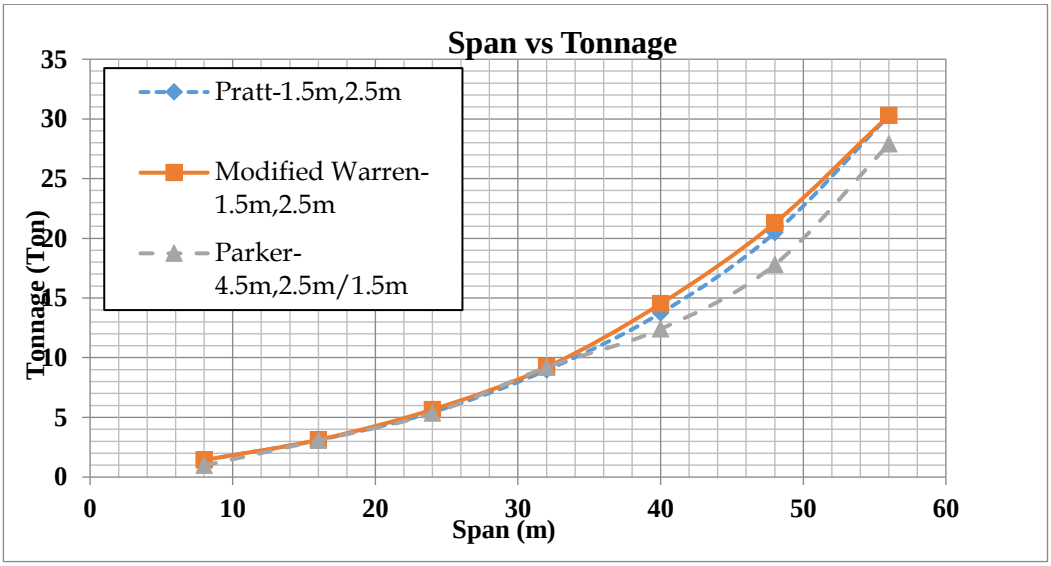

Figure 3.12: Span vs.tonnage graphs for three trusses

3.3.4. Discussion of results

The analytical investigation was carried out for the assessment of steel tonnage reduction with the change of minimum width to 1.5 m and height to 2.5 m, compared to that of 2 m width and specified minimum height (2.5 m) used by previous research (Baskaran et al., 2011). These results are summarized in Table 3.2.

Table 3.2: Steel tonnage reduction for each truss type

Truss type /span(m)	Modified Warren	Pratt	Parker
8	23%	8%	5%
16	23%	7%	11%
24	13%	11%	9%
32	15%	11%	9%
40	15%	13%	20%
48	14%	10%	20%
56	12%	7%	8%

It is evident that the reduction of the steel tonnage noticeably varies with the span for all selected truss types. According to the results, Modified Warren truss type is more applicable for the smaller spans since it gives higher tonnage reduction for spans of 8 m, 16 m and 24 m. Pratt type shows above behaviour for spans 24 m, 32 m, 40 m and 48 m. Parker truss also contributed to a considerable average reduction of 11.82%. It's maximum reduction yields when span reaches 40 m and 48 m. Parker truss is the truss type which consumes the least tonnage for any particular span. It is due to the variable shape of the truss.

Table 3.3: Average steel tonnage reduction

Truss type	Average steel tonnage reduction
Modified Warren	17%
Pratt	10%
Parker	12%

It can be seen that there are many significances in the Parker truss. Initially, the

tonnages for particular spans are comparatively lesser compared to Modified Warren and Pratt trusses. The maximum Tonnage which has yielded for the 56 m span is about 30 tons, while above two truss types yielding 35 tons. It is a positive point when we are selecting a truss type considering the most economical considerations. Also, the tonnages have not been changed significantly up to 32 m spans in Parker truss. Thereafter, a significant difference in tonnages can be identified. Especially for the graph of 1.5 m width, the tonnage values yielded are noticeably less compared to other two truss types. Initially for top chord and bottom chord BS 178x102x19 and for vertical members BS 127x76x13 sections were used for all the trusses and according to optimization, section properties were changed accordingly.

3.4. Identification of the problems in the existing pedestrian bridges and propose strengthening measures

There were several cases reported in past about the failure of truss type pedestrian bridges as well as highway bridges. Ehalakanda Bridge is one such case, which failed due to self-weight, while it was launching. Old bridges built in Ehalakanda area have failed several times due to heavy flooding in the Gin Ganga. Figure 3.15 shows the ruins of an old bridge pier, while the existing truss type pedestrian bridge at Ehalakanda is located above that. Width of this section is higher

Figure 3.13: Parts of the old bridge under existing Ehalakanda Bridge

and the water depth is also much higher. Therefore, piers could have damaged and it could be the reason for the failure of the bridge trusses.

Figure 3.16 shows the image of an old truss type pedestrian bridge in Ehalakanda, which had failed during launching. As in Figure 3.16, top chord members in either sides have failed due to lateral torsional buckling with the load transferred by its member weight. Without any triangulation in the load path, the bridge had only vertical members, with the absence of the diagonal members. So, both top and bottom chord members were rigidly connected at the joints, in the plane of the truss and in lateral direction.

Figure 3.16: Failed Ehalakanda Bridge when launching

Obeying to the RDA standards and general practice, minimum head room of a pedestrian bridge should be in the range of 2.5-3.0 m. Hence, the top chord members close to the support in either sides could not be braced in lateral direction. Slenderness ratio of those members in lateral direction was more than the recommended value. Even though the maximum capacity has not been reached in particular members, failure had occurred by buckling of the top chord member. The failure analysis of the Ehelakanda Bridge has been presented in a previous research (Baskaran et al., 2011).

As discussed above, top chord members near the supports in a variable height steel truss type pedestrian bridge cannot be braced to provide the minimum headroom requirement. These members have a higher effective length in lateral direction, and hence are prone buckle laterally as they are subjected higher compressive forces than those at the middle. As a solution, providing a portal frame in either sides of the truss, using bigger sections for members which are prone to lateral buckling and also changing the geometry of those member elements etc. have been assessed in past. In Sri Lankan context, an onsite economical solution is needed for this problem as variable height truss type steel bridges are frequently used, especially as pedestrian bridges. Hence, infilling self-compacting high strength concrete into top chord members which are prone to fail in lateral buckling would be an ideal solution in terms of the cost as well. Therefore, this study is directed towards assessing the applicability of CFST sections in truss type pedestrian bridges. An extensive experimental program has been conducted to investigate the strength enhancement of CFST compared to their counterparts (hollow GI tubes). Results of this study are presented in Chapter IV.

3.5. Chapter Summary

Common practice is to use the sections designed for a larger span bridge to that of a smaller span bridge. The gap between the tonnage graphs of different truss types increased considerably when it comes to higher spans. By comparing span vs. tonnage graphs for different truss types with specified dimensions, it can be said that almost all the pedestrian bridges consume similar tonnage up to 30 m spans. So, by considering ease of construction, both Pratt and Modified Warren truss type bridges can be recommended for spans less than 30 m.

For higher spans, Parker truss consumes a noticeably less tonnage compared to the other two truss types and hence could be recommended for higher spans. The reduction in the steel tonnage when the minimum width and height are reduced to 1.5 m and 2.5 m respectively are not that significant and hence bridges with those modifications can be recommended only at locations where the access can be provided only for pedestrians. With the present study, it is recommended to follow the RDA regulations, where a minimum 2 m width and 3 m headroom height should be used for pedestrian bridges to allow the access of light vehicles.

Based on the field visits and questionnaire surveys with people who are living along the Gin Ganga area yielded that there are lot of locations that need to be connected by a bridge. With the results of the above parametric study, Parker truss type has been identified as the most economical truss type to be proposed for higher spans since our focused area has a river width above 30 m. Therefore, Parker truss type is further studied to use as an economical solution for higher span bridges for the context of the study.

CHAPTER IV

4. EXPERIMENTAL PROGRAM PHASE 1 - COMPRESSION TESTING OF SQUARE HOLLOW GI SECTIONS AND CFST

4.1. Introduction

Even though lot of practical applications have been processed all over the world, in local context CFST has not been much popular among bridge designers. Therefore, commercially available steel tubes were selected to check the practical applicability of proposed solution. Present steel industry has focused more on Galvanized Iron (GI) steel. Considering the maximum size of the aggregates to be 37.5 mm (< according to testing), 50 mm square sections were selected to proceed with the experimental testing of GI. In total, 32 number of GI columns were tested for compression. Lengths were taken as 1.5 m and 1.0 m and section thicknesses were selected as 1.2 mm, 1.4 mm, 1.6 mm and 2.0 mm. Three specimens were tested for 1.5 m high hollow and CFST members for each thickness and one specimen from each thickness was tested for 1.0 m high hollow and CFST members.

Before member testing, tensile strength of the steel was generated using tensile testing machine inside the structural testing laboratory in the Department of Civil Engineering. Generated loads vs displacement curves and stress vs strain curves are presented in annex.

Compressive load was applied along the vertical axis even though there were some unevenness present in the upper and lower cross-sections of the steel tubes. However, necessary precautions were taken to level the surfaces using angle grinder to a considerable level. Especially in CFST tubes concrete shrinkages were observed along the vertical axis direction and accordingly extra concrete were filled into CFST tubes to achieve the required level. Thereafter top and bottom surfaces were levelled using an angle grinder. Figure 4.1 illustrates the application of compressive load to a 1.5 m high hollow GI specimen having a 1.2 mm thickness, while the Figure 4.2 shows that for a 1.5 m high CFST specimen having a 1.2 mm thick GI section.

Figure 4.1: Compressive load test of hollow GI section (1.5 m high, 1.2 mm thick)

Figure 4.1: Compressive load test of CFST grade 40 section (1.5 m high, 1.2 mm thick)

4.2. Theoretical prediction of the failure loads and modes

Steel sections can be classified into four classes (Class 1, 2, 3 and 4) as specified in the EN 1993-1-1 2005. Out of these sections belong to Class 4 will fail by local buckling (LB). Sections belong to Classes 1, 2 and 3 will fail by compression (CF) or by global buckling (GB) depending on several parameters such as sectional properties, support condition, eccentricity of loading and presence of material imperfection.

Hollow GI tubes used for the experiment were classified according to the information given in the Table 5.2 of EN 1993-1-1 2005 as presented below.

Square section with 50mm cross-section and 1.2mm thickness

$c/t = 47.6/1.2 = 39.6$; $42*(\sqrt{\frac{235}{f_y}}) = 42*(\sqrt{\frac{235}{320}}) = 36$

Since $c/t > 42\epsilon$; section is categorized as class 4.

Square section with 50mm cross-section and 1.4mm thickness

$c/t = 47.2/1.4 = 33.71$; $42*(\sqrt{\frac{235}{f_y}}) = 42*(\sqrt{\frac{235}{320}}) = 36$

Since $c/t < 42\epsilon$; section is categorized as class 3.

Square section with 50mm cross-section and 1.6mm thickness

$c/t = 46.8/1.6 = 29.25$; $38*(\sqrt{\frac{235}{f_y}}) = 38*(\sqrt{\frac{235}{320}}) = 32.56$

Since $c/t < 38\epsilon$; section is categorized as class 2.

Square section with 50mm cross-section and 2.0mm thickness

$c/t = 46.0/2.0 = 23.0$; $33*(\sqrt{\frac{235}{f_y}}) = 33*(\sqrt{\frac{235}{320}}) = 28.28$

Since $c/t < 33\epsilon$; section is categorized as class 1.

It is evident from the above calculations that, the 1.2 mm thick hollow sections belong to Class 4 irrespective of the length, and hence they will fail in local buckling. For 1.2

mm thick specimens (both of 1.0 m and 1.5 m high), effective cross-sectional areas were determined using the BS EN 1993-1-5:2006 to calculate their compression capacity. Specimens having 1.4 mm, 1.6 mm, and 2.0 mm thicknesses belong to classes 3, 2 and 1 respectively, and hence they will fail either by compression or global buckling depending on the length and the other factors as specified above. As explained in Section 2.5, Euler's formula was used to predict the buckling failure load, while the EN 1993-1-1 2005 was used to calculate the compression failure load. The lowest value was selected as the critical theoretical failure load and those are presented in Table 4.1.

CFST sections were checked for local buckling of sections according to EN 1994-1-1:2004. For CFST sections having a square shape, $h/t < 50*(\sqrt{\frac{235}{f_y}})$ condition has to be satisfied to prevent them from local buckling. All the CFST specimens satisfy the above criterion and hence local buckling (LB) will not be prioritised in those. Compression failure load (CF) and the Euler Buckling (EB) load of the CFST sections were determined as explained in Section 2.5 and those are presented in Table 4.2.

Table 4.1: Theoretical failure loads and modes of the hollow GI specimens

Height (m)	**Thickness (mm)**	**Euler's formulae (kN)**	**Section capacity (kN)**	**Critical failure load (kN)**	**Failure mode**
1.0	1.2	172	68	**68**	LB
	1.4	212	87	**87**	CF
	1.6	239	99	**99**	CF
	2.0	292	123	**123**	CF
1.5	1.2	76	68	**68**	LB
	1.4	94	87	**87**	CF
	1.6	106	99	**99**	CF
	2.0	130	123	**123**	CF

It is evident from the Table 4.1 that the section capacities of all the 1 m high specimens are considerably less than their Euler buckling failure loads, and probably they will fail in compression by exceeding the compression capacity. However, it should be noted that the 1.2 mm thick specimens will fail by local buckling irrespective of the height as discussed earlier. Compression capacity of the 1.5 m high specimens are slightly less than their Euler buckling failure loads and hence they will also fail by compression similar to 1 m high specimens. However, it could be noted that the Euler buckling load can vary due to several parameters such as sectional properties, support condition, eccentricity of loading and presence of material imperfections. So, change in the failure mode can be expected in the experiment for the 1.5 m high specimens.

Table 4.2: Theoretical failure loads and modes of the CFST

Height (m)	**Thickness (mm)**	**Euler's formulae (kN)**	**Section capacity (kN)**	**Critical failure load (kN)**	**Failure Mode**
1.0	1.2	269	154	**154**	CF
	1.4	294	165	**165**	CF
	1.6	319	176	**176**	CF
	2.0	366	197	**197**	CF
1.5	1.2	122	154	**122**	GB
	1.4	133	165	**133**	GB
	1.6	144	176	**144**	GB
	2.0	165	197	**165**	GB

According to Table 4.2, it is clear that the section capacities of 1 m high CFST are considerably less than their Euler buckling failure loads for all the thicknesses and probably they will fail in compression by exceeding the compression capacity. However, section capacities of 1.5 m high CFST are higher than their Euler buckling failure loads for all the thicknesses and probably they will fail in global buckling.

Failure loads and modes seen from the experiment are presented in the following section.

4.3. Failure loads and modes obtained from the experiment

Failure loads and modes obtained from the experiment for the hollow GI specimens are presented in Table 4.3, while those obtained for the CFST are presented in Table 4.4. Only one specimen from each thickness was tested for 1 m height both hollow and CFST. However, three specimens from each thickness were tested for 1.5 m high both hollow and CFST and the average failure loads are present for those in the following tables. Failure modes of the tested specimens are shown in Figure 4.3-4.6.

Table 4.3: Experimental failure loads and modes of the hollow GI specimens

Height (m)	**Thickness (mm)**	**Failure Load (kN)**			**Average Failure Load (kN)**	**Failure mode**
		S1	**S2**	**S3**		
1.0	1.2	42	-	-	**42**	LB
	1.4	88	-	-	**88**	CF
	1.6	101	-	-	**101**	CF and GB later
	2.0	143	-	-	**143**	CF and GB later
1.5	1.2	60	56	62	**59**	LB
	1.4	84	81	80	**82**	CF and GB later
	1.6	89	86	95	**90**	CF and GB later
	2.0	126	126	135	**129**	CF and GB later

Table 4.4: Experimental failure loads and modes of the CFST

Height (m)	**Thickness (mm)**	**Failure Load (kN)**			**Average Failure Load (kN)**	**Failure mode**
		S1	S2	S3		
1.0	1.2	140	-	-	140	CF and GB later
	1.4	159	-	-	159	CF and GB later
	1.6	178	-	-	178	CF
	2.0	204	-	-	204	CF
1.5	1.2	140	131	128	133	GB
	1.4	143	126	141	137	GB
	1.6	151	125	141	139	GB
	2.0	173	198	198	190	GB

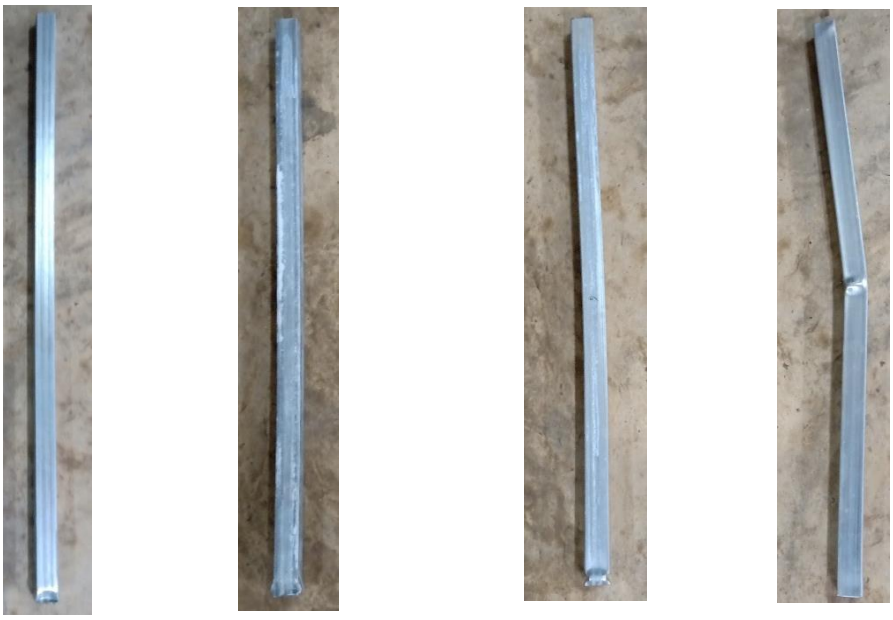

LB | CF | CF initially and GB later | CF initially and GB later

(a) 1.2 mm | (b) 1.4 mm | (c) 1.6 mm | (d) 2.0 mm

Figure 4.3: Failure modes of the 1 m height hollow specimens

LB

(a) 1.2 mm

CF initially and GB later

(b) 1.4 mm

CF initially and GB later

(c) 1.6 mm

CF initially and GB later

(d) 2.0 mm

Figure 4.4: Failure modes of the 1.5 m height hollow specimens

CF initially and GB later

(a) 1.2 mm

CF initially and GB later

(b) 1.4 mm

CF

(c) 1.6 mm

CF

(d) 2.0 mm

Figure 4.5: Failure modes of the 1 m height CFST

GB

(a) 1.2 mm

GB

(b) 1.4 mm

GB

(c) 1.6 mm

GB

(d) 2.0 mm

Figure 4.6: Failure modes of the 1.5 m height CFST

4.4. Comparison of the experimental results with the theoretical predictions

Failure modes obtained from the experiment are agreed well with those predicted from the theory as indicated in Figure 4.3-4.6. Local buckling could be seen in the both hollow 1 m and 1.5 m high specimens having 1.2 mm thickness. All the other hollow GI specimens failed in compression, but later global buckling was also seen with the increment of loading. 1m high CFST specimens failed in compression, while 1.5 m high of those failed in global buckling as predicted from the theoretical calculations. A comparison of the failure loads obtained from the theoretical calculations and the experiment for hollow and CFST are given in Table 4.5 and Table 4.6 respectively.

Table 4.5: Comparison of the failure loads obtained for the hollow GI specimens

Section	**Height (m)**	**Thickness (mm)**	**Exp. failure Load (kN)**	**Theoretical Failure Load (kN)**	**Failure Mode**	**% change in exp. load**
Hollow Section	1.0	1.2	**42**	**68**	LB	38.2%
		1.4	**88**	**87**	CF	1.1%
		1.6	**101**	**99**	CF	2.0%
		2.0	**143**	**123**	CF	16.3%
	1.5	1.2	**59**	**68**	LB	13.2%
		1.4	**82**	**87**	CF	-5.7%
		1.6	**90**	**99**	CF	-9,1%
		2.0	**129**	**123**	CF	4.9%

Table 4.6: Comparison of the failure loads obtained for the CFST

Section	Height (m)	Thickness (mm)	Experimental failure Load (kN)	Theoretical failure load	Failure Mode	% change in exp. load
CFST Section	1.0	1.2	**140**	**154**	CF	-9.1%
		1.4	**159**	**165**	CF	-3.6%
		1.6	**178**	**176**	CF	1.1%
		2.0	**204**	**197**	CF	3.6%
	1.5	1.2	**133**	**122**	GB	9.0%
		1.4	**137**	**133**	GB	3.0%
		1.6	**139**	**144**	GB	-3.5%
		2.0	**190**	**165**	GB	15.2%

According to Table 4.5, it is evident that the experimental failure loads are agreed well with those predicted from the theoretical calculations for all the GI hollow specimens (% change is less than 15% for most of them), except for the specimen having 1 m height and 1.2 mm thickness which failed in local buckling (% change of 38.2%). Overall, it is clear that the theoretical and experimental failure loads are agreed well for the specimens failed in compression compared to those failed in local buckling.

According to Table 4.6, it is evident that the experimental failure loads are agreed well with those predicted from the theoretical calculations for all the CFST specimens (% change is less than 10% for all of them except the CFST specimen having a 1.5 m height and 2 mm thickness). For most of the specimens failed in global buckling, experimental failure loads are slightly higher than the theoretical predictions, probably due to the increased fixity at the ends due to frictional forces whereas pin support condition was assumed in the theoretical calculations.

4.5. Strength enhancement of CFST compared to hollow GI tubes

Figure 4.7 compares the experimental and theoretical failure loads of the specimens with 1 m high (both hollow and CFST), and the variations of those for specimens with 1.5 m high are shown in Figure 4.8. Overall, these figures further confirm that the experimental results and theoretical predictions are agreed well and this trend can be mostly seen for the 1.4 mm and 1.6 mm thick GI specimens (both hollow and CFST) which are belong to classes 3 and 2 respectively. These figures also illustrate the increase in the failure loads of the CFST compared to hollow GI tubes with identical dimension.

This has been further illustrated in Table 4.7, which compares the percentage increase in the theoretical failure loads of the CFST compared to hollow GI tubes with identical dimension. For 1 m high specimens, increase in the failure load has reduced from 126% to 60% when the thickness of the GI tube is increased from 1.2 mm to 2.0 mm, while it has reduced from 79% to 34% for 1.5 m high specimens. Table 4.8 compares the percentage increase in the experimental failure loads of the CFST compared to hollow GI tubes with identical dimension. For 1 m high specimens, increase in the failure load has reduced from 233% to 43% when the thickness of the GI tube is increased from 1.2 mm to 2.0 mm, while it has reduced from 125% to 47% for 1.5 m high specimens. Overall, the strength enhancement of CFST seen from the experiment is more than those predicted from theoretical calculations.

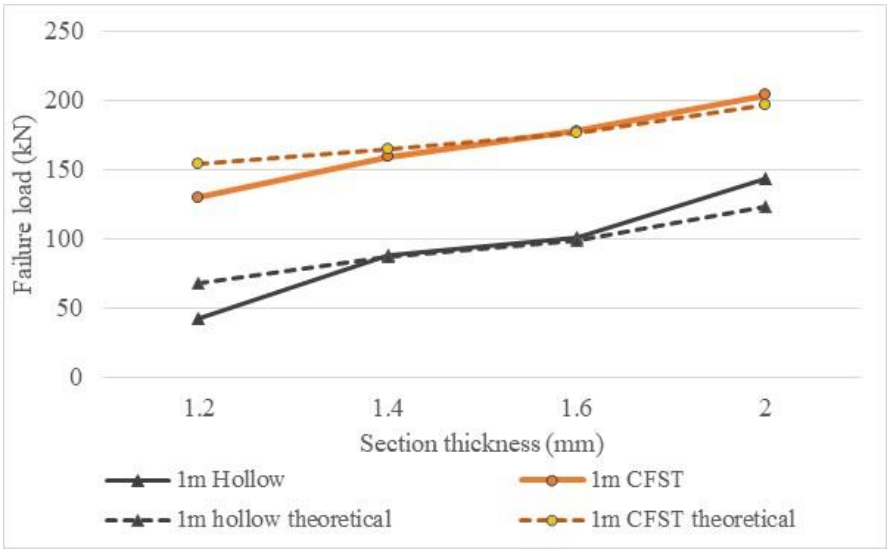

Figure 4.7: Comparison of experimental and theoretical failure loads of the 1 m height specimens

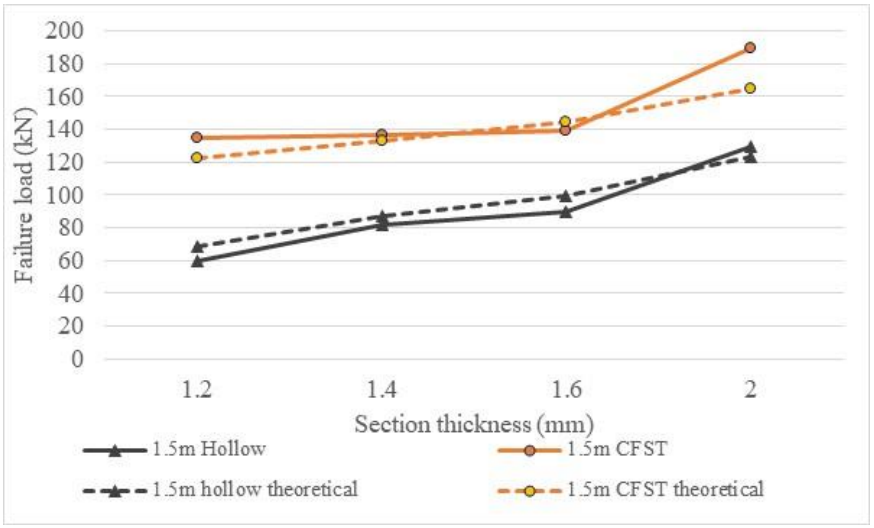

Figure 4.8: Comparison of experimental and theoretical failure loads of the 1.5 m height specimens

Table 4.7: Comparison of the improvement in the theoretical failure loads of the CFST compared to hollow GI tubes

Height (m)	Thickness (mm)	Hollow		CFST		% increase in CFST
		Failure Load (kN)	Failure Mode	Failure Load	Failure Mode	
1.0	1.2	**68**	LB	**154**	CF	**126%**
	1.4	**87**	CF	**165**	CF	**90%**
	1.6	**99**	CF	**176**	CF	**78%**
	2.0	**123**	CF	**197**	CF	**60%**
1.5	1.2	**68**	LB	**122**	GB	**79%**
	1.4	**87**	CF	**133**	GB	**53%**
	1.6	**99**	CF	**144**	GB	**45%**
	2.0	**123**	CF	**165**	GB	**34%**

Table 4.8: Comparison of the improvement in the experimental failure loads of the CFST compared to hollow GI tubes

Height (m)	Thickness (mm)	Hollow		CFST		% increase in CFST
		Failure Load (kN)	Failure Mode	Failure Load	Failure Mode	
1.0	1.2	**42**	LB	**140**	CF	**233%**
	1.4	**88**	CF	**159**	CF	**81%**
	1.6	**101**	CF	**178**	CF	**76%**
	2.0	**143**	CF	**204**	CF	**43%**
1.5	1.2	**59**	LB	**133**	GB	**125%**
	1.4	**82**	CF	**137**	GB	**67%**
	1.6	**90**	CF	**139**	GB	**54%**
	2.0	**129**	CF	**190**	GB	**47%**

It is therefore clear that the failure load improvement in CFST has reduced with the increase of the thickness of the GI tube, where the section type is changed from Class 4 to Class 1. On the other hand, improvement in the failure loads is less in the specimens with 1.5 m height compared those of 1 m height, which might be due to the change in the failure mode of those from compression failure (1 m CFST) to the global buckling failure (1.5 m CFST). So, it is evident that the strength enhancement with CFST is more significant in the short columns compared to the long columns.

4.6. Chapter Summary

This chapter presents the uni-axial compression test results of hollow GI and CFST specimens having lengths of 1 m and 1.5 m for four different thicknesses (1.2 mm, 1.4 mm, 1.6 mm and 2.0 mm). Both 1 m and 1.5 m high hollow GI specimens having a 1.2 mm thickness failed in local buckling irrespective of the height. Both 1m and 1.5 m high hollow GI specimens having 1.4 mm, 1.6 mm and 2.0 mm thicknesses failed in compression. Compression capacities of the 1 m high columns are considerably higher than their Euler buckling loads, while that trend is quite low in the 1.5 m high specimens. Experimental failure modes agreed well with the theoretical predictions. Overall, it is evident that the theoretical and experimental failure loads are agreed well for the specimens failed in compression (change is less than 10%) compared to those failed in local buckling.

1 m high CFST specimens with all the thicknesses failed in compression as their Euler buckling failure loads are considerably higher than the compression capacities. However, 1.5 m high CFST specimens with all the thicknesses failed in global buckling as their Euler buckling failure loads are lower than the compression capacities. Experimental failure modes agreed well with the theoretical predictions. Overall, experimental failure loads agreed well with those predicted from the theoretical calculations for all the CFST specimens (change is less than 15%)

For 1 m high specimens, increase in the failure load has reduced from 126% to 60% theoretically (from 233% to 43% experimentally) when the thickness of the GI tube is increased from 1.2 mm to 2.0 mm, while it has reduced from 79% to 34% theoretically (from 125% to 47% experimentally) for 1.5 m high specimens. It is clear

that the failure load improvement in CFST has reduced with the increase of the thickness of the GI tube, where the GI section type is changed from Class 4 to Class 1. On the other hand, improvement in the failure load is less in the specimens with 1.5 m height compared those of 1 m height, where the failure mode is changed from compression failure (1 m CFST) to the global buckling failure (1.5 m CFST). So, it is evident that the strength enhancement with CFST is more significant in the short columns compared to the long columns. It was also observed that strength enhancement of CFST seen from the experiment is more than those predicted from theoretical calculations.

CHAPTER V

5. EXPERIMENTAL PROGRAM PHASE 2 – TESTING MODEL BRIDGES

5.1. Introduction

5.2. Details of the model bridges

A truss structure following the shape of the bending moment diagram was selected to assess the performance of the geometrical shape and also to maintain a pleasant esthetical shape to the truss. Proportionate to the shape of the bending moment diagram of an idealized model of a truss bridge withstanding for a uniformly distributed load along its span, a 2 m long truss bridge model was selected as shown in Figure 5.1.

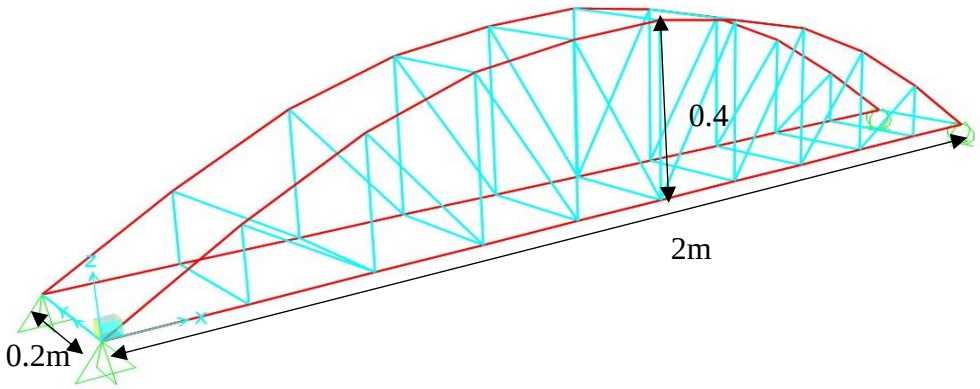

Figure 5.1: Dimensions of the selected truss bridge for testing

When selecting cross sections for each member, top and bottom chord members were selected with higher thickness (0.9 mm) than vertical and diagonal members which have a lower thickness (0.65 mm) as shown in Figure 5.2. However, the section sizes were kept same as 12.5 mm x 12.5 mm to ensure the consistency as indicated in Figure 5.3.

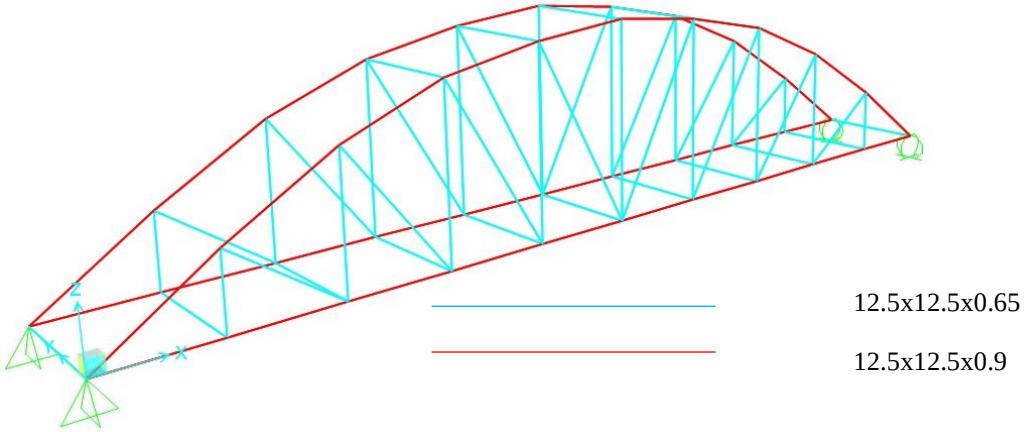

Figure 5.2: Aluminum cross-section details

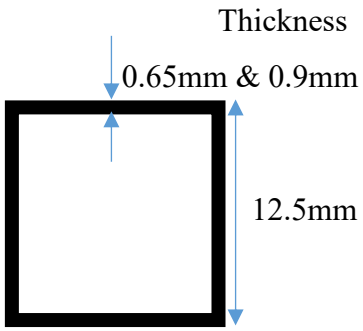

Figure 5.3: Cross-section dimensions

The first three members located at each end of a truss were identified as critical members, which does not have enough lateral bracings as shown in Figure 5.4. These members were replaced with GFAT to see the strength enhancement in the Truss B compared to that of hollow Aluminium sections (Truss A). These unbraced members have lengths of 240 mm, 230 mm and 210 mm respectively starting from the support, and have a thickness of 0.9 mm. Before testing the bridge as a whole, the effectiveness of infilling the grout into individual Aluminium members was studied. These members were tested for compression and their experimental failure loads and failure modes were compared with theoretical predictions and those are presented in the Section 5.4. The standard tensile test was done to investigate the material properties of the Aluminium sections used for the experiment and the results are presented in the Section 5.3.

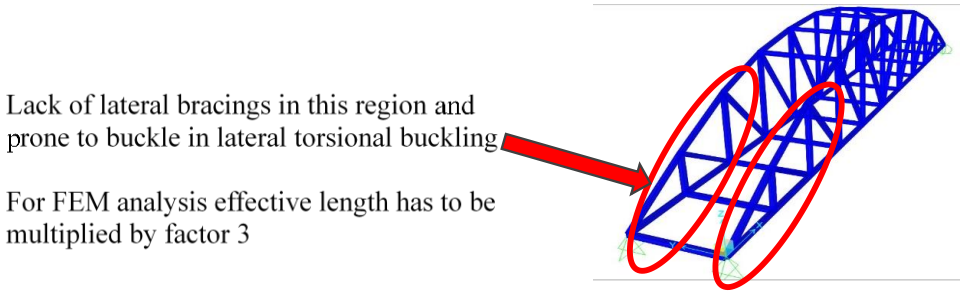

Figure 5.4: Compression members which are prone to fail in buckling

5.3. Tensile test on Aluminium sections

The tensile strength of Aluminium was determined according to ASTM E8/E8M standard specification using the "Hounsfield Tensiometer". Since these 0.65 mm and 0.9 mm thick sections could not be gripped into chucks of universal tensile testing machine, manually operated Hounsfield tensiometer was used. Dimensions of a specimen used for the tensile test is shown in Figure 5.5, while the Hounsfield tensiometer used for the testing is shown in Figure 5.6. Average tensile strength of Aluminium was found to be about 157 N/mm^2.

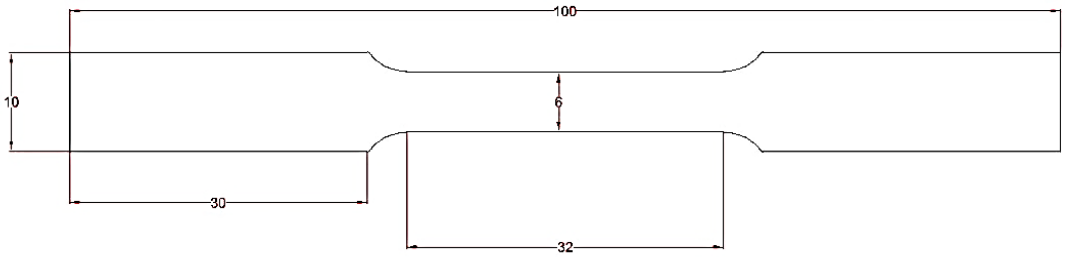

Figure 5.5: Dimensions of tested specimens (in mm)

Figure 5.6: Hounsfield Tensiometer

5.4. Compression testing of Aluminium hollow and Aluminium grout filled tubes (GFAT)

Before testing the truss as whole, critical individual members of the two trusses (length same as in the truss models) with and without infilling cement grout were also tested for compression. As shown in Figure 5.7, individual truss members prepared as for the same length as the members in the truss model were tested for compression.

Figure 5.7: Testing of individual members of model trusses

5.4.1. Theoretical prediction of the failure loads and modes

Theoretical calculations were done to predict the failure loads and failure modes of the tested Aluminium hollow and GFAT specimens. According to EN.1994.1.1 (EC 9), 12.5 mm x 12.5 mm square hollow Aluminium section having thickness of 0.9 mm is categorised into Class1, by referring to the formulae given and the shape of the stress strain diagram of the used Aluminium material (EC 9 - Section 6.1.4.2).

$$\frac{\beta}{\epsilon} = \frac{0.4\, b/t}{\sqrt{250/f_y}} \qquad \text{(Eq. 5.1)}$$

Using above equation $\beta/\in$ value is calculated as 4.4 which lies below the slenderness limit (11) defined for class 1 in EC 9 (Su M., 2017). Compression

capacities of the sections were determined by multiplying the cross-sectional area of the Aluminium by the Yield stress as given in EC 9. Buckling capacity was estimated using the Euler formula as discussed in Section 2.5.1.

Theoretical compression capacity of GFAT was calculated based on the procedure specified in the Euro code 4, by assuming the material properties of Aluminium and cement grout instead of steel and concrete respectively as followed in a previous research (Ran f., 2017). Water cement ratio for infilled cement grout was 0.65 and corresponding compressive strength was taken as 25 N/mm^2 referring to 28 days strength of the cement grout (Hari D.,2011). The Euler Buckling load of the GFAT was calculated as discussed in Section 2.5.2, by assuming the material properties of Aluminium and cement grout. The theoretical failure loads and modes obtained for the Aluminium hollow and GFAT are presented in Table 5.1.

Table 5.1: Theoretical failure loads and modes of the Aluminium hollow and GFAT

Section Type	Length (mm)	Euler's formulae (kN)	Section capacity (kN)	Critical failure load (kN)	Failure mode
Hollow	210	14.6	6.6	**6.6**	CF
	230	12.1	6.6	**6.6**	CF
	240	11.2	6.6	**6.6**	CF
GFAT	210	19.5	9.4	**9.4**	CF
	230	16.2	9.4	**9.4**	CF
	240	14.9	9.4	**9.4**	CF

It is evident that the section capacities of all the specimens are considerably less than their Euler Buckling loads, and hence both Aluminium hollow and GFAT would fail in compression (CF). Experimental failure loads and modes of those specimens are presented in Section 5.4.2.

5.4.2. Experimental failure loads and modes

The failed Aluminium hollow specimens and GFAT after testing are shown in Figure 5.8. These test specimens failed initially in compression (CF) and later buckle laterally

showing global buckling (GB). The failure modes are agreed with the theoretical predictions. Three samples were tested for each of the lengths and the average failure load was determined. A summary of the experimental failure loads and modes are presented in Table 5.2.

(a) Hollow Aluminium (b) GFAT

Figure 5.8: Samples of Aluminium specimens after testing

Table 5.2: A summary of the failure loads and modes of Aluminium hollow and GFAT

Section Type	**Length (mm)**	**Failure load (kN)**			**Average failure load (kN)**	**Failure Mode**
		S1	**S2**	**S3**		
Hollow	210	6.0	6.6	7.6	6.7	CF and GB later
	230	6.2	6.5	6.4	6.4	CF and GB later
	240	5.8	5.6	5.8	5.7	CF and GB later
GFAT	210	7.0	9.2	9.3	8.5	CF and GB later
	230	6.7	6.8	7.6	7.0	CF and GB later
	240	6.3	7.2	7.3	6.9	CF and GB later

5.4.3. Comparison of the experimental failure loads and modes with theoretical predictions

The experimental failure loads obtained for both Aluminium hollow and GFAT were compared with those obtained from theoretical calculations and those are presented in Table 5.3. According to theoretical predictions, both Aluminium hollow and GFAT fail in compression irrespective of the length. Theoretical failure loads of Aluminium hollow sections are greater than the experimental failure loads for both 230 mm and 240 mm specimens while it is slightly lesser than that for the 210 mm length specimen. The percentage change is less than 15% for all three lengths (for hollow sections), which seems to be increased with the length of the specimen.

For GFAT, experimental failure loads are quite lower than the theoretical failure loads and this trend is mostly seen for higher lengths, where the percentage change in the experimental failure load is increased from 9.6% to 26.6% when the length is increased from 210 mm to 240 mm. Overall, it seems that for higher lengths the experimental failure loads of both Aluminium hollow and GFAT are getting lower than the theoretical failure loads. This might be due to the effect of global buckling, as the predicted Euler buckling loads can be reduced due to many parameters such as eccentricity of loading, material imperfections, etc.

Table 5.3: Comparison of experimental failure loads with those obtained from the Theoritical calculations

Section Type	**Length (mm)**	**Average exp. failure load (kN)**	**Critical Theoretical failure load**	**Failure Mode**	**% change in the exp. load**
Hollow	210	6.7	6.6	CF	1.5%
	230	6.4	6.6	CF	-3.0%
	240	5.7	6.6	CF	-13.6%
GFAT	210	8.5	9.4	CF	-9.6%
	230	7.0	9.4	CF	-25.5%
	240	6.9	9.4	CF	-26.6%

5.4.4. Strength enhancement of GFAT compared to hollow Aluminium tubes

Change in the experimental failure load of both hollow and GFAT depending on the length of the specimens are illustrated in Figure 5.9. GFAT shows a noticeable strength enhancement compared to Aluminium hollow sections and this trend can be clearly seen for the 210 mm height specimens. Table 5.4 compares the strength enhancement of GFAT compared to Aluminium hollow sections as reported from the experiment as well as predicted from the theoretical calculations. It is evident that the strength enhancement of GFAT seen from the experiment (9% - 27%) is quite lower than that predicted from theoretical calculations (42.4%).

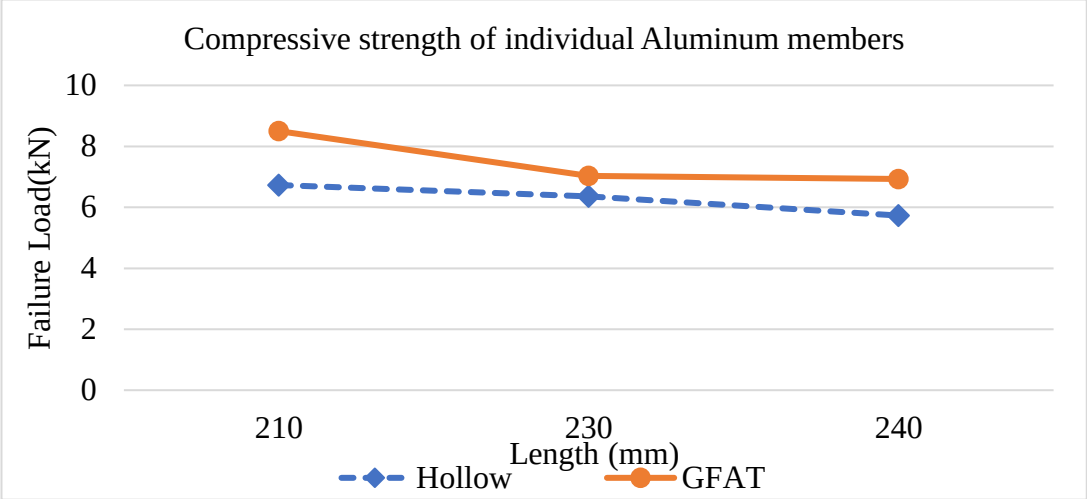

Figure 5.9: Compressive strength of individual Aluminum members

Table 5.4: Comparison of strength enhancement GFAT compared to Aluminium hollow sections

Length (mm)	Experimental			Theoretical		
	Failure Load (kN)		% increase in GFAT	Failure Load (kN)		% increase in GFAT
	Al hollow	GFAT		Al hollow	GFAT	
210	6.7	8.5	26.9%	6.6	9.4	42.4%
230	6.4	7.0	9.4%	6.6	9.4	42.4%
240	5.7	6.9	21.1%	6.6	9.4	42.4%

Based on the information presented in Section 5.4, it can be said that the GFAT shows a noticeable strength enhancement compared to Aluminium hollow sections similar to that observed with CFST in the Chapter IV. Hence, the use of GFAT to strengthen the model bridges instead of CFST for the experimental program can be justified.

5.5. Laboratory testing of model bridges

The selection of the bridge type and the dimension of the bridge were discussed in the Sections 5.1 and 5.2 in this chapter. A Parker truss type bridge with a top chord having a shape of bending moment diagram of a simply supported beam was selected. For the scaled down testing, a real truss having a length of 20 m, maximum height of 4 m and width of 2 m was considered. The scale was set to 1:10 and hence 2 m span model bridge was constructed with a maximum height of 0.4 m and width of 0.2 m. Figure 5.10 illustrates the side view of the model bridge used for the testing, while Figure 5.11 illustrates the sectional view that.

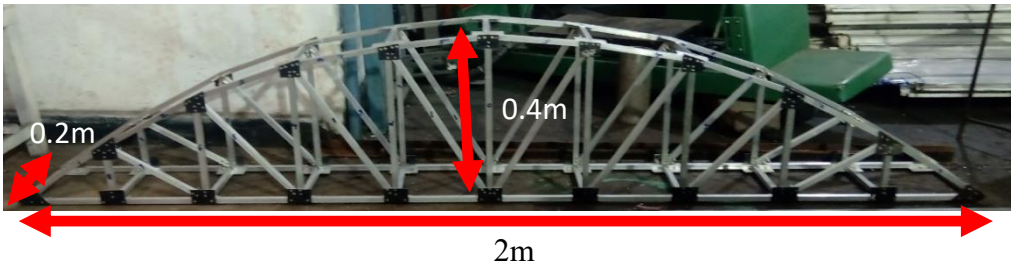

Figure 5.10: Side view of the bridge model

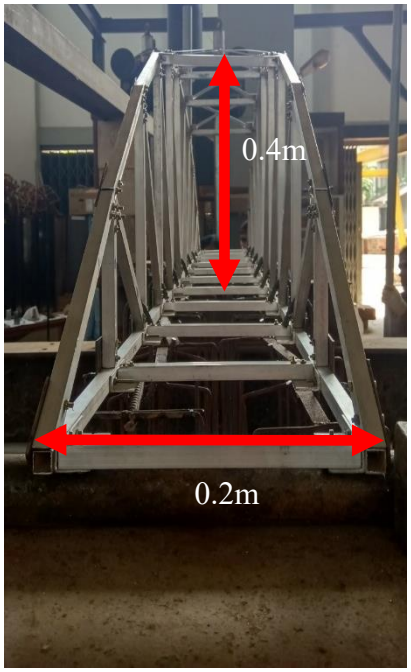

Figure 5.11: Sectional view of the bridge model

First three members close to the support from each end of the truss cannot be braced laterally to meet the minimum head room requirement. These members are highlighted in Figure 5.12. Initially, a truss made out of Aluminium hollow sections (Truss A) was tested. Later, a truss having identical dimensions was made by replacing the unbraced top chord members with GFAT, while using identical Aluminium hollow sections for the remaining members (Truss B). Steel gusset plates of 0.2 mm thickness were used and 2 nuts were used to connect each member to a gusset plate. 3 mm steel nuts and bolts were used to connect all the compression and tension members along with the concrete infilled members.

When above truss is simply supported in both ends and a uniformly distributed load is applied, bottom chord will be subjected to tensile force which is increased

Figure 5.12: Concrete grout infilled members in truss B

towards the centre, while the top chord will be subjected to compressive force which is increased towards the supports. Horizontal bracings in the experimental model were not provided because in actual model more than 2.5 m clearance must be provided according to RDA design manual. Therefore, first three horizontal bracings had to be avoided when building the model and it is the most critical point in this study.

5.5.1. Predicting the theoretical failure loads of the bridge models

Selected truss bridges were modelled using SAP2000 software package and material properties were defined as per those used for the theoretical calculations. Two FEM models were developed, in which one consists with only hollow sections (Truss A) and the other consists with identical sections, but using GFAT for the unbraced top chord members (Truss B). For the preliminary analysis, Truss B was modelled in SAP2000 using an equivalent section for GFAT.

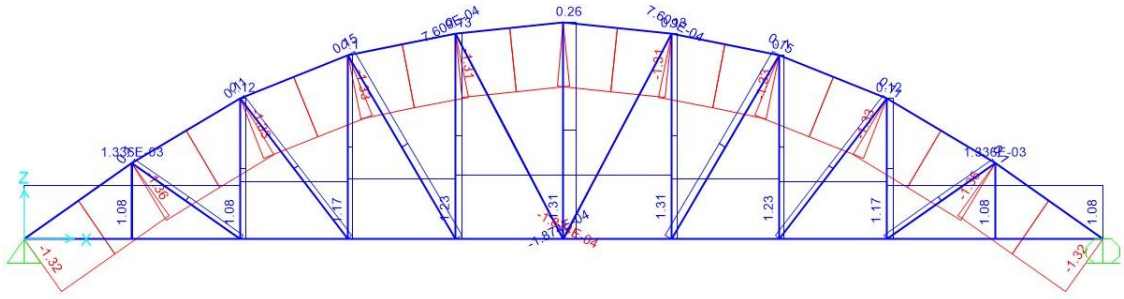

Figure 5.13: Axial force diagram of Truss A at the theoritical failure load of 2.98 kN

The effective length of the unbraced top chord members in the lateral direction is assumed to be about 680 mm, while that of individual unbraced members in the plane of the truss are about 240 mm, 230 mm and 210 mm respectively from the end of the truss. The sectional capacity of the 12.5 mm x 12.5 mm size Aluminium section having 0.9 mm thickness was found to be about 6.6 kN irrespective of the length as stated in Section 5.4.1. When the length is increased to 680 mm, the Euler Buckling load of the Aluminium hollow section was reduced to 1.39 kN, which is less than the compression capacity of the section and hence will become the theoretical failure load of the member. The loads applied at the nodal points of the bridge were increased until the critical failure load of 1.39 kN is obtained in at least one of the unbraced top chord members. The total load applied on the FE model at this instance was considered as

the theoretical failure load of the truss bridge. The theoretical failure load of the Truss A was found to be about 2.98 kN, and the axial force diagram of the truss under this load is shown in Figure 5.13.

For a GFAT section having a length of 680 mm, overall size of 12.5 mm x 12.5 mm and an Aluminium thickness of 0.9 mm, the section capacity was found to be about 9.4 kN as discussed in Section 5.4.1. The Euler buckling failure load of this member was found to be about 1.86 kN, and hence will become the theoretical failure load of the member. Similar to the analysis done for truss A, the total theoretical failure load of the Truss B was determined using the SAP2000 model. It was found to be about 3.81 kN, and the axial force diagram of the truss under that load is shown in Figure 5.14.

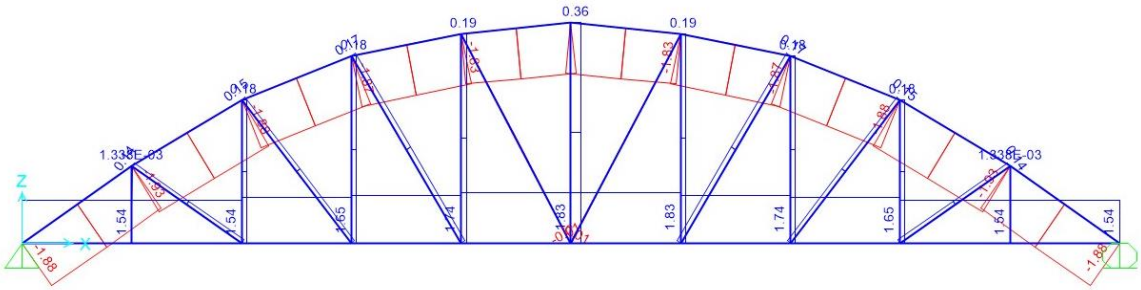

Figure 5.14: Axial force diagram of Truss B at the theoritical failure load of 3.81 kN

5.5.2. Experimental model loading

Loading cages each weighs 2 kg and concrete cubes having an average weight of 8.1 kg were used to load two experimental truss models. A cage could bear 8 number of concrete cubes having dimension of 150 mm x 150 mm x 150 mm. Truss A had a weight of 3.9 kg and truss B was 4.4 kg. One end of the truss was pin supported and other end was roller supported as shown in Figure 5.15.

Figure 5.15: Support conditions of tested trusses

When testing the bridge, it was planned to apply nodal gravity forces at the connections considering the practical applicability.14 nodal forces were applied on the bottom chord joints. Loading sequence was planned as explained in Figure 5.16 to minimize the eccentric effects to truss bridge models.14 nodal loads were simulated by 14 cages in both sides of the bottom chords of trusses. Loading the bridge during the experiment is shown in Figure 5.17. Four dial gauges were used to measure the deflection at the critical points in the truss as shown in Figure 5.18. One dial gauge was set at top of the bridge to measure vertical deflection, another gauge to measure lateral deflection at the middle of the truss and two gauges to measure lateral deflection of unbraced top chord members.

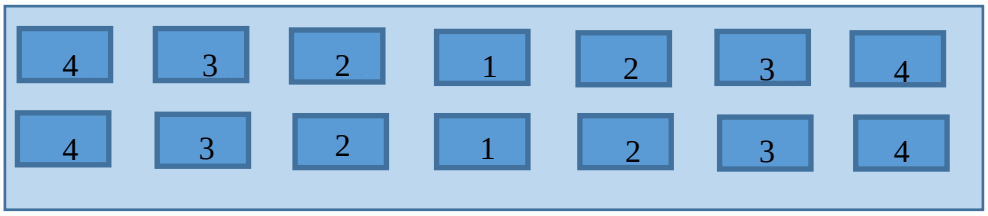

Figure 5.16: Loading sequnce

Figure 5.17: Loading of truss bridge in the laborotary

Figure 5.18: Dial gauge setup

5.5.3. Experimental test results

Two trusses were tested as described above. Dial gauge readings were recorded, and finally the failure load and failure modes were observed. Truss A failed as in the Figure 5.19 yielding a total failure load of 433 kg (4.25 kN), which is higher than the theatrically predicted a failure load of 2.98 kN. “C” shape failure mode was observed along the span. Unbraced top chord members failed laterally when applying the loads uniformly along the span as shown in the Figure 5.21.

Truss B also showed a “C” shaped failure mode along its span showing a behaviour similar to the truss A, as elaborated in Figure 5.20. ‘’However, the failure load was increased to 514 kg (5.04 kN), which is quite higher than the theoretical failure load which is about 3.81 kN. As Figure 5.22 shows, truss initially deformed laterally and with the failure of the unbraced members in the top, it shrunk into the bay and finally achieved a “C” shape.

Figure 5.19: Failure mode of truss A

Figure 5.20: Failure mode of truss B

The reasons for the failures of the two trusses were investigated by a thorough visual inspection of all the elements of the trusses. An unbraced member located in the top chord had critically damaged than the other members. As shown in Figure 5.21, a tearing had occurred near a bolt hole of the top chord member connection due to the buckling occurred in lateral direction. As predicted from the theoretical analysis, unbraced top chord members have failed in lateral buckling. As a result, after applying 433 kg (4.25 kN) load, truss A has lost its load carrying capacity and failed in buckling.

Figure 5.21: Initiating point of the crack of truss A

As in the truss A, top chord members of which were prone to fail in lateral buckling failed first as shown in Figure 5.22. When examining the failed members of the truss B in the top chord, it was identified that the damage has initiated in the same place as in truss A, but slightly downward to the connection as shown in Figure 5.22. The unbraced top chord members failed in lateral buckling. After applying a load of 514 kg (5.04kN), an unbraced top chord member has teared and lost its capacity against lateral buckling. A comparison of failure modes of Truss A and B is further illustrated in Figure 5.23, according to which both show a similar failure pattern.

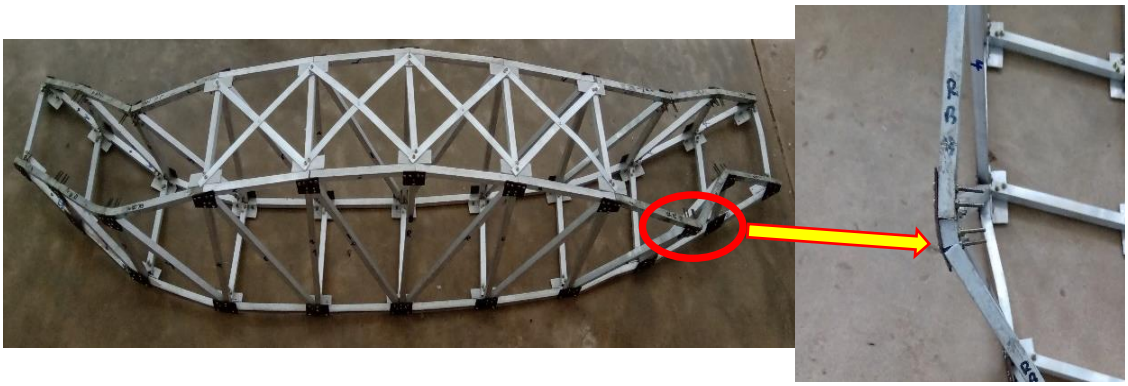

Figure 5.22: Initiating point of failure for the truss B

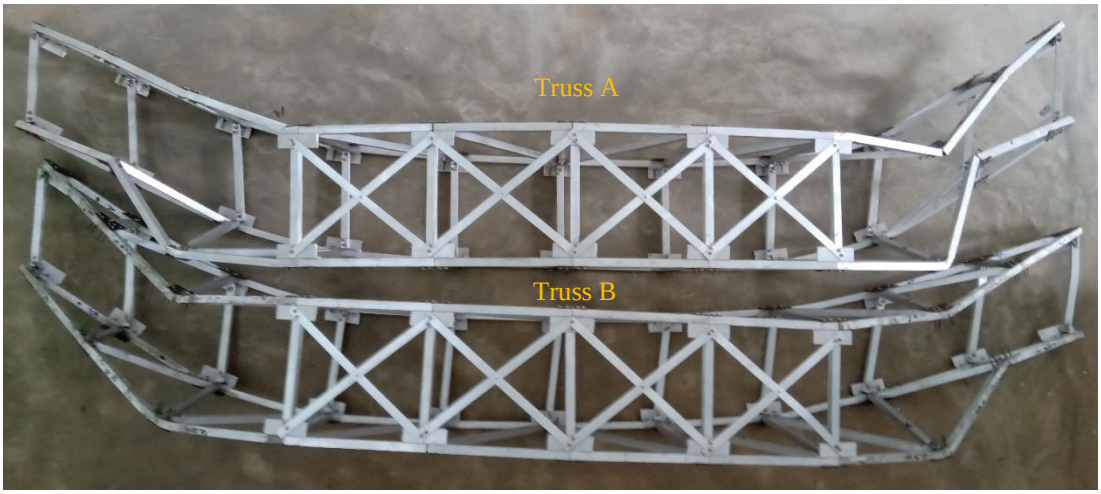

Figure 5.23: Comparison of failure modes of truss A and B

Load vs. deflection curves obtained from different dial gauges for truss A and B are presented in the Figures 5.24 and 5.25 respectively. Two trusses have followed the same failure pattern and it can be considered to support the fact that loading has been applied in the same way to both of these trusses. Vertical gauge at the middle top most point of the top chord showed a linear increment of deflection in both trusses. Also, the horizontal deflection at the middle of the truss in the top most point of top chord has showed a diversion of the direction of deflection. However, at the end top chord has deflected laterally and failed. Horizontal dial gauges which were set to measure horizontal deflection in the area of focused have deflected slowly in the first few layers of loading and suddenly increased the deflection. Top chord members which are prone to fail in lateral buckling also followed a deviation in the direction of deflection.

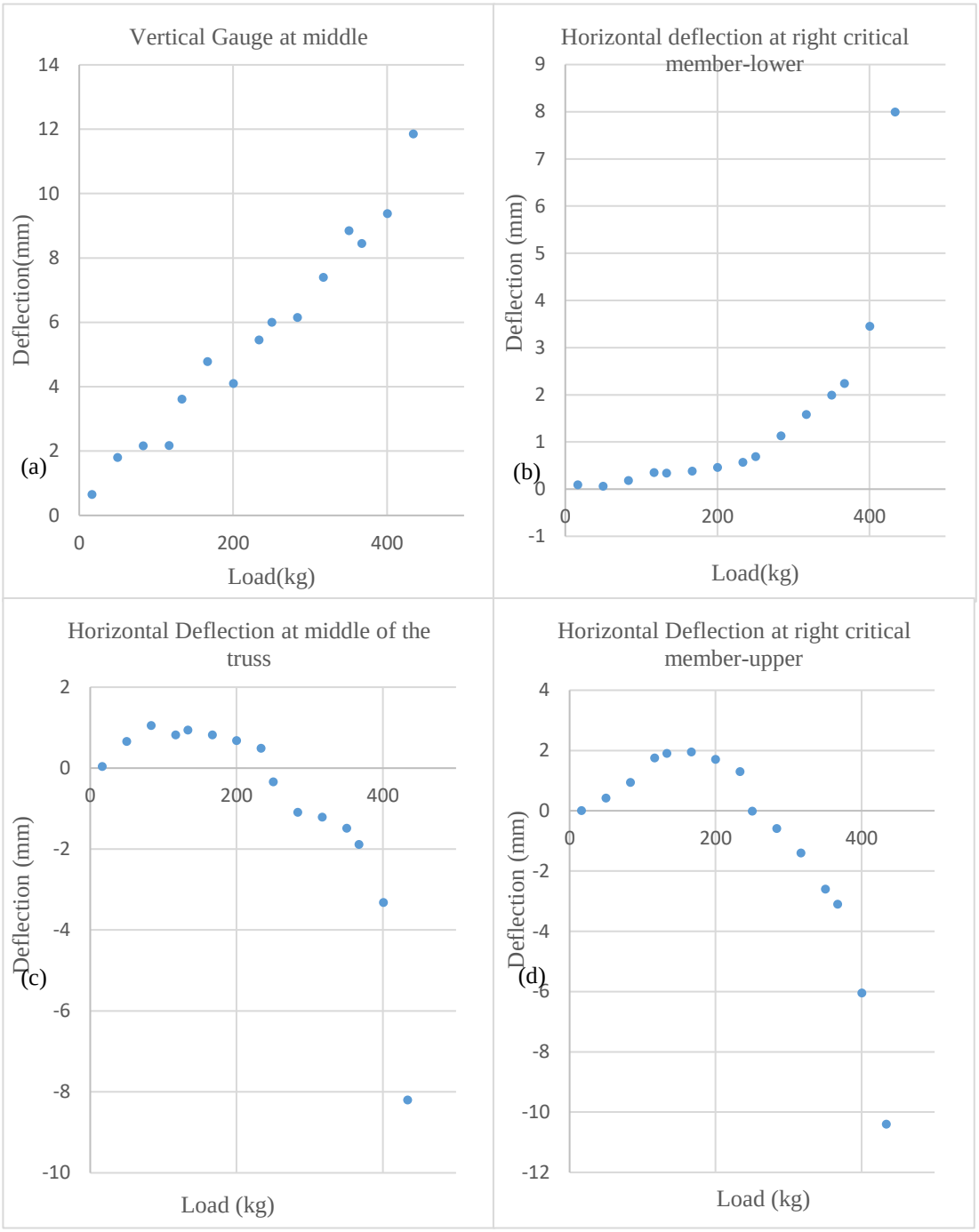

Figure 5.24: Load vs. Deflection curves obtained for different dial gauges for truss A

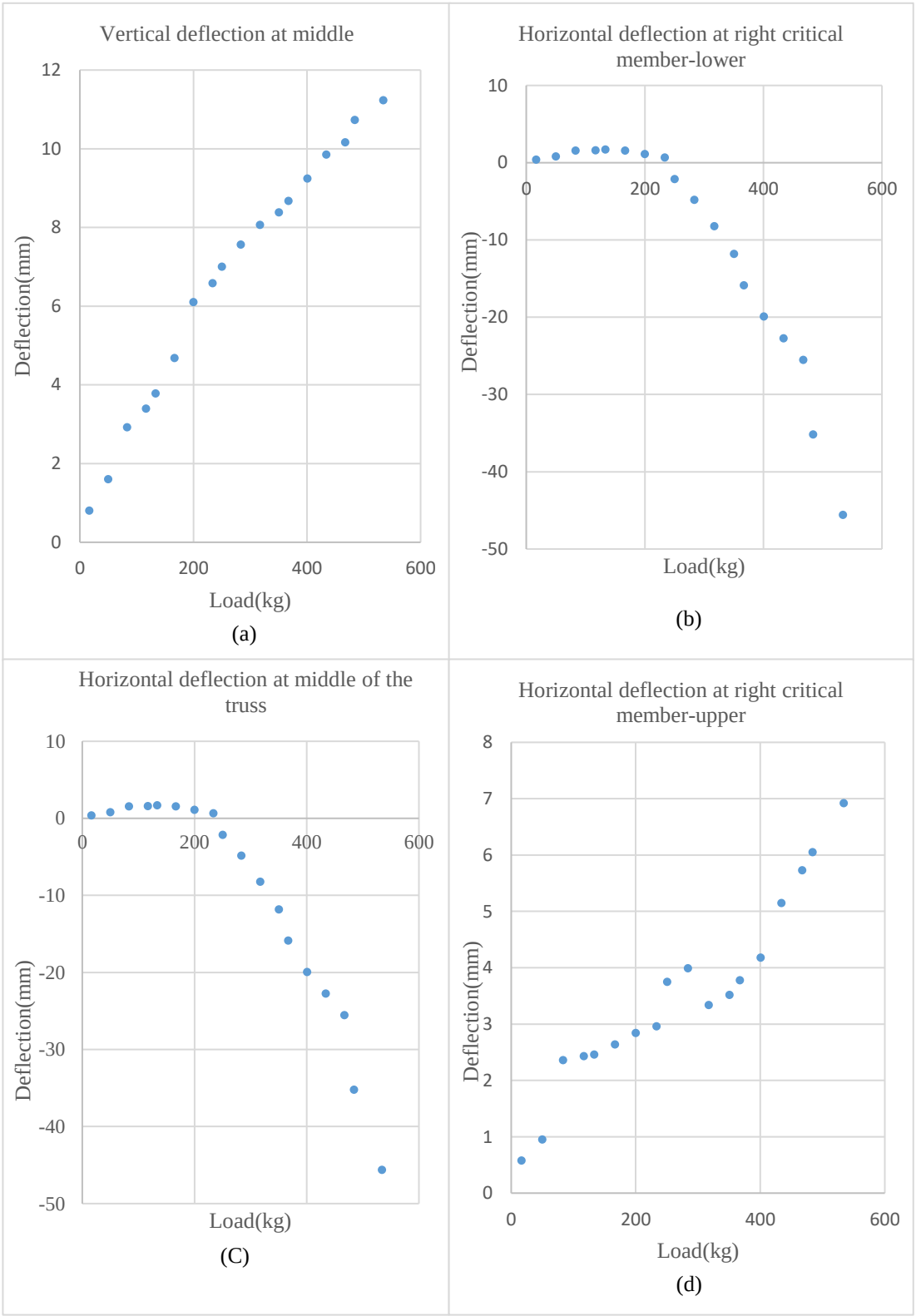

Figure 5.25: Load vs. Deflection curves obtained from different dial gauges for truss B

5.5.4. Comparison of the experimental results with the theoretical predictions

The failure loads obtained in the experiments were applied to the FE models of the both trusses A and B, and the member forces getting in the critical unbraced members under actual failure loads were obtained. Axial force diagrams obtained for the Trusses A and B under their experimental failure loads are shown in Figure 5.26 and Figure 5.27 respectively. The maximum axial forces obtained in the unbraced top chord members were found to be 1.93 kN and 2.41 kN in the Trusses A and B respectively.

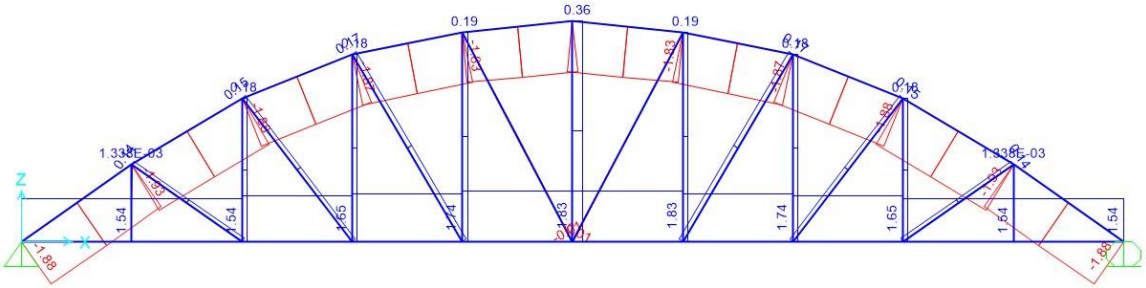

Figure 5.26: Axial force diagram of Truss A at experimental failure load of 4.25 kN

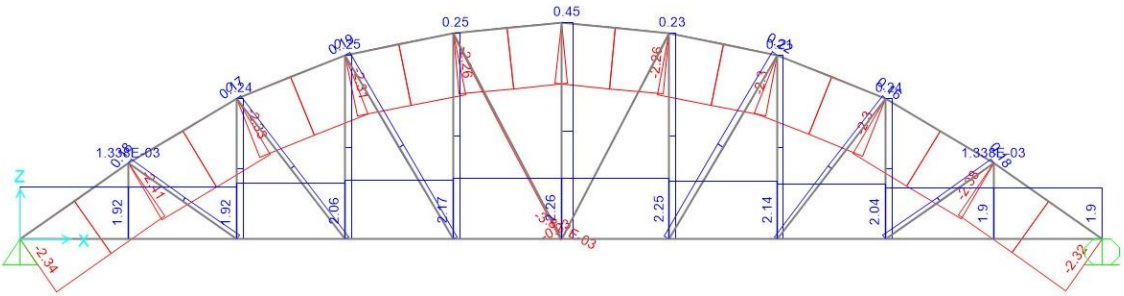

Figure 5.27: Axial force diagram of Truss B at experimental failure load of 5.04 kN

Table 5.5 compares the theoretical failure loads of the critical members and the entire truss for those obtained from the experiments for both of the Trusses A and B. Theoretical failure load of the critical (unbraced) members were obtained based on the Euler buckling load by considering the unbraced length as 680 mm. Theoretical failure load of the truss was obtained by increasing the loads applied on the 14 nodes in the FE model (similar sequence of loading used for the testing). Experimental failure load of the truss was the collapse load of the truss during the experiment. Experimental

failure load of the critical member was obtained by applying the actual failure load to the FE model. According to Table 5.5, it is evident that the experimental failure loads are noticeably higher than the theoretical failure loads and this trend is more visible in Truss A than Truss B. In both of the trusses, percentage increase in the experimental failure load of the critical member is very much close to the percentage increase in the total failure load.

Table 5.5: Comparison of theoretical and experimental failure loads of the trusses

Truss Type	**Critical member force/ Total failure load**	**At the theoretical failure load of the critical member**	**At the experimental failure load of the truss**	**% increment in the Exp. load**
A	Critical member force (kN)	1.39	1.93	38.8%
	Total failure load of the truss (kN)	2.98	4.25	42.6%
B	Critical member force (kN)	1.86	2.41	29.6%
	Total failure load of the truss (kN)	3.81	5.04	32.3%

A few reasons were identified for the increment in the experimental failure loads compared to the theoretical predictions. When calculating the theoretical failure load of the unbraced members, Euler buckling equation was used by assuming unbraced length in the lateral direction as 680 mm, and pin condition at both ends. However, in the actual bridge, the unbraced top chord members get some lateral stability with the presence of steel gusset plates, vertical and diagonal members at the intermediate points. There will be some fixity at the ends of the unbraced members and hence practically it will be less than 680 mm. Even though member connections are modelled as pin ended members in the FE model, actual connection does not act as pin ended connection with the presence of two bolts and the steel gusset plate, which add extra rigidity to the connections. These could be the reasons of getting a higher failure load in the experiment than the theoretical predictions. On the other hand, even the collapse load was noted in the experiment, lateral buckling of the top chord might have happened at an earlier load as seen from the deflection measurements.

5.5.5. Strength enhancement in the truss with GFAT (Truss B) compared to that with Aluminium hollow sections (Truss A)

Table 5.6 compares the failure loads (both theoretical and experimental) of the critical members and the truss as a whole in both Truss A and Truss B. According to both theoretical and experimental investigations, it is clear that the failure load increment in the truss is less than that of individual members. With the introduction of the GFAT for the unbraced top chord members, it was expected to achieve a 27.9% strength enhancement theoretically, but that achieved in the experiment was about 18.6% which is quite less than the theoretical value. However, it should be noted that still the experimental failure loads are greater than the theoretical predictions in both truss A and B. Overall, it is evident that there is a noticeable strength enhancement in Truss B compared to Truss A, highlighting the effectiveness of infilling the unbraced top chord members in a variable height truss types towards their strength enhancement.

Table 5.6: Comparison of failure loads between truss A and B

Theoretical/ Experimental	**Critical member force/ Total failure load**	**Truss A**	**Truss B**	**% increment in Truss B**
Theoretical	Critical member force (kN)	1.39	1.86	33.8%
	Total failure load of the truss	2.98	3.81	27.9%
Experimental	Critical member force (kN)	1.93	2.41	24.9%
	Total failure load of the truss	4.25	5.04	18.6%

5.6. Chapter Summary

This chapter investigated the applicability of infilled sections to enhance the strength of the variable height truss type bridges. Aluminium was used instead of steel to construct the model bridges to lower the failure loads which can be applied with in the laboratory. Aluminium sections were filled with cement grout instead of concrete by considering the practical construction of those without getting honeycombs.

Initially, the behavior of Aluminium hollow and Grout Filled Aluminium Tubes (GFAT) was studied under compression loading. According to theoretical predictions, both Aluminium hollow and GFAT fail in compression irrespective of the length. Theoretical failure loads of Aluminium hollow sections are greater than the experimental failure loads for both 230 mm and 240 mm specimens while it is slightly lesser than that for the 210 mm length specimen. The percentage change is less than 15% for all three lengths (for hollow sections), which seems to be increased with the length of the specimen.

For GFAT, experimental failure loads are quite lower than the theoretical failure loads. This could be mostly seen for higher lengths, where the percentage change in the experimental failure load is increased from 9.6% to 26.6% when the length is increased from 210 mm to 240 mm. Overall, it seems that for higher lengths the experimental failure loads of both Aluminium hollow and GFAT are getting lower than the theoretical failure loads. This might be due to the effect of global buckling, as the predicted Euler buckling loads can be reduced due to many parameters such as eccentricity of loading, material imperfections, etc.

GFAT shows a noticeable strength enhancement compared to Aluminium hollow sections and this trend can be clearly seen for the 210 mm height specimens. It is evident that the strength enhancement of GFAT seen from the experiment (9% - 27%) is quite lower than that predicted from theoretical calculations (42.4%).

A variable height Parker truss type was used for the study. Initially, a truss was made by using only Aluminium hollow sections (Truss A), and then an identical truss was made (Truss B) by replacing the unbraced top chord members with GFAT. Experimental failure loads are noticeably higher than the theoretical failure loads and

this trend is more visible in Truss A than Truss B. In both of the trusses, percentage increase in the experimental failure load of the critical member is very much close to the percentage increase in the total failure load.

Failure load increment in both trusses is less than that of individual members. With the introduction of the GFAT for the unbraced top chord members, it was expected to achieve a 27.9% strength enhancement theoretically, but that achieved in the experiment was about 18.6% which is quite less than the theoretical value. However, still the experimental failure loads are greater than the theoretical predictions in both truss A and B. Overall, it is evident that there is a noticeable strength enhancement in Truss B compared to Truss A, highlighting the effectiveness of infilling the unbraced top chord members in a variable height truss types towards their strength enhancement.

CHAPTER VI

6. NUMERICAL ANALYSIS

6.1. Introduction

In this research FEM was used for two purposes. FEM was used to model the behaviour of the CFST subjected to compression, and also for the design of the truss bridge. Calibrated properties of the CFST is required to design the truss bridge. Therefore, modelling of the CFST subjected to the compression was carried out first. Also, hollow steel tubes were modelled in FEM software to examine the capacity and failure mode.

6.2. FEM Software

There are many FEM software that are used for finite element modelling such as ANSYS, ABAQUS CAE and MIDAS FEA etc. ABAQUS CAE was used in this research to model the experiment carried out at the laboratory. Midas Civil was selected as the most suitable FEM software to model the bridge because it has updated features to model a truss bridge more precisely incorporating the latest design codes.

6.3. FEM Details

Two materials were defined in the FE model which are, concrete infill and the confining steel tube. In order to idealize the accurate behaviour of the CFST column, it is essential to define properties of the both materials correctly. Stress- strain curve details of both materials were accounted to define material properties.

6.3.1. Concrete

Non-linear concrete properties were used. Grade 40 concrete was used to model the CFST tubes and its ultimate compressive strength and ultimate tensile strength were obtained from compressive strength test for 150 mm x 150 mm x 150 mm square test cubes. These results are presented in Table 6.1.

Table 6.1: Propertise of self compacting grade 40 concrete

Ultimate compressive strength	42.9 N/mm^2
Ultimate tensile strength	2.55 N/mm^2

As the failure will occur in plastic state, a plasticity model was simulated. Mainly, there are three types of plasticity-based crack models for concrete and they are concrete smeared cracking model, cracking model for concrete, and concrete damaged plasticity model (User, n.d.). Among these three models, Concrete damaged plasticity model has been proved successful in many concrete simulations. Therefore, in this study a concrete damaged plasticity model has been selected which can represent complete inelastic behaviour in tension and compression including damage characteristics. Both elastic and plastic properties used for this study are tabulated in the Table 6.2. given below.

Table 6.2: Mechanical properties of grade 40 concrete (Sümer & Aktaş, 2015)

Density (ρ)	2400kg/m^3
Elastic modulus (E)	25.4 GPa
Poisson ratio (υ)	0.2
fb0/fc0 (ratio of the strength in the biaxial state to the strength in the uniaxial state)	1.16
Eccentricity (e)	0.1
K (porosity)	0.667
Dilation angle	37°
Viscosity	0

Concrete Damage Plasticity Model

The concrete plasticity model considers two main failure mechanisms. Compressive crushing and tensile cracking models are those two mechanisms. In this model, to define the stress-strain relation of concrete, it is required to input the stresses (σ_c / σ_t) and inelastic strains ($e^{/}$), cracking strains (εt^{-ck}) and corresponding damage properties (d_c / d_t).

Compressive stress-strain Relationship

The inelastic strains can be calculated using total strain (ε_c), and elastic strain corresponding to the undamaged material (ε_{oc}^{el}) by following equation (1).

$$\varepsilon_c^{-in} = \varepsilon_c - \varepsilon_{oc}^{el} \quad (1)$$

Where $\varepsilon_{oc}^{el} = \sigma_c / E_0$ (E_0. Initial tangential modulus)

The plastic strain values will be calculated using following equation (2) by the software itself.

$$\varepsilon_c^{-pl} = \varepsilon_c^{-in} - \frac{d_c}{(1-d_c)} \frac{\sigma_c}{E_0} \quad (2)$$

The compressive damage parameter d_c is the ratio between the inelastic strain (ε_c^{-in}) and total strain (ε_d) The complete compressive stress-strain relationship of concrete including the damage properties is illustrated in Figure 6.1.

Tension stiffening Relationship

The tensile cracking strain can be calculated using total strain (ε_t), and elastic strain corresponding to the undamaged material (ε_{ot}^{el}) by following equation (3).

$$\varepsilon_t^{-ck} = \varepsilon_t - \varepsilon_{ot}^{el} \quad (3)$$

Where $\varepsilon_{ot}^{el} = \sigma_t / E_0$

The plastic strain values are calculated using following equation (4) by the software itself.

$$\varepsilon_t^{-pl} = \varepsilon_t^{-in} - \frac{d_t}{(1-d_t)} \frac{\sigma_t}{E_0} \quad (4)$$

The tensile damage parameter d_t is the ratio between the cracking strain (ε_t^{-ck}) and total strain (ε_d). The complete tensile stress-strain relationship model of concrete including the damage properties (tension stiffening relationship) is illustrated in Figure 6.1.

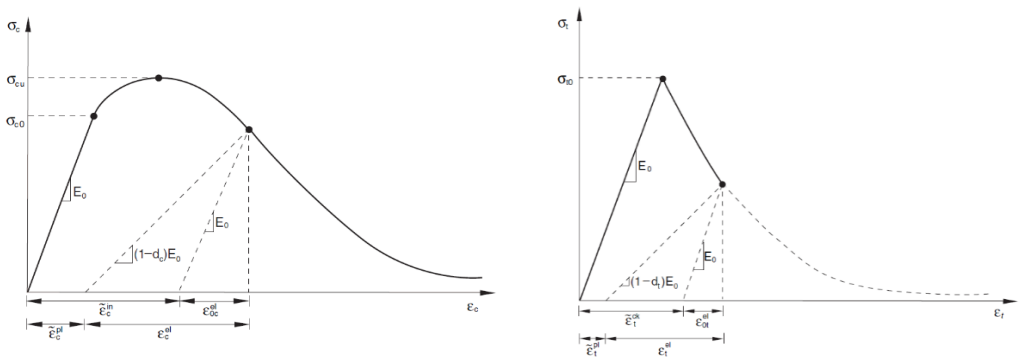

Figure 6.1: Response of concrete to uniaxial loading in compression and tension

Simplified Concrete Damage Plasticity Model

To develop the compressive stress-strain relationship, a method by Hsu & Hsu, (1994) and Wahalathantri et al. (2011) was used in this study. This numerical model is used to calculate the compressive stress values (σ_c) from the yield point (0.5 σ_c) to 0.3 σ_c in the descending portion using equation (5). And the developed strain-stress curve by Wahalathantri et al. is illustrated by Figure 6.2.

$$\sigma_c = \frac{\beta(\frac{\varepsilon_c}{\varepsilon_0})}{\beta - 1 + \frac{\varepsilon_c}{\varepsilon_0}} \sigma_{cu} \tag{5}$$

Where,

β - shape of the stress-strain diagram

ε_0 – strain at peak stress

and β, and ε_0 are given by equation (6) and (7) respectively.

$$\beta = \frac{1}{1 - [\frac{\sigma_{cu}}{\varepsilon_0 E_0}]} \tag{6}$$

$$\varepsilon_0 = 8.9 \times 10^{-5} \sigma_{cu} + 2.114 \times 10^{-3} \tag{7}$$

Where,

$$E_0 = 124.31\, \sigma_{cu} + 3283.12 \tag{8}$$

Note: σ_c , σ_{cu} , E_0 in equations (3), (4), an (5) are in kip/in^2.

The tension stiffening model developed by Nayal & Rasheed (2006) and Gilbert & Warner (1978) was modified for ABAQUS by Wahalathantri et al. (2011), and it was used to derive the complete strain-stress behaviour of the concrete in tension. The modified Tension stiffening model is illustrated in Figure 6.3 below.

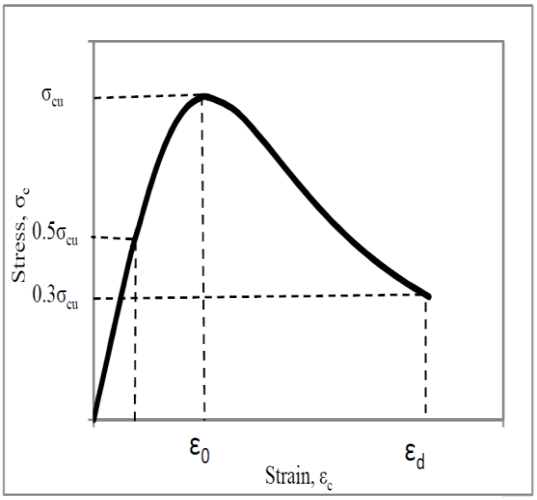

Figure 6.2: Modified Compressive stress-strain model for ABAQUS

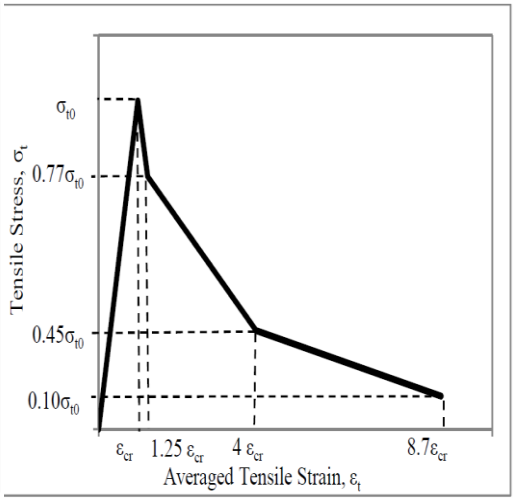

Figure 6.3: Modified Tension stiffening model for ABAQUS

The derived stress-strain behaviour for both tension and compression are tabulated below.

Table 6.3: Theoretically obtained Compressive parameters using Wahalathantri's model (Wahalathathri et.al, 2011)

Stress (Pa)	**Inelastic strain**
0	0.00E+00
1.97E+07	7.50E-04
2.09E+07	8.00E-04
2.52E+07	1.00E-03
3.83E+07	2.00E-03
3.96E+07	3.00E-03
3.59E+07	4.00E-03
3.13E+07	5.00E-03
2.71E+07	6.00E-03

2.35E+07	7.00E-03
2.06E+07	8.00E-03
1.82E+07	9.00E-03
1.63E+07	1.00E-02
1.46E+07	1.10E-02
1.33E+07	1.20E-02
1.21E+07	1.30E-02
1.11E+07	1.40E-02
1.03E+07	1.50E-02

Table 6.4: Theoretically obtained Tensile parameters using Wahalathantri's model (Wahalathanthri et.al, 2011)

Stress (Pa)	**Inelastic strain**
3.00E+06	1.10E-04
2.31E+06	1.38E-04
1.35E+06	4.40E-04
3.00E+05	9.57E-04

6.3.2. Steel

Material properties of steel were determined by steel coupon test. Young's modulus of the steel was determined as 200 GPa according to the testing results. Poisson's ratio of the steel was used as 0.3 and the density was used as 7800kg/m^3. Steel sections were modelled as a linear elastic material by using the stress-strain curve obtained from the steel coupon test.

6.3.3. Parts

FE model mainly includes three parts; concrete cylinder, steel tube and rigid plates. Each part modelled separately and sections were assigned. Solid element (C3D8R) was used for concrete fill and shell element (S4R) was used to model steel tube. R3D4 elements were used for the rigid plate.

6.3.4. Interaction

Surface-to-surface contact was used to model the interaction between concrete and steel interface. Since the stiffness of steel is higher than concrete, inner surface of the steel tube was simulated as the master surface and the concrete surface was simulated as the slave surface. No slip conditions were assigned between steel and concrete surface because they are loaded simultaneously.

When defining normal behaviour, hard contact type was assigned, and it avoids material penetrate into each other under compression. In tangential behaviour, friction formulation selected as Lagrange multiplier model. Friction coefficient was defined as 0.4 initially according to literature (Lidong et. at, 2018). It was calibrated with experimental results.

6.3.5. Loading and Boundary Conditions

Bottom end of the column was modelled as a pin support while the top end was modelled as a roller support, allowing the movement only in longitudinal (vertical) direction. Movement along the longitudinal direction was allowed at the top end of the section for the purpose of simulating the experimental support conditions.

For loading, there are two methods available in ABAQUS; load control method and displacement control method. Load control method was used for the model to simulate actual loading scenario performed in experimental testing. Load was applied at a specific rate to the CHS. To simulate loading condition, load was applied to the nodes of the loading end in steel.

6.4. Results of FEM

Using the ABAQUS CAE software, nonlinear buckling analysis was performed for the hollow and CFST tubes. The most preferable analysis type has to be decided to get a better representation of the experimental failure shape for hollow and CFSTs. In linear buckling analysis, there are advantages such as less processing time, easy to define appropriately, no convergence problems and no experience required to define the problem, but at the same time it has disadvantages such as in many cases the outcome may be wrong and inability to account for the material and geometrical non linearity. Considering the disadvantages of the linear buckling analysis as

discussed above, nonlinear buckling analysis was used in this research. It yields more precise results with the advantages such as ability to animate instability failure process, providing a robust outcome and ability to account for nonlinearity of material. Even though it requires more experience and computational time, it converges the problem precisely.

Nonlinear analysis was performed to simulate the failure loads and the modes observed in the experiments. For hollow GI tubes, first local buckling phenomena was demonstrated and later compression failure was observed for 1 m and 1.5 m length 1.2 mm thick sections. Similar failure patterns could be seen from the FE analysis and presented in Figure 6.4.

In the specimens (1.2 mm thick 1 m and 1.5 m members) failed in local buckling, the failure could be seen at the bottom most point in the experiment. However, in the numerical model the failure could be seen at an upper level of the tube (refer Figure 6.4). This might be due to the simplifications used in the FE model when simulating the support conditions. However, failure modes of 1 m and 1.5 m length 1.2 mm thick members confirmed the local buckling failure mode as in the experimental testing (refer Figure 6.5).

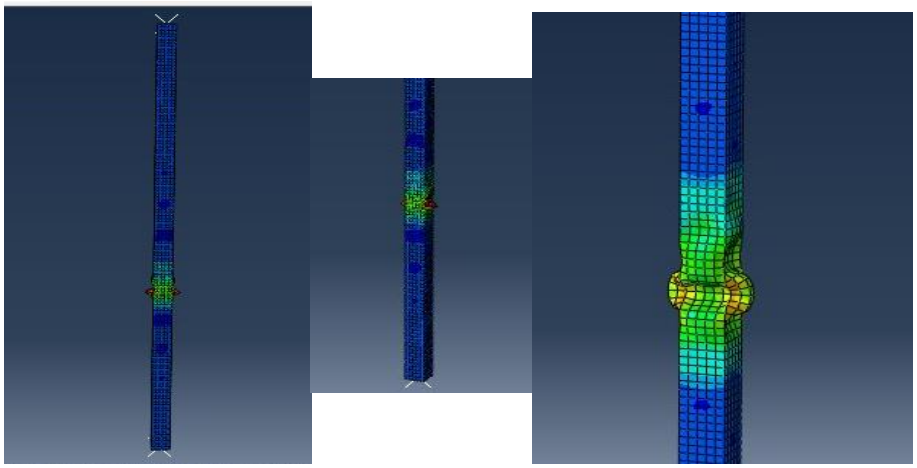

Figure 6.4: Failure modes of the Class 4 hollow GI sections (local buckling) as seen from numerical analysis

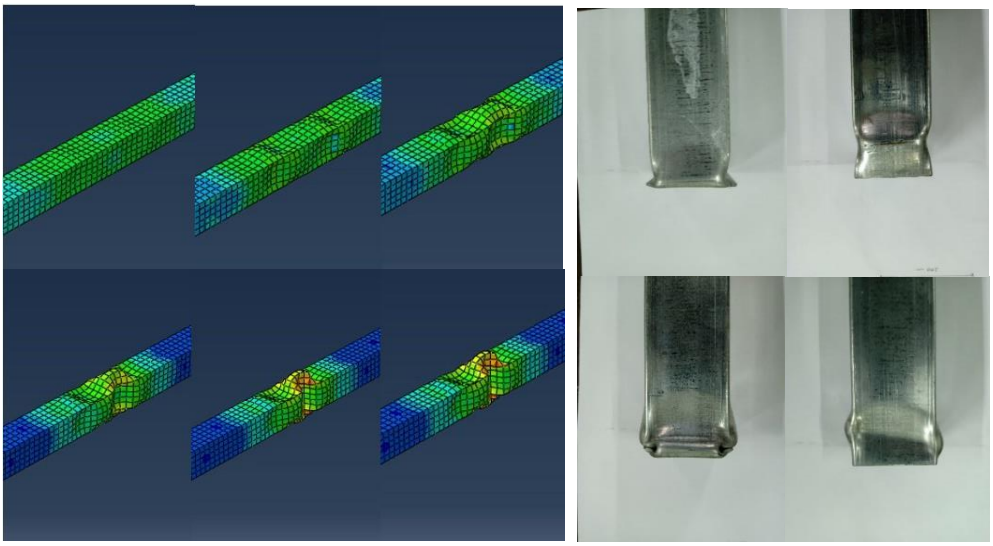

Figure 6.5: Comparison of failure modes of hollow GI sections (1.2 mm thick) between experimental and numerical results

Hollow GI sections having thicknesses 1.4 mm, 1.6 mm, 2.0 mm and all the 1.0 m length CFST sections failed in compression initially and with further application of loading global buckling was generated. Comparison of failure modes with those obtained from their numerical models are presented in Figures 6.6 and 6.7 respectively.

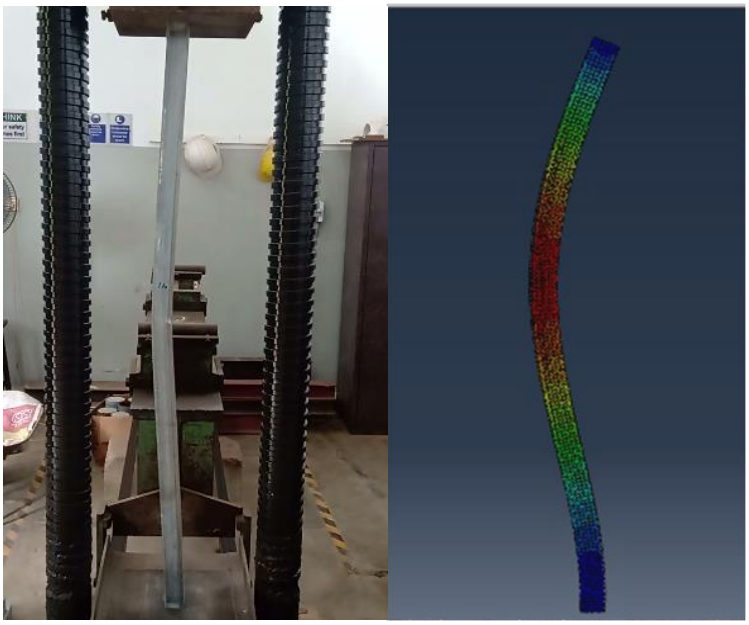

Figure 6.6: Comparison of failure modes of hollow GI sections between experimental and numerical results

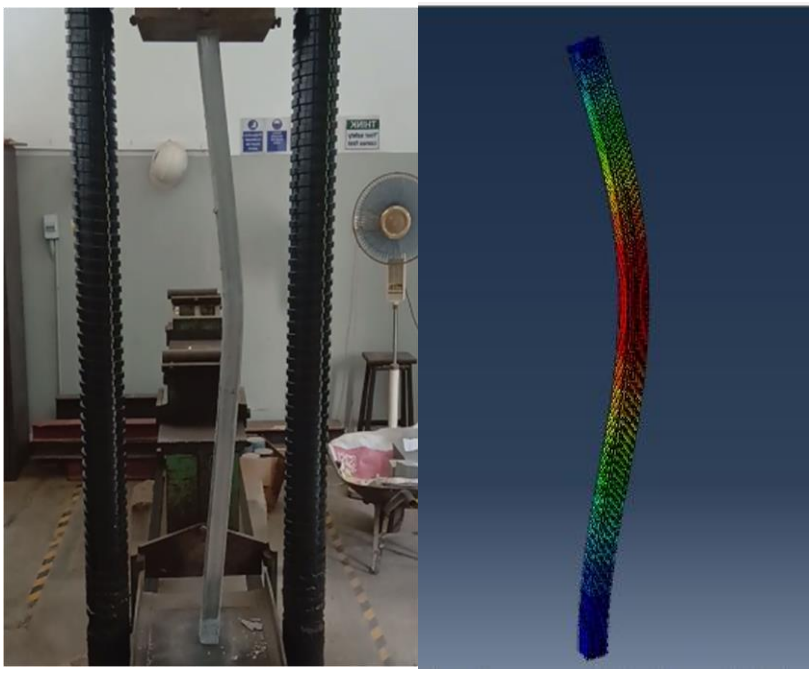

Figure 6.7: Comparison of failure modes of CFST specimens between experimental and numerical results

CFST sections of 1 m length first demonstrated a compression failure while moving into global buckling shape for all members with further increase of load. Also, in the numerical analysis, experimental failure shape was recorded as described in Figure 6.7. 1.5 m length CFST demonstrated global buckling mode since starting of loading.

Table 6.5 gives the failure loads and modes obtained from the numerical analysis using the ABAQUS CAE software. It is evident that the failure modes obtained from the numerical analysis are agreed well with those seen from the experiment. Table 6.6 compares the failure loads obtained from the numerical analysis with those obtained from the experiment and theoretical calculations.

Table 6.5: Failure loads and failure modes of the specimens obtained from numerical analysis using the ABAQUS CAE software

Section	**Height (m)**	**Thickness (mm)**	**Average Failure Load (kN)**	**Failure mode** (LB/CF/GB)
Hollow Section	1m	1.2	43.4	LB
		1.4	89.9	CF
		1.6	102.5	CF
		2.0	144.8	CF
	1.5m	1.2	61.8	LB
		1.4	84.9	CF
		1.6	93.3	CF
		2.0	131.1	CF
CFST Section	1m	1.2	143.6	CF
		1.4	160.1	CF
		1.6	179.6	CF
		2.0	205.7	CF
	1.5m	1.2	137.6	GB
		1.4	138.5	GB
		1.6	140.9	GB
		2.0	188.0	GB

Table 6.6: Comparison of failure loads obtained from numerical analysis with those obtained from experiment and Theoretical values

Section	**Height (m)**	**Thickness (mm)**	**Theoretical failure load (kN)**	**Exp. failure load (kN)**	**Numerical failure load (kN)**	**Failure mode**	**% change in numerical compared to exp.**
Hollow Section	1	1.2	68	42	43.4	LB	3.3%
		1.4	87	88	89.9	CF	2.2%
		1.6	99	101	102.5	CF	1.5%
		2.0	123	143	144.8	CF	1.3%
	1.5	1.2	68	59	61.8	LB	4.7%
		1.4	87	82	84.9	CF	3.5%
		1.6	99	90	93.3	CF	3.7%
		2.0	123	129	131.1	CF	1.6%
CFST Section	1	1.2	154	140	143.6	CF	2.6%
		1.4	165	159	160.1	CF	0.7%
		1.6	176	178	179.6	CF	0.9%
		2.0	197	204	205.7	CF	0.8%
	1.5	1.2	122	133	137.6	GB	3.5%
		1.4	133	137	138.5	GB	1.1%
		1.6	144	139	140.9	GB	1.4%
		2.0	165	190	188.0	GB	-1.1%

From the Table 6.6, it is evident that the failure loads obtained from the numerical analysis agreed well with those obtained from the experiment showing a less than 5% variation for all the cases. Numerical failure loads are slightly higher than the experimental failure loads for all of the cases except for the 1.5 m length 2 mm thick CFST specimen. All three methods yielded a similar failure mode. However, failure loads predicted from the theoretical calculations deviate from those obtained

from the experiment and numerical analysis for some of the cases. Overall, it is clear that the non-linear FE analysis conducted using the ABAQUS CAE software can be used to predict the behaviour of both Aluminium hollow and CFST sections under uni-axial compression loading.

6.5. Chapter Summary

This chapter presented the detailed information of modelling the behaviour of steel hollow and CFST under uni-axial compressive loading using the ABAQUS CAE finite element software. Steel sections were modelled as a linear elastic material with shell elements by using the stress-strain curve obtained from the steel coupon test. Concrete was modelled with solid elements using the concrete damaged plasticity model which can represent complete inelastic behaviour in tension and compression including damage characteristics. Surface-to-surface contact was used to model the interaction between concrete and steel interface in CFST. When assigning boundary conditions, bottom end of the column was modelled as a pin support while the top end was modelled as a roller support, allowing the movement only in longitudinal (vertical) direction to simulate the experimental conditions.

Numerical models could predict the failure modes, where they agreed well with those obtained from both experiment and theoretical predictions. Failure loads obtained from numerical analysis agreed well with those obtained from the experiment showing less than 5% variation for all the tested samples. However, they slightly deviate with values obtained from theoretical calculations for some of the samples.

CHAPTER VII

7. APPLICATION OF CFST IN TRUSS TYPE LIGHT VEHICULAR BRIDGES

7.1. Introduction

This chapter investigates the applicability of using CFST in steel truss type light vehicular bridges. Modified Warren, Pratt and Parker (variable height truss) truss type light vehicular bridges were analysed incorporating CFST members into appropriate positions. Finally, the advantages and disadvantages of different truss types in cooperating CFST are discussed to come up with an economical solution for the lack of pedestrian bridges in Sri Lanka. Basic details of the selected truss types are shown in Table 7.1. Additional details and graphical views are included in the Annex.

Table 7.1: Details of selected truss models

	Parker	Modified Warren	Pratt
Bridge length (m)	50	50	50
Road way width (m)	2	2	2
Maximum height (m)	5	3	3
Head Room (m)	3	3	3

7.2. Methodology

3D models of the selected structures were developed using MIDAS Civil software. Design data which was used to develop 3D model is included in the Annex. After developing 3D FE models of the trusses, loads and boundary conditions were applied to the model. Dead, superimposed dead, live and wind loads were treated in the analysis. Application of these loads and different load patterns considered in the analysis were discussed in Section 3.3.3.

Compression members of the structure were identified during the analysis. Several alternative truss types were considered by replacing different compression members with CFST. Finally, performance of all the structures were compared to identify the effect of using CFST in the selected truss types.

7.3. FE Analysis of the selected bridge types

According to the design details of the structure, 3D models were developed by using Midas Civil software. Developed FE models of the selected truss types are shown in Figure 7.1. One end of the truss was pinned and the other end was roller supported in the analysis. Members were modelled as pin ended members.

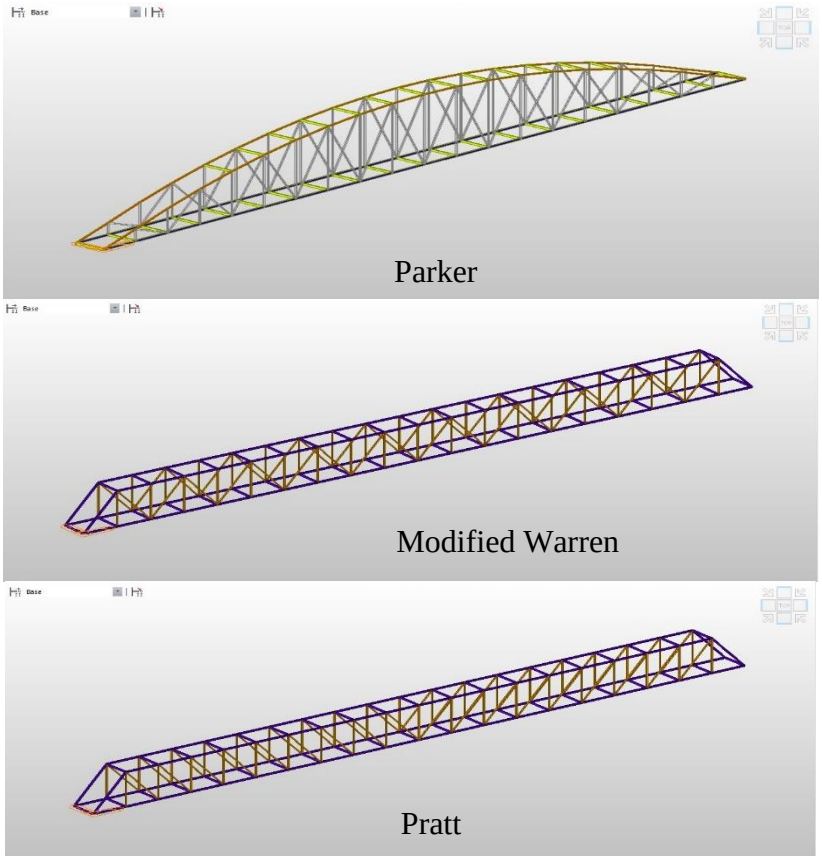

Figure 7.1: Developed FE Models of the selected truss bridges

7.3.1. Bridge loading

Bridge structure can be subjected to various types of loading. Following loads which are specified in BS 5400: Part 2 (1978) were considered in the analysis.

1. Dead load (weight of the structural elements)

2. Superimposed dead load (weight of the non-structural elements including the surfaces and finishing)
3. Live loads (10 kN/m^2 load was considered by considering access of pedestrians and light vehicles)
4. Wind load (wind load acting on the pedestrians standing on the bridge was assumed to be transferred to the deck of the bridge)

Different live load patterns were considered by considering the present of pedestrians on different parts of the deck slab. Load factors and load combinations which are specified in Euro code 3 were considered in the analysis. Load envelope was created considering all the cases, and the results were determined according to the final load envelope.

7.3.2. Material properties

In these composite CFST structures both steel and concrete are present. Properties of the both materials as used in the FE analysis are given below.

Young's modulus of steel = 210 GPa

Yield stress of steel = 320 N/mm^2

Poisson's ratio of steel = 0.3

Density of steel = 78.5 kN/m^3

Density of concrete = 2400 kg/m^3

Compressive strength of concrete = 42.9 N/mm^2

Tensile strength of concrete = 2.55 N/mm^2

7.4. Design of CFST truss bridge

Initial cross section of CFST sections was determined by using Euro code 4. Initial axial forces for CFST design was taken as the compression value of the corresponding I section in original structure. Self-weight of the CFST Bridge is higher than steel truss bridge due to extra weight of concrete. Therefore, CFST sections should be able to resist at least the maximum compressive force of the original structure.

As described earlier, different compression members of the truss bridges were replaced with CFST members. Four different CFST structures were designed along with 3 different steel truss type light vehicular bridge structures. For steel truss bridges all the members were designed with I sections. CFST members are assumed to be made by infilling concrete into 200 mm square hollow steel sections having 5 mm thickness. Members which were replaced by CFST are highlighted in Figure 7.2.

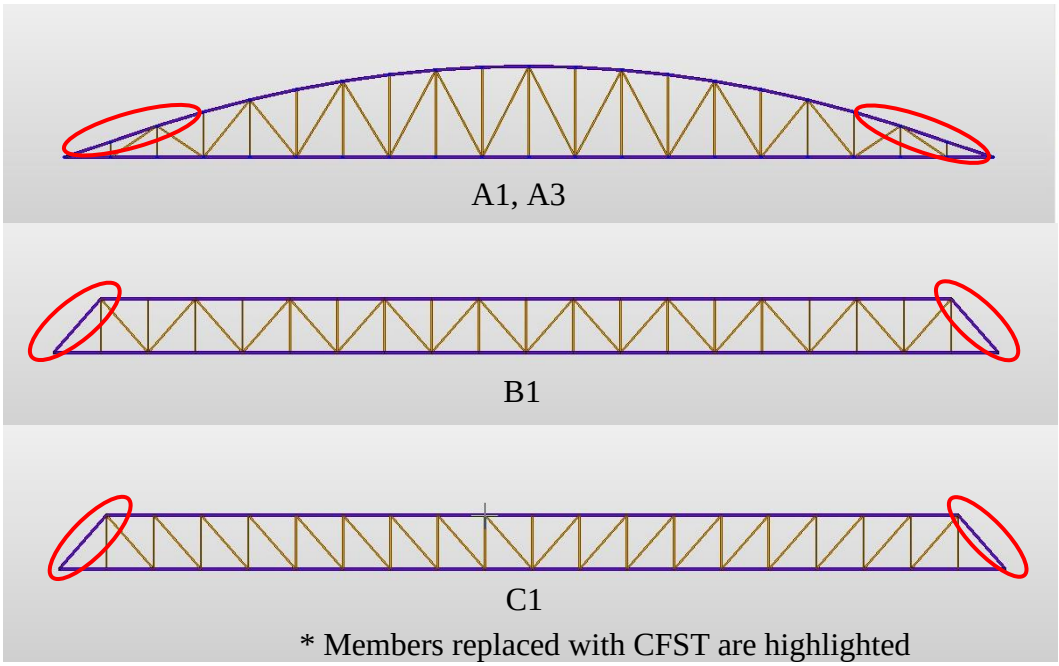

Figure 7.2: Members replaced with CFST in different truss types

Above cases were analysed using previous material properties incorporating into the model. Sections were designed according to Euro code 4. Four different cases analysed can be categorized as follows,

1) Parker truss type light vehicular bridge with unbraced members replaced with CFST – A1
2) Parker truss type light vehicular bridge full top chord replaced with CFST – A2
3) Parker truss type light vehicular bridge with unbraced top chord members replaced with bigger steel section – A3
4) Modified Warren truss type light vehicular bridge with end rakers replaced with CFST – B1

5) Pratt truss type light vehicular bridge with end rakers replaced with CFST-C1

Details of the sections used for different structures are shown in Table 7.2. CFST (made by infilling concrete into 200 mm square steel hollow sections having 5 mm thickness) were used by limiting the demand/ capacity ratio to 0.85. In all truss types steel I sections of size 203x203x71 were used for the bottom chord. The same section was used for the all top chord in the trusses B1 and C1. In the truss A2, CFST as mentioned above used for the entire top chord. In trusses A1 and A3 unbraced top chord members were replaced with CFST and bigger I sections of size 254x 254 x 167 respectively, while the remaining top chord members in those could be provided with a smaller I sections of size 203x203x52. Because the introduction of CFST or bigger I sections to unbraced top chord members at the corners has caused a reduction of demand /capacity ratio for other top chord members. It also contributes to an improvement of cost figures. These additional sections were chosen in order to limit the deflection to prescribed limitation according to AASHTO's guidelines. Axial forces, deflection, support reaction and demand/capacity values for top and bottom chords for the case of steel Parker truss is presented in Annex.

Table 7.2: Details of the truss members

Member	**Section type**	**Section Dimensions (mm)**
Top chord	I section	203x203x71 and 203x203x52
Vertical	I section	89x89x19.35
Bottom chord	I section	203x203x71
CFST	Box section	200x200x5
Top chord (bigger section for case A3)	I section	254x254x167

7.5. Results and comparison

Maximum compressive forces occurred at the corner most members of the top chord were considered when selecting the sections while considering the envelop for load combinations. Axial forces have increased when more members are replaced with CFST in Parker truss. When number of CFST is increased, it adds extra concrete weight to the structure. Therefore, axial forces of the members are increased when a greater number of members are replaced with CFST. Maximum axial forces are recorded in Modified Warren and Pratt trusses due to higher tonnages inherent to them.

Support reactions under the self-weight is increased, when number of replaced members (with CFST) are increased in Parker trusses. This is due to the extra weight of concrete in CFST members, and necessary precautions have to be taken when foundation structure is designed. Modified Warren and Pratt trusses yield higher weight and hence they cause the higher support reactions compared to Parker varieties.

AASHTO's Guide Specifications for Design of Pedestrian Bridges, 1997, Section 1.3.1 describes the limits for deflections of the truss type pedestrian bridges at serviceability condition. It allows maximum deflection of 1/400 of span at serviceability state. Therefore, 50 m span truss bridge has to be designed limiting the deflection to 125 mm. Deflections obtained from the FE models for each truss type is presented in the Table 7.3.

Table 7.3: Deflection in each truss

Case	**Maximum deflection (mm)**
Parker	96
A1	77
A2	38
A3	37
Modified Warren	146
B1	139
Pratt	143
C1	138

The parker truss and all its modifications (A1, A2 and A3) show a deflection well below 125 mm. The deflection of the parker truss is about 96 mm and it has reduced to 77 mm in truss A1, when the unbraced top chord members are replaced with CFST. The introduction of the CFST to the entire top chord (truss A2), has caused a noticeable reduction in the deflection, where it has reduced to about 38 mm. Similarly, replacement of unbraced top chord members with a bigger I section (truss A3) has also caused a reduction in the deflection to about 37 mm.

Both modified Warren and Pratt truss types have shown deflections of about 146 mm and 143 mm respectively, while the replacement of end rakers with CFST has lowered their deflections slightly to about 139 mm (in truss B1) and 138 mm (in truss C1) respectively. Overall, it is evident that the Modified Warren and the Pratt truss types do not satisfy the deflection limit given in the AASHTO's Guide with the selected sections.

7.6. Feasibility study

Feasibility of using CFST in truss bridges in Sri Lanka is discussed in this chapter. Mainly economic feasibility of the CFST is focused during the discussion.

7.6.1. Economic feasibility

Above sections indicated the material usage for different cases considered for the analysis. Over the time, steel and concrete have been used alone as popular construction materials in bridge construction. However, bridges made out of entirely with steel or concrete yields extensive cost values in terms of design and construction. But for light vehicular and pedestrian bridges composites with steel and concrete can be used in a more economical cost figures as this study yields.

The total cost of a bridge can be estimated using the Eq. 1. The economic feasibility of a bridge using CFST sections compared to that using solid GI sections can be generated using the Eq. 2.

$$\text{Total cost} = P_{stl} \times W_{stl} + P_{conc} \times W_{conc} + P_{CFSTstl} \times W_{CFSTstl} \quad (1)$$

$$P_{conc} \times W_{conc} + P_{CFSTstl} \times W_{CFSTstl} \lessgtr P_{stl} \times W'_{stl} \quad (2)$$

Where,

$P_{conc.}$ = Cost of concrete (Rs. 8.33/kg)

$W_{conc.}$ = Weight of concrete

$P_{CFSTstl}$ = Cost of hollow GI in CFST (Rs. 280/kg)

$W_{CFSTstl}$ = Weight of hollow GI in CFST

$P_{stl.}$ = Cost of solid GI (Rs. 210/kg)

$W_{stl.}$ = Weight of solid GI steel

$W'_{stl.}$ = Weight of replaced steel members in normal truss bridge

It was found that the market prize of Grade 40 ready-mixed self-compacting concrete (SCC) by accommodating for infilling is about Rs. 8.33/kg. The price of solid GI was found to be about Rs. 210/kg, while that of rectangular hollow (box) GI sections was found to be about Rs. 280/kg. Since the price of GI is considerably higher than that of infilled concrete, the introduction of CFST into top chord members would lead to an economical solution. However, it should be also noted that the introduction of CFST would increase the total weight of the structure, creating higher axial forces in the members, which may lead to replace those with bigger sections. The increase in the tonnage will also have to account when designing the foundations. The cost of the selected bridges calculated using Eq. 1 is shown Table 7.4.

A1 and A2 can be identified as the most economical structures among all structures. Even though A3 structure has more rigidity against mid deflection it costs more to have a larger steel I section at the corner members of the top chord. When the cost difference between concrete and steel is higher, saving is much higher by using CFST. The amount that can be saved, depends on the weight of the steel that is replaced by CFST (refer Eq. 2). Since CFST uses less steel amount, higher amount of cost can be reduced when the number of replaced members are increased. In A2 structure, the amount saved is higher than in A1 structure when material cost is considered. In A2 structure a greater effort has to put to in the construction phase. That means replacing the entire top chord with CFST may not be the best solution for this type of truss by considering practical implementation. Modified Warren and Pratt trusses consume a comparatively higher steel tonnage and replacement of end rakes has not been yielded a considerable structural performance to be used as an economical truss type.

Table 7.4: Steel and concrete tonnage for 8 cases of truss analysis

Case	Steel Tonnage (Ton) 210 Rs/kg	CFST		Weight (Ton)	Cost (LKR)
		CFST Steel (Ton) 280 Rs/kg	Concrete Tonnage (Ton)		
Parker	24.77	-	-	24.77	5.20 m
A1	21.80	1.27	3.85 (1.60)	26.92	4.97 m
A2	17.50	3.11	9.42 (3.92)	30.03	4.62 m
A3	28.80	-	-	28.8	6.05 m
Modified Warren - steel	25.05	-	-	25.05	5.26 m
B1	23.96	0.46	1.40 (0.58)	25.82	5.17 m
Pratt - Steel	25.05	-	-	25.05	5.26 m
C1	23.96	0.46	1.40 (0.58)	25.82	5.17 m

Even though the usage of CFST reduces the deflection and the cost of the overall structure, it increases the weight of the structure. It is clear that, with the inclusion of CFST members, weight of both A1 and A2 trusses have increased by 2.15 and 5.26 tons respectively compared to the Parker truss with only steel members. Both A1 and A2 trusses show 4.4% and 11.2% cost reduction compared to Parker truss, but show 8.7% and 21.2% weight increase respectively compared to that. The increase in the weight has to be accommodated when designing the abutment, which will affect the cost of the construction. Therefore, to determine the feasibility of the structure more accurately, structural design and cost analysis for these bridges have to be conducted by accounting for the connections, substructure and superstructure.

Numerical results state the fact that concrete infilling has increased the capacity of the truss bridges by a larger proportion. Hence, to achieve the economy in variable height truss bridges, one of the optimum solutions is to concrete infilling into top chord members.

7.7. Constructability

Even though using CFST in truss bridges has economic and structural advantages, constructability and the suitability as a construction material in Sri Lanka has to be analysed.

There are several geometric sections that are used for CFST as described earlier. Square and rectangular shapes of CFST have better characteristics when considered the connections and confining of concrete. Even though circular CFST performed better than square or rectangular type in terms of compression capacity, there are difficulties occur during the construction. One of the difficulties is the type of joint when using circular CFSTs. Members have to be welded or have to use a gusset plate at the joint.

Quality of concreting is a main factor which governs the strength of a CFST member. If there are honeycomb in the concrete, it will reduce the strength of the CFST in large amount. After concreting, it will be hard to identify any concreting defects by naked eye. Special equipment has to be used to identify concrete defects. One of the main disadvantages in CFST is, there is no way to treat concrete defects like honeycombs. The whole CFST will have to remove, if it does not have the required strength because of the strength reduction due to honeycombs. Therefore, necessary steps should be taken to ensure the quality of the concreting. Using high flow type concrete, proper compaction method and proper inspection during the concreting will help to reduce the defects of the CFST.

Even though CFST has less corrosion rate than normal steel tubes and I sections, corrosion of the CFST is another fact, which determines the suitability of the material. Therefore, proper measures have to be taken to reduce the corrosion of CFST.

7.8. Chapter summary

The performance of eight different truss types (Parker, Parker with unbraced top chord members replaced with CFST (A1), Parker with entire top chord replaced with CFST (A2), Parker with unbraced top chord members replaced with bigger I sections (A3), Modified Warren, Modified Warren with end rackers replaced with CFST (B1), Pratt and Pratt with end rackers replaced with CFST (C1)) having a 50 m

length was studied using the MIDAS CIVIL software for their applicability as light vehicular bridges. The Parker truss and all its modifications (A1, A2 and A3) show a deflection below 125 mm (span/400), which is the limiting value specified in the AASHTO's Guide Specifications for Design of Pedestrian Bridges, 1997. Both Modified Warren, Pratt and their modifications with CFST show a deflection in the range of 135- 150 mm, which are slightly greater than the recommended value. The use of CFST for the entire top chord (A2) and larger I sections for the unbraced top chord members (A3) have considerably lowered the deflection of the Parker truss. The use of CFST for the end rackers has not shown noticeable influence on the deflection of the Modified Warren and Pratt truss types.

Cost of concrete is considerably less that the cost of steel sections (both hollow and solid GI). Therefore, the introduction of CFST has led to a noticeable cost reduction in the Parker truss. Both A1 and A2 trusses show 4.4% and 11.2% cost reduction compared to Parker truss. However, introduction of CFST has increased the weight by 8.7% and 21.2% respectively compared to the Parker truss. The use of bigger I sections for the unbraced top chord (A3), is not a favourable option in terms of both cost and the weight. The use of CFST for the end rackers in the Modified Warren and the Pratt trusses does not have a noticeable influence on the weight and hence the cost. However, to determine the feasibility of a structure more accurately, structural design and cost analysis for the bridges have to be carried out by accounting for the connections, substructure and the superstructure.

CHAPTER VIII

8. CONCLUSION

Behaviour of CFST members in truss bridges, under axial compression was studied in this research as an economical solution for lack of higher span pedestrian and light vehicular bridges in Sri Lanka. Following conclusions were drawn based on the result of this research.

The developed span vs. tonnage graphs for different truss types with specified dimensions indicated that almost all the pedestrian bridges consume similar tonnage up to 30 m spans. By considering ease of construction, both Pratt and Modified Warren truss type bridges can be recommended for spans less than 30 m. For higher spans, Parker truss consumes noticeably less tonnage compared to the other truss types and hence could be recommended for higher spans.

The reduction in the steel tonnage when the minimum width and height of a truss are reduced to 1.5 m and 2.5 m respectively are not that significant and hence bridges with those modifications can be recommended only at locations where the access can be provided only for pedestrians. It is recommended to follow the RDA regulations, where a minimum 2 m width and 3 m headroom height should be used for pedestrian bridges to allow the access of light vehicles.

Uni-axial compression test was carried out for hollow GI and CFST specimens having lengths of 1 m and 1.5 m for four different thicknesses (1.2 mm, 1.4 mm, 1.6 mm and 2.0 mm). Both 1 m and 1.5 m high hollow GI specimens having a 1.2 mm thickness failed in local buckling irrespective of the height. Both 1m and 1.5 m high hollow GI specimens having 1.4 mm, 1.6 mm and 2.0 mm thicknesses failed in compression. Compression capacities of the 1 m high columns are considerably higher than their Euler buckling loads, while that trend is quite low in the 1.5 m high specimens. Experimental failure modes agreed well with the theoretical predictions. The theoretical and experimental failure loads are agreed well for the specimens failed in compression (change is less than 10%) compared to those failed in local buckling.

1 m high CFST specimens with all the thicknesses failed in compression as their Euler buckling failure loads are considerably higher than the compression capacities. However, 1.5 m high CFST specimens with all the thicknesses failed in global buckling as their Euler buckling failure loads are lower than the compression capacities. Experimental failure modes agreed well with the theoretical predictions. Overall, experimental failure loads agreed well with those predicted from the theoretical calculations for all the CFST specimens (change is less than 15%)

For 1 m high specimens, increase in the failure load has reduced from 126% to 60% when the thickness of the GI tube is increased from 1.2 mm to 2.0 mm, while it has reduced from 79% to 34% for 1.5 m high specimens. It is therefore clear that the failure load improvement in CFST has reduced with the increase of the thickness of the GI tube, where the GI section type is changed from Class 4 to Class 1. On the other hand, improvement in the failure load is less in the specimens with 1.5 m height compared those of 1 m height, where the failure mode is changed from compression failure (in hollow GI tubes) to the global buckling failure (in CFST). So, it is evident that the strength enhancement with CFST is more significant in the short columns compared to the long columns.

Uni-axial compression test was carried out for Aluminium hollow and Grout Filled Aluminium Tubes (GFAT) having a 0.9 mm thickness for three different lengths (210 mm, 230 mm and 240 mm). According to theoretical predictions, both Aluminium hollow and GFAT fail in compression irrespective of the length. Theoretical failure loads of Aluminium hollow sections are greater than the experimental failure loads for both 230 mm and 240 mm specimens while it is slightly lesser than that for the 210 mm length specimen. The percentage change is less than 15% for all three lengths (for hollow sections), which seems to be increased with the length of the specimen.

For GFAT, experimental failure loads are quite lower than the theoretical failure loads. This could be mostly seen for higher lengths, where the percentage change in the experimental failure load is increased from 9.6% to 26.6% when the length is increased from 210 mm to 240 mm. Overall, it seems that for higher lengths

the experimental failure loads of both Aluminium hollow and GFAT are getting lower than the theoretical failure loads. This might be due to the effect of global buckling, as the predicted Euler buckling loads can be reduced due to many parameters such as eccentricity of loading, material imperfections, etc.

GFAT shows a noticeable strength enhancement compared to Aluminium hollow sections and this trend can be clearly seen for the 210 mm height specimens. It is evident that the strength enhancement of GFAT seen from the experiment (9% - 27%) is quite lower than that predicted from theoretical calculations (42.4%).

The applicability of GFAT to enhance the strength of a variable height Parker truss made out of Aluminium hollow sections was studied. Initially, a truss was made by using only Aluminium hollow sections (Truss A), and then an identical truss was made (Truss B) by replacing the unbraced top chord members with GFAT. Experimental failure loads are noticeably higher than the theoretical failure loads and this trend is more visible in Truss A than Truss B. In both of the trusses, percentage increase in the experimental failure load of the critical member is very much close to the percentage increase in the total failure load.

Failure load increment in both trusses is less than that of individual members. With the introduction of the GFAT for the unbraced top chord members, it was expected to achieve a 27.9% strength enhancement theoretically, but that achieved in the experiment was about 18.6% which is quite less than the theoretical value. However, still the experimental failure loads are greater than the theoretical predictions in both truss A and B. Overall, it is evident that there is a noticeable strength enhancement in Truss B compared to Truss A, highlighting the effectiveness of infilling the unbraced top chord members in a variable height truss types towards their strength enhancement.

The behaviour of steel hollow and CFST under uni-axial compressive loading was studied using the ABAQUS CAE finite element software. Numerical models could predict the failure modes, where they agreed well with those obtained from both experiment and theoretical predictions. Failure loads obtained from numerical analysis agreed well with those obtained from the experiment showing less than 5% variation

for all the tested samples. However, they slightly deviate with the values obtained from theoretical calculations for some of the samples. Overall, it can be concluded that numerical results agreed well with those obtained from the experiment compared to the theoretical predictions. This might be due to the accountability of both geometric and material nonlinearities in the numerical model where as a linear elastic behavior was treated in the theoretical calculations.

The performance of eight different truss types (Parker, Parker with unbraced top chord members replaced with CFST (A1), Parker with entire top chord replaced with CFST (A2), Parker with unbraced top chord members replaced with bigger I sections (A3), Modified Warren, Modified Warren with end rackers replaced with CFST (B1), Pratt and Pratt with end rackers replaced with CFST (C1)) having a 50 m length was studied using the MIDAS CIVIL software for their applicability as light vehicular bridges. The Parker truss and all its modifications (A1, A2 and A3) show a deflection below 125 mm (span/400), which is the limiting value specified in the AASHTO's Guide Specifications for Design of Pedestrian Bridges, 1997. Both Modified Warren, Pratt and their modifications with CFST show a deflection in the range of 135- 150 mm, which are slightly greater than the recommended value. The use of CFST for the entire top chord (A2) and larger I sections for the unbraced top chord members (A3) have considerably lowered the deflection of the Parker truss. The use of CFST for the end rackers has not shown noticeable influence on the deflection of the Modified Warren and Pratt truss types.

Cost of concrete is considerably less than the cost of steel sections (both hollow and solid GI). Therefore, the introduction of CFST has led to a noticeable cost reduction in the Parker truss. Both A1 and A2 trusses show 4.4% and 11.2% cost reduction compared to Parker truss. However, introduction of CFST has increased the weight by 8.7% and 21.2% respectively compared to the Parker truss. The use of bigger I sections for the unbraced top chord (A3), is not a favourable option in terms of both cost and the weight. The use of CFST for the end rackers in the Modified Warren and the Pratt trusses does not have a noticeable influence on the weight and hence the cost. However, to determine the feasibility of a structure more accurately, structural design

and cost analysis for the bridges have to be carried out by accounting for the connections, substructure and the superstructure.

RECOMMENDATION FOR FUTURE WORK

Main objective of this study is to identify the feasibility of using CFST in truss bridges in Sri Lanka as an economical solution for lack of higher span truss type light vehicular bridges. After processing the results of the research, it was concluded that CFST can be used to design economic and better structurally performed truss bridges. There are some other aspects which were not studied during this study and which need to be addressed. Some of them are mentioned below.

The experimental program was conducted for the small scale bridges made out of Aluminium sections where infilling was done with cement grout. This has to be extended for large scale bridges using steel sections, where the infilling has to be done with concrete. Connection details should also be considered in the design and it should be accounted for the costing,

In this study, square hollow sections were used for the infilling. However, applicability of the circular hollow sections should also be investigated. Concrete infilling has to be studied with different types of concretes having various grades and workability.

Occurring honeycombs in CFST was identified as a reason which prevents the use of that as a construction material. Impact of honeycombs and suitable methods to rectify or reduce those defects should be studied. Further studies about the durability of CFST should be carried out.

Steel hollow sections used to concrete infilling can be stiffened using steel plate parts and improve the load carrying capacity and it has to be tested against different patterns of stiffening.

Dynamic analysis of the CFST truss bridge can be carried out to determine the seismic performance to identify the most effective CFST structure.

REFERENCE

AASHTO's Guide Specifications for Design of Pedestrian Bridges, 1997, American association of state highway and transportation officials.

American Concrete Institute (ACI). (1999). ‘‘Building code requirements for structural concrete and commentary.’’ ACI 318-99, Detroit.

Baskaran. K, Karunarathna W.W.N., Hidallana Gamage H.D., 2011. “Finite Element Analysis of Truss Type Steel Bridges.”

BS 4: Part 1: 1993, British Standards for structural steel sections, p. 14.

BS 5400: Part 2: 2006, Concrete and composite bridges, classification for loads, p. 60.

Burak, E., Kivanc, T., Tuncan, A., (2014). Structural behaviour of concrete filled steel tubular sections (CFT/CFST) under axial compression. Thin-Walled structures, (80), 46-56.

Chandrasiri, B., & Jayasinghe, M. (2001). Rehabilitation of steel bridges in Sri Lanka.

Dushyant A. Zamre, Aditi H. Deshmukh, 2015. Seismic Design Considerations of Foot Bridge. International Journal for Research in Applied Science & Engineering Technology (IJRASET), 3(2).

European Committee for Standardization (CEN). (1992). Design of composite steel and concrete structures, part 1.1—General rules and rules for buildings. Euro code 4.

Fong, M., Chan, S. L., Uy, B., (2011). Advanced design for trusses of steel and concrete-filled tubular section. *Engineering Structures,* 33(12), 3162-3171.

Geetha, H., and Swedha, T., (2015). An experimental study on concrete filled tubular columns using varying steel materials. *International J Innovative Science, Engineering & Technology,* 2(5), 737-742.

Gupta, P.K., Sarda, M., Kumar, M.S., (2007). Experimental and computational study of concrete filled steel tubular columns under axial loads. *J Constr Steel*, 63(2), 182–193.

Han, L.H., He, S.H., Liao, F.Y., (2011). Performance and calculations of concrete filled steel tubes (CFST) under axial tension. *J Constr Steel*, 67(11), 699–709.

Han, L.-H., Hou, C.C., Wang, Q.-L., (2014). Behaviour of circular CFST stub columns under sustained load and chloride corrosion. *J Constr Steel*, 103, 23-36.

Hibbitt, Karlsson, and Sorensen, Inc. (2000). ABAQUS theory manual and user manuals. Version 5.8, Providence, R.I

Hu, H.T, Huang, C.S., Wu, M.H., Wu,Y.M., (2003). Nonlinear analysis of axially loaded concrete-filled tube columns with confinement effect. *J Struct Eng*, 129(10), 322–99.

Jorge T., Alberto G., (2010). "Structural evaluation of a truss pedestrian bridge.", American Society for Engineering Education, 2010.

Karunarathna, H.M.G.U., & Susantha, K.A.S., (2015). Concrete Filled Steel Tubes for Performance Improvement of Steel Truss Bridges. 6th International Conference on Structural Engineering and Construction Management, 84-90.

Keil, A., (2013). Detail Practice Pedestrian Bridges. Institut fur internationale Architektur-Dokumentation GmbH & Co. KG (28 Feb. 2013) (January 1, 1600)

Lee, J., Fenves, G. L., (1998). Plastic-damage model for cyclic loading of concrete structures. *J Eng Mech*, (124), 892–900.

Lidong Z., Wanlin C., Huazhen G., Yang Z., Yu S. and Zhaoyuan Y., (2018). Experimental and Numerical Analysis of Large-Scale Circular Concrete-Filled Steel Tubular Columns with Various Constructural Measures under High Axial Load Ratios. Appl. Sci. 2018, 8, 1894.

Lubliner, J., Oliver, J, Oller, S., Oñate, E. A., (1989). Plastic-damage model for concrete. *International J Solids and Structures*. 25(3), 299–329.

Mander, J. B., Priestley, M. J. N., and Park, R., (1988). Theoretical stress-strain model for confined concrete. *J. Struct. Eng*, (114), 1804–1848.

Martin, D., O'Shea, and Russell Q. Bridge, (2000). Design of circular thin-walled concrete filled steel tubes. *J. Struct. Eng*, 126(11), 1295-1303.

Meng, Z., Li-Yan, X., Mu-Xua, T., Jerome, F., (2017). Experimental study on confining- strengthening, confining-stiffening, and fractal cracking of circular concrete filled steel tubes under axial tension. Engineering structures. 133,186-199.

Miss, W. (n.d.). Truss bridge, Bridge design, Bridge construction. Pinterest. Retrived 01 December, 2019 from https://www.pinterest.com/pin/175358979215181118/

Mohanad M., (2007). "The Behaviour and Design of Thin Walled Concrete Filled Steel Box Columns". (Doctoral dissertation, The University of New South Wales, Sydney, Australia). Retrieved from http://unsworks.unsw.edu.au/fapi/datastream/unsworks:1443/SOURCE01?view=true

Monika M, Pradeep A R, Guruprasad T N, (2017). "Comparative study on Time period and Frequency of Full Arch and Vierendeel Truss Steel Pedestrian Bridge". International Research Journal of Engineering and Technology (IRJET),4(6).

Moon J., Roeder, C.W., Lehman, D.E., Lee, H.-E, 2012. Analytical modeling of bending of circular concrete-filled steel tubes. *Engineering Structures*, 42, 349-361.

Pan, Y.G., Zhong, S.T., (1990). *Constitutive relations of concrete filled steel tube under tension. Ind Constr, 20.*

Ran F., Yu C., Wenzhi G., 2017. Flexural behaviour of concrete-filled aluminium alloy thin-walled SHS and RHS tubes. *Engineering Structures*, 137, 33-49.

Rohitha S. D. K., Jayasuriya C.C.W., Jayasinghe M.T.R., 2001. "Computer Modelling of Suspension Bridges for Light Vehicular Traffic."

Shosuke M., Keigo T., 2003. Design and Construction of Concrete-Filled Steel Tube Column System in Japan. Earthquake Engineering and Engineering Seismology, Vol. 4, No. 1.

Taylor, A., Sejal, P., Dalal. Desai, A.K., (2016). Comparative Performance Evaluation of Steel Column Building & Concrete Filled Tube Column Building under Static and Dynamic Loading, *Procedia Engineering*, 173, 1847–1853.

Weiwei L., Teruhiko Y., (2017), "Applied Loads and Stability of Steel and Steel-Concrete Composite Bridges", Bridge Engineering.

Zhijuan Tian, Yongjian Liu, Lei Jiang, Weiqing Zhu, Yinping Ma, 2019. A review on application of composite truss bridges composed of hollow structural section members. journal of traffic and transportation engineering (English Edition).

ANNEX

Euler's buckling failure load demonstration

Euler's formulae for 1.5 m height, 2.0 mm thick, 50 mm x 50 mm sections: -

$$N = \frac{n\prod^2 EI}{L^2} \quad (1)$$

Where,

n = factor accounting for the end conditions = 1 (pinned ended at both ends)

E = modulus of elasticity = 2 x 10^{11} Pa (N/m^2)

L = length of column = 1.5 m

I = Moment of inertia = 1.47 x $10^{-7}m^4$

$$N = \frac{1\ x\ 3.14^2\ x\ 2 \text{ x } 10^{11} \text{ x } 1.47 \text{ x } 10^{-7}}{1.5^2}$$

N = 128.8 kN

L/r = 1500/19.92 = 75.2

Therefore, 40 < L/r < 120 and categorises into "intermediate columns" where failure mode is a combination of crushing (yielding) and buckling.

Eurocode 4 has given a reasonable approach to design composite columns. This method is based on steel design approach and work out the buckling load for concentrically loaded column and modifies incorporating reinforced concrete design approach. The squash load N_{sq}, ultimate moment Mu and Euler critical load N_{crit} are basic parameters used by Eurocode 4. (Mohanad M, 2007)

The Euler critical load is calculated as

$$F = \frac{\prod^2 (EI)_e}{L^2{}_e}$$

where the effective elastic flexural stiffness $(EI)_e$ about the axis of bending is determined by

$$(EI)_e = E_s I_s + 0.8 E_c I_c$$

Sample of Steel tensile test output – steel coupon test

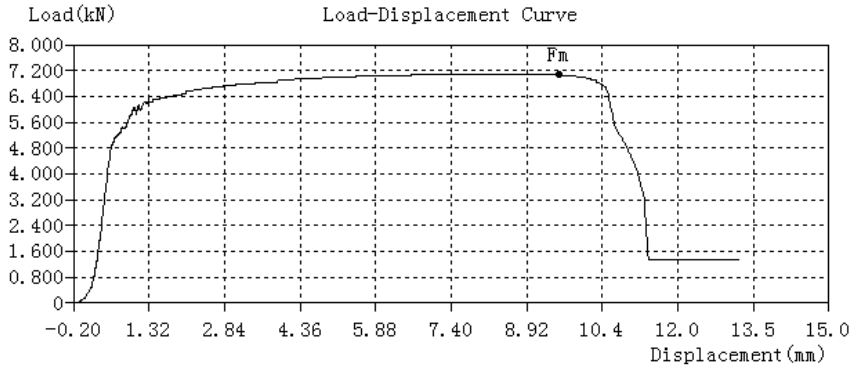

Average yield strength = 4.8 kN

Average yield stress = 320 N/mm^2

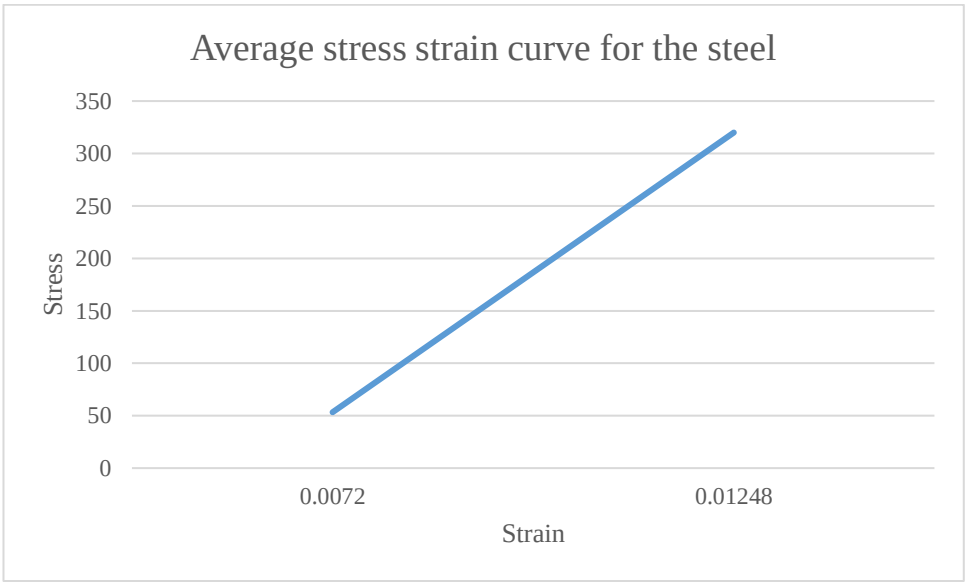

FEM CFST bridge truss models dimensions

Parker truss

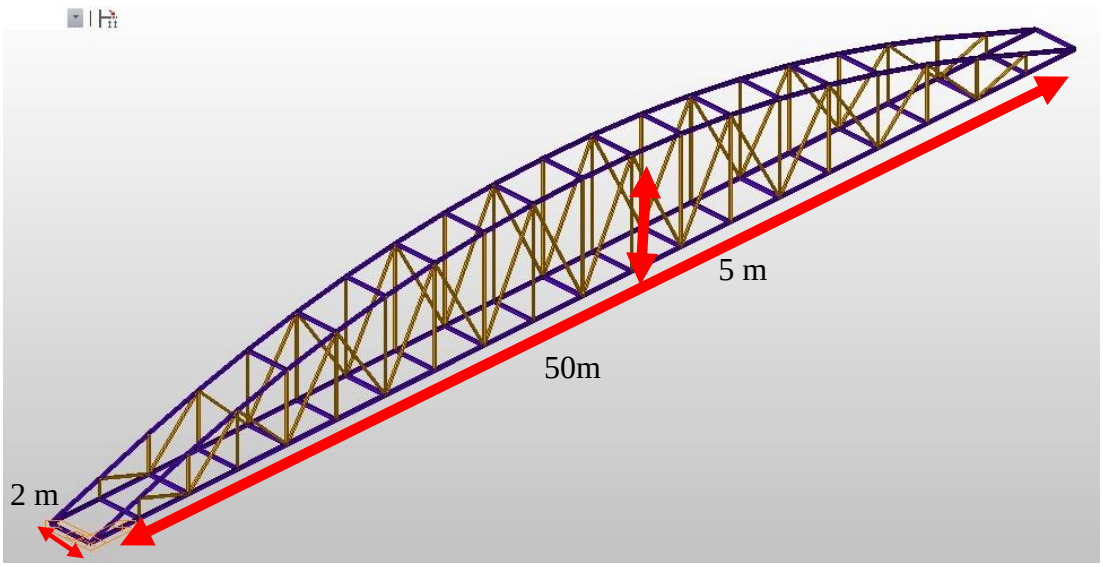

Modified Warren

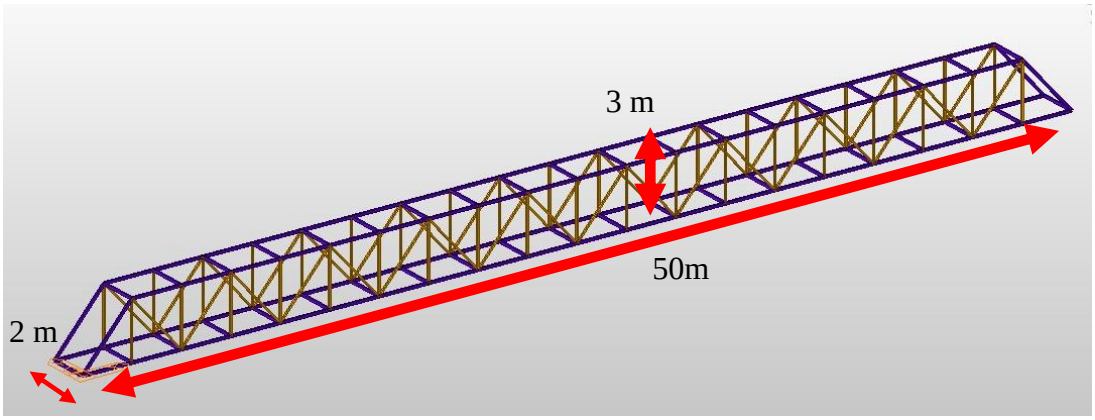

Pratt

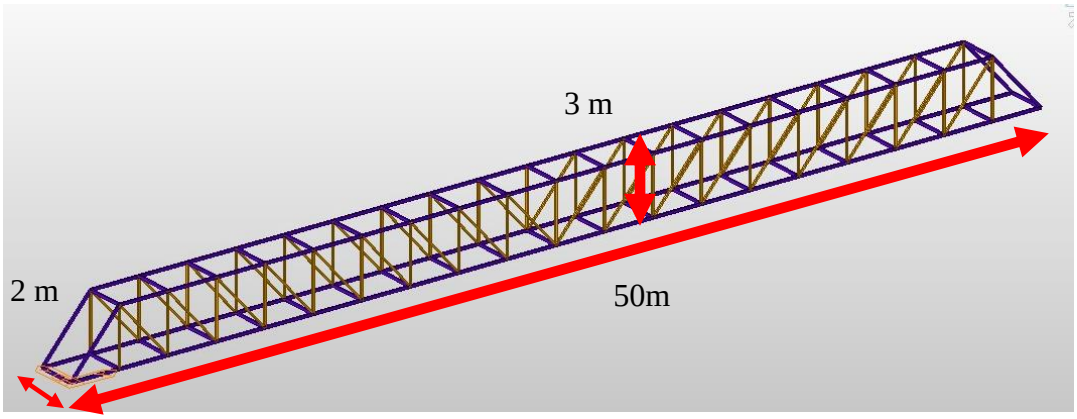

Analysis details – Parker steel

Section details – Parker steel truss

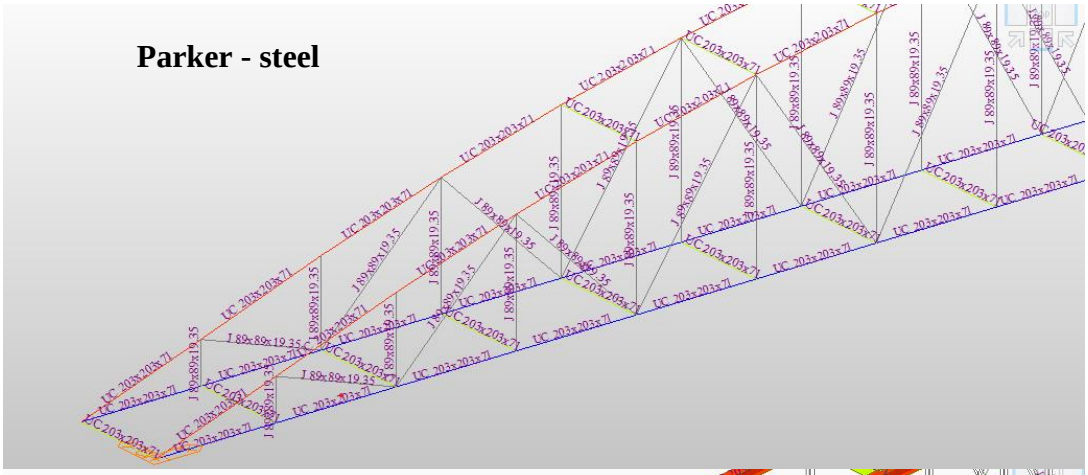

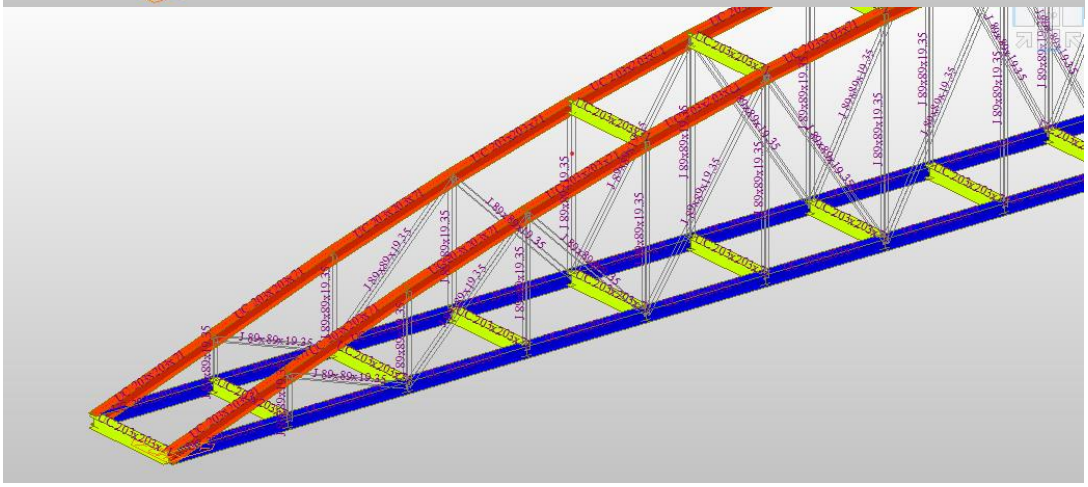

Support reactions

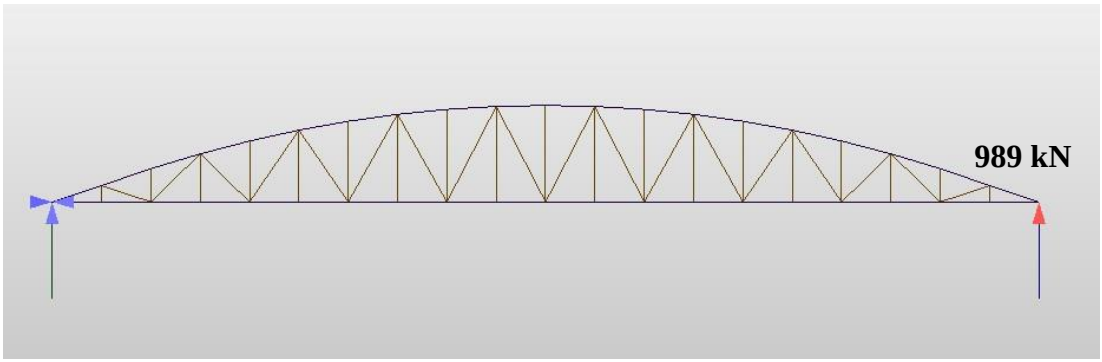

Maximum axial forces

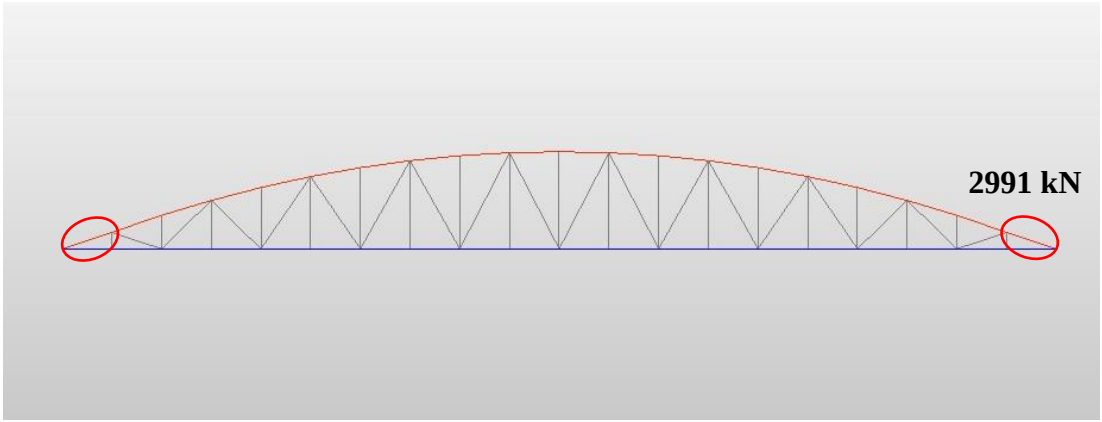

Deflections

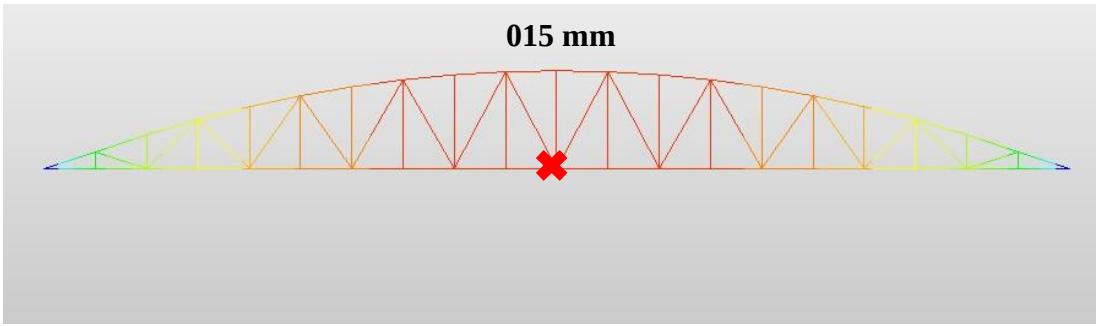

Section/capacity ratios